NTNU – Trondheim
Norwegian University of
Science and Technology

Mechanisms of Cellular Uptake and Intracellular Degradation of Polymeric Nanoparticles

Einar Sulheim

Nanotechnology
Submission date: June 2014
Supervisor: Catharina de Lange Davies, IFY

Norwegian University of Science and Technology
Department of Physics

Preface

This master thesis concludes 5 years of education within the Master of Science - Nanotechnology program at the Norwegian University of Science and Technology, with specialization in bionanotechnology. This work is part of a collaboration between NTNU Department of Physics, St.Olavs hospital and SINTEF termed "Multifunctional nanoparticles in diagnosis and therapy of cancer" that is led by Professor Catharina de Lange Davies who was also my supervisor.

Foremost, I would like to thank Professor Catharina de Lange Davies for introducing me to this field of research and letting me write both my 5th year project thesis and master thesis on this topic. For the last 3 years, my education has been aimed at working with nanomedicine, and I am very happy that I could complete my master degree working on a relevant and challenging project. During the experimental work I was given full freedom to follow the results I found most interesting with my own choice of methods, and I was supported to present my work at a biophysics conference in Oslo. I am very grateful for giving me that opportunity and for having confidence in me. I am also grateful for all the support, suggestions and advice given, and for being invited to the weekly meetings in the research group, these meetings have been an excellent forum for discussing future experiments and results. I would also like to thank the rest of the nanoparticle group at NTNU biophysics for taking time to discuss results and experiments and including me both in academic and social arguments and arrangements.

Further I would like to thank research scientist Yrr Mørch and SINTEF Materials and Chemistry for providing the nanoparticles evaluated in this thesis, for inviting me to do experiments at SINTEF when necessary and for much needed suggestions and advice throughout this year. Yrr Mørch was my co-supervisor in the 5th year project thesis.

I would also like the thank Kristin Grenstad Sæterbø for introducing me to the cell laboratory, Astrid Bjørkøy for help figuring out the sometimes confusing peculiarities of the CLSM and Professor Emeritus Thor Bernt Melø for suggestions and advice in regards to the lifetime measurement.

Einar Sulheim
Trondheim June 2014

Abstract

The effect of cancer therapy could be greatly improved by encapsulating existing drugs into nanoparticles. Nanoparticles can facilitate delivery of hydrophobic drugs with poor solubility in water, and allow you to target cancer cells specifically either through passive targeting, active targeting or triggered drug delivery. This thesis explores the cellular uptake and intracellular degradation of a novel, multimodal polymeric nanoparticle developed at SINTEF Materials and Chemistry.

Two types of nanoparticles were evaluated for drug delivery purposes. Fluorescence lifetime imaging and analysis of emission spectra were used to assess the intracellular degradation, confocal laser scanning microscopy and flow cytometry were used to characterized the uptake. It was found that the poly(butyl cyanoacrylate) particle has degraded considerably after 24 hours intracellularly and is taken up through clathrin-mediated endocytosis. It was found that the cellular uptake was highly dependent on cell confluency and maturation. The poly (octyl cyanoacrylate) nanoparticle was not found to degrade readily within the first week of cell contact and is therefore less promising for drug delivery purposes. However, it was found that after 3 hours the particle had at least 3-fold higher uptake in prostate cancer cells than the poly(butyl cyanoacrylate) particle and that both clathrin- and caveolin-mediated uptake was important mechanisms in this uptake. This particle might be useful either for slow delivery or imaging. It was found indications that the nanoparticles escape the lysosomes and degrades in cytosol which is beneficial for drug delivery.

Sammendrag

Dagens kreftbehandling kan forbedres betydelig ved å bruke nanopartikler til å frakte kreftmedisinen gjennom kroppen og levere den i tumor. Nanopartikler gjør det mulig å utnytte cytotoksiske stoffer som normalt er for hydrofobe eller ustabile til å brukes i fri form. I tillegg kan nanopartikler gjøre det mulig å rette behandlingen mer spesifikt mot kreftceller ved passiv/aktiv målsøking, eller ved hjelp av ekstern stimuli som for eksempel ultralyd. Denne masteroppgaven beskriver cellulært opptak og intracellulær nedbrytning av en nye type multimodale polymernanopartikler utviklet ved SINTEF Materialer of Kjemi. Et nytt, svært hydrofobt fluoriserende fargestoff har blitt utviklet for å kunne merke partiklen utene at fargestoffet lekker ut. I denne oppgaven er det vist at dette fargestoffet også kan brukes til å måle nedbrytningen av partiklene ved å se på levetiden til den eksiterte tilstanden i fluoroforen.

To partikkeltyper har blitt vurdert for bruk til medisinlevering basert på nedbrytning. Det ble funnet at poly (butyl cyanoakrylat) partikkelen brytes ned i et tempo som er godt egnet for levering av kreftmedisin. Disse partiklene ble tatt opp av prostatakreftceller ved clathrinmediert endocytose. Opptaket var sterkt avhengi av celletetthet og modenhet, det vil si antall dager etter at cellene ble sådd ut. Partikler av poly (oktyl cyanoakrylat) ble ikke brutt ned i betydelig grad i løpet av den første uken i kontakt med celler. Dette er for tregt for medisinlevereng, men kan være ideelt for avbildingsapplikasjoner. Etter 3 timer var tre ganger mer av disse partiklene tatt opp enn av poly (butyl cyanoakrylat) partiklene, trolig fordi også caveolinmediert endocytose bidro til opptaket. Fluoresenslevetid og analyse av emisjonsspekter ble brukt for å kartlegge nedbrytningen av partiklene. Konfokalmikroskop og flow cytometer ble brukt for å kartlegge opptaket. Det ble vist at fluoresenslevetid med fargestoffet NR668 er en svært følsom metode for å måle intracellulær nedbrytning.

Contents

List of abbreviations

CLSM	Confocal laser scanning microscopy
DMEM	Dulbecco's modified eagles medium
ECM	Extra-cellular matrix
EPR	Enhanced permeability and retention
FCM	Flow cytometry
FD	Frequency domain
FLIM	Fluorescence lifetime imaging
FRET	Förster resonance energy transfer
IRF	Instrument response function
NP	Nanoparticle
PACA	Poly(alkyl cyanoacrylate)
PBCA	Poly(butyl cyanoacrylate)
PBS	Phosphate buffered saline
PEG	Poly(ethylene glycol)
POCA	Poly(oktyl cyanoacrylate)
RES	Reticuloendothelial system
ROI	Region of interest
TCSPC	Time-correlated single photon counting
TD	Time domain
TICT	Twisted intramolecular charge transfer

Chapter 1

Introduction

Treating cancer is one of the main challenges in modern healthcare, cancer being one of the most deadly diseases in the developed world. The disease arises from cells that through mutations acquire the ability to proliferate uncontrolled and avoid systematic and intracellular control systems. Existing therapy is often insufficient and suffers from adverse side effects.

Nanotechnology has been introduced as the toolbox necessary to create novel platforms both for drug delivery and for cancer diagnostics. A wide array of systems have been proposed, but few have made it through the trial stage. The concept suggested is often to bind or encapsulate an existing drug to a nano sized carrier that will selectively deliver the drug at the tumor site. This is an intriguing thought that has proven very challenging. These systems would in principle both increase the amount of drug delivered to the tumor and lower the dose released systemically. Nano sized particles are known to target solid tumors through the enhanced permeability and retention (EPR) effect[1][2]. Exploiting the EPR effect is known as passive targeting. Systems using active targeting (selectively binding surface molecules)[3] and triggered drug delivery[4] have also been proposed.

A novel drug delivery platform based on biodegradable polymeric nanoparticles (NPs) has been designed at SINTEF Materials and Chemistry (data not published). The NPs are made through polymerization of poly(alkyl cyanoacrylate)(PACA) in an one-step miniemulsion synthesis. The particles can be loaded with drugs and imaging agents, and the surface can be functionalized with targeting proteins and poly ethylene glycol (PEG). These NPs can also be used to stabilize microbubbles, this system has been demonstrated for triggered drug delivery and imaging using ultrasound [5]. Drug delivery based on PACA NPs is considered very promising due to the biocompatibility and tunable biodegrada-

tion of the material and several systems based on these particles are under clinical development for cancer treatment[6].

In order to further develop this platform, it is important to throughly understand how these particles interact with cells. This includes the rate and pathway of cellular uptake, and the intracellular fate of the NPs. To maximize the effect of the encapsulated drug, it should be delivered at its target by the NP, this is in most cases intracellularly. Characterizing that properties that dictate the uptake and if receptors are involved would help in further development of the NPs However, uptake through endocytosis often leads to lysosomal degradation and inactivation of the drug. The particles produced at SINTEF Materials and Chemistry has a tunable degradation depending on the choice of monomer. Detailed knowledge of the rate and location of the intracellular delivery of the drug is crucial in order to accurately characterize the drug delivery platform. In this study, two PACA NPs with different rate of degradation[7] was used. These particles are made from either poly(octyl cyanoacrylate) (POCA) or poly(butyl cyanoacrylate)(PBCA).

1.1 Project motivation

The purpose of this master thesis was to evaluate the uptake and intracellular fate of PACA NPs in human cancer cells in vitro. If the NPs were internalized by the cells, the intracellular degradation or clearance would be assessed. An important goal of this project was to establish a method for evaluating the intracellular degradation of the NPs and this was done using imaging techniques such as fluorescence lifetime imaging (FLIM) and spectral analysis. The overall goal was to evaluate the potential for degradation dependent drug delivery of the two different NPs.

Chapter 2

Theory

This thesis is a continuation of the 5th year project thesis written fall 2013 [8] and some of the theory, especially the section on the properties of the NPs (section 2.3) has been adapted from that thesis.

2.1 Cancer

Cancer is one of the main health problems in the world, according to the World Health Organization accounting for around 13% of deaths[9]. According to the Cancer registry of Norway, every third norwegian will be diagnosed with cancer before turning 75[10]. In 2011, we had 30000 new cases of cancer in Norway.

Cancer is a collection of diseases based on uncontrolled growth and lack of regulation of our own cells. The disease can be of different nature and can have multiple causes[11]. Cancer typically starts as a single cell malfunctioning due to mutations in its DNA. The change could either up regulate a cancer promoting gene (oncogene), or down regulate a tumor suppressing gene. Either way, the mutation leads to uncontrolled duplications of this cell. The evolution of the disease typically goes through invasion of surrounding tissue and metastasis to near and distant sites. These traits distinguish cancer from benign growths. There are many exceptions to these steps, exemplified by cancers circulating in the blood or in the lymphatic system such as leukemia and lymphoma. There is a wide array of genes that through mutations can promote cancer, cancer cells are therefore both very similar to our healthy cells yet extremely diverse making them hard both for the immune system to identify and to medicate without also causing extensive damage to the patient. There are intense research in the field and according to The Association of the Pharmaceutical Industry in Norway (LMI), the survival chances of cancer patients have doubled during the last 50 years.

Still, chemotherapy, radiotherapy and surgery which are the current treatment options all have drawbacks in terms of efficiency and side effects. New knowledge of genes promoting and suppressing cancer (oncogenes and tumor suppressor genes) has paved way for the development of better, more tailored chemotherapy. However, this method still suffers from systemic distribution after intravenous delivery which results in the necessity of high drug doses resulting in side effects. Increasing the specificity of chemotherapy has been a holy grail in cancer medicine for decades[12].

2.1.1 Cancer treatments

Many cancer types are greatly affected by lifestyle and environment. The most effective way to fight cancer is by prevention. All other treatments today have different severe side effects and often yield limited results. The classic methods of treatment can be divided into radiotherapy, chemotherapy and surgery, these are often used in combination. While surgery and radiotherapy are options for solid, non-metastasized tumors, chemotherapy is the most common option for developed, late stage cancer. Surgery is the best option for superficial cancers, while radiotherapy is often used if surgery is difficult for example in brain tumors[11]. Radiotherapy is based on radiating the tumor cells from many directions to create a high dose of exposure only at the tumor. The radiation will then create fractures in the DNA strands of these cells, inducing chromosomal aberration and mitotic death[13]. Radiation is carcinogenic and reoccurring cancers are common, making it a non-ideal therapy[11][14].

Chemotherapy is the use of cytotoxic or cytostatic drugs that kill malignant cells or stop them from proliferating. They often target steps in the cell cycle making them effective towards all proliferating cells. In addition to malignant cells, this involves cells in the immune system or blood cells and stem cells producing hair in the hair follicles. Also, targeting dividing cells makes chemotherapy work poorly on tumor stem cells or quiescent G0 cells[15]. While traditional chemotherapy generally targets all dividing cells, intense work is directed towards more intelligent chemotherapy targeting the signaling pathway being up or down regulated in the specific case of cancer[16].

2.1.2 The biology of a tumor and therapeutic barriers

One main attribute of a tumor is the fact that the cells are proliferating. This process has a high demand for oxygen and nutrients. Up to a size of $2mm^3$, the tumor is being fed by passive diffusion[17]. Larger tumors will suffer hypoxia unless blood vessels are formed, and at this point, successful tumors start angiogenesis, or blood vessel formation[18]. Typical for angiogenesis in tumors is that is occurs rapidly and unorganized. This creates areas of poor vascularization resulting in

local necrosis, and areas of dense vascularization[17]. Another effect of this rapid angiogenesis is that created vessels typically are branched, short-circuited and of uneven diameter, with poorly constructed leaky walls. The size of the gaps between the endothelial cells are reported to be from 200nm to 1.2μm depending on tumor type[19]. However, it is documented that the vascularization and leakiness of the vessel is very heterogeneous within a tumor[20][21]. The gap between endothelial cells in healthy vessels is approximately $5 - 10$nm. Leaky vesicles in tumors are a possibility for passive targeting by exploiting the EPR-effect (enhanced permeability and retention)[22]. The leaky vesicles lead to the enhanced permeability, the retention effect is caused by a poorly developed or non-existing lymphatic system in the tumor. While the lymphatic system normally would remove NPs from the extracellular compartment, NPs can often remain in the tumor[23]. While the leakiness of the new vesicles around the tumor can be used to target tumors, it can also present a challenge. A natural effect of an immature vesicle system is low blood flow making it hard to get a sufficient concentration of drugs and NPs. It is seen that areas of low blood flow are hard to treat and often survive therapies[24].

One significant effect of the late and poor vascularization is that tumors evolve under a lack of oxygen and nutrients. This forces the tumor cells to perform anaerobe metabolism. It is unclear what mechanisms lead tumors into performing glycolysis, but it is well documented that most tumors use glycolysis also when oxygen is sufficiently provided (normoxia)[18]. Glycolysis is ineffective and produces only two ATP while complete oxidation results in 32 ATP produced[25]. Therefore, tumors normally have a very high consumption of nutrients, which can be exploited both for imaging and targeted therapy. Glycolysis results in the production of lactic acid which gives lower pH in tumors compared to healthy tissue. While the pH of blood is held around 7.4, tumors have been reported to have pH values down to 5.6[26].

While angiogenesis, leaky vesicles and acidic environments are properties that can be exploited for targeted delivery, there are also properties of tumors that make drug delivery challenging. Due to the poor vascularization, there will be tumor cells surviving on marginal conditions, far from any blood vessels. These cells are hard to reach with classical drug delivery and require new methods. Tumors also typically have a higher interstitial pressure than the surrounding tissue[27]. The interstitial pressure in a tumor is highest at its center, and decreases towards the periphery[28]. This high pressure is a result of the retention caused by the lack of a lymphatic system in the tumor. This phenomenon reduces the convection of molecules towards the center of the tumor because of the counter acting convection created by the interstitial pressure and makes it difficult to deliver drugs to this central area.

Non-tumor related obstacles

Getting a drug to the tumor intact, functioning and at a sufficient concentration is very challenging. Therapeutic agents are typically given intravenously, and once in the blood many processes and a series of obstacles will be presented to make sure the drug/NP is removed from the circulatory system[11]. The innate immune system consists amongst others of complement protein that will bind anything foreign and of a notable size. Protein coverage called opsonization leads to phagocytosis by monocytes and macrophages. This is called the reticuloendothelial system (RES)[29].

The extra cellular matrix (ECM) also presents a challenge for drug transport. ECM is a combination of networks of fibrous proteins such as collagen and elastin and highly viscous fluids. Although ECM is often degraded in a tumor, ECM reduces the flow of drugs once the drug has left the circulatory system. Another limiting obstacle is cell internalization. Most drugs must be delivered inside the cell in order to function. This often means going through endocytosis (cell-eating), where the drug is encapsulated in early endosome, late endosome and finally lysosome. In this process, the drug faces pH ranging from 7.4 and down to 5[25][29].

2.1.3 Cancer targeting and nanoparticles

The drugs being used in chemotherapy are toxic to many healthy cells. By finding better ways of targeting the tumor cells one could limit the adverse effects by both interacting less with healthy cells and lowering the dose due to increased concentration around the tumor[30]. In order to find ways to target these cells, detailed knowledge about the environment in and around a tumor is a prerequisite.

Nanotechnology could be the toolbox necessary to overcome limitations of current chemotherapy. While chemotherapeutic agents can not be altered without also changing the cytotoxic function of the molecule, NPs are promising platforms for delivering these toxic agents to the cells in the tumor[31]. NPs can be loaded with conventional chemotheraputics and increase the load delivered at the wanted location. Besides targeting, nanocarriers are also a way of delivering drugs that have properties that have made them unsuitable so far, such as adverse side effects and poor solvability in water/hydrophobicity. Targeting of cancer cells is a huge field of research, and multiple strategies and platforms are being developed. The strategies can be divided into three categories; passive targeting, active targeting and triggered drug delivery. These three options will be discussed in the following section.

Passive targeting

Passive targeting of NPs to cancer tissue relies on the EPR effect[32]. NPs that circulate in the vasculature will not be able to penetrate through the endothelial layer of healthy tissue and will therefore remain in circulation until removed by the RES-system. The enhanced permeability often present in cancers will allow the NPs to leave the bloodstream and the lack of functional lymphatic system will allow the particles to accumulate in the tissue[23]. The potential of passive targeting depends on the vascularity and leakiness of the veins in the tumor, but the process has low efficiency, and long-circulating NPs are necessary[33]. Drug delivery is also normally limited by very slow diffusion, especially of bigger NPs (>100nm), in the tumor tissue, but is has recently been shown that by increasing the amount of poly ethylene glycol (PEG), particles above 100nm can diffuse effectively through brain tissue and this result is likely valid for other tissues as well[34]. Covering a surface with PEG (pegylation) is a method to decrease the hydrophobicity and increase the biocompatibility of the particle that is further described in section 2.3.2.

Active targeting

In active targeting, the particles are surface functionalized with molecules selectively targeting receptors on the target cells and tissue. Targeting nanocarriers that are approved or in phase one trials have typically utilized antibodies, transferrin or interleukin 2 (Il-2) for targeting[35]. Transferrin receptors are expressed by many cancer types while Il-2 receptors are highly expressed on malignant T-cells (T-cell leukemia)[36]. Particles have also been targeted to avoid the P-glycoprotein (P-gp) efflux pump upregulated in many cancers and often responsible for multidrug resistance[37].

Triggered drug delivery

Triggered drug delivery is a targeting tactic where external stimuli is used to direct the NP or to release the drug. This can be changes in local environment such as temperature, pH or salt concentration[38][4], or external sources such as light, heating and ultrasound[39][40]. Ultrasound is also being developed for drug delivery in combination with microbubbles[41].

2.2 Nanoparticles and medicine

Intense research is currently being aimed at creating NPs for biomedical applications such as drug delivery, biosensing and as contrast agents for imaging[42]. The concept is to create a particle that can be functionalized to target specific cells or

organs. The drug or contrast agent can either be attached to the surface of the particle, encapsulated by a shell or mixed into the particle material. Common to all potential systems are some necessary features. The particle must be biocompatible. This means that it should not be toxic nor should it be taken up by phagocytes in the immune system. Biocompatible also means that the particle is either degraded in the body or removed by the kidneys to avoid accumulation[43].

Nanosized objects have some intrinsic characteristics for biomedical applications. NPs have a high surface to volume ratio making their properties highly dependent on their surface. The properties of a NP can be changed significantly based only on the surface chemistry. There is a wide range of developed particles, in terms of material, size and shape, where many have all ready been approved either for phase one trials or for clinical use[44]. NPs are also able to carry drugs. Drugs are small molecules that are distributed in the blood and are typically taken up non-specifically by cells or simply diffuse through cell membranes. This makes it impossible to target cells or organs. NPs on the other hand are small enough to flow through small capillaries and leak through the capillary walls in tumors, but are too large to escape healthy blood vessels or diffuse through cell layers. Diffusion through cell ECM is limited and highly dependent on properties such as charge and pegylation[34]. Also, they require active transport to be taken up by cells[45][46]. At least in theory, this makes it possible to design the particle to interact only with specific cells. Practically, this is still difficult but is being studied intensively.

NPs generally have properties controlled by their size and shape, biological properties are also highly dependent on surface chemistry and targeting groups[47]. Most proposed and developed NPs, shape and structural options and some examples of possible surface chemistries and targeting groups are summarized in figure 2.1. The particles used in this study falls under the category polymeric NPs and will be described in detail in the next section.

2.3 Poly (alkyl cyanoacrylate) nanoparticles

The particles used in this project are polymer NPs made from polymerization of alkyl cyanoacrylate giving poly(alkyl cyanoacrylate)(PACA). PACA was initially developed for use as a surgical glue due to its biocompatibility and quick polymerization[6]. The material is now intensively studied and developed to be used for therapy and diagnostics as a nanocarrier of drugs or contrast agents for imaging. Two different subgroups have been studied, poly (butyl cyanoacrylate)(PBCA) and poly(octyl cyanoacrylate) (POCA). The most widely used material is PBCA, but also POCA is being studied and has the advantage of slower degradation and lower toxicity[48]. PACA NPs are typically produced through a miniemulsion process giving a tunable size often in the 100-300nm region[49][50].

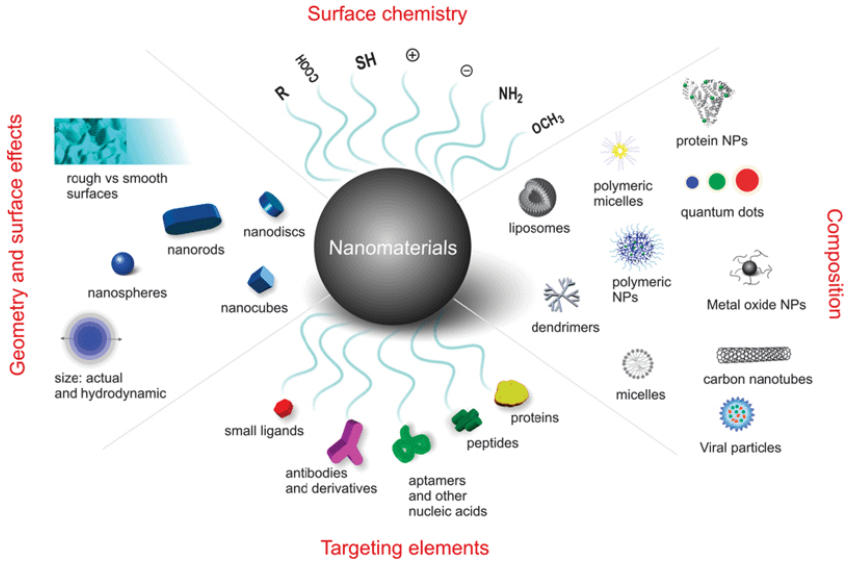

Figure 2.1: Illustration summarizing different NPs and characteristics important for their properties. Adapted from [47].

The miniemulsion process also makes it possible to mix in other hydrophobic molecules and is normally stabilized by a surfactant that organizes at the particle surface. Through choosing surface molecules and load, PACA NPs can be produced with different properties dependent on the application. Often though, the surface is covered by PEG (poly ethylenglycol) to sterically stabilize the particle and improve the biocompatibility[51]. Figure 2.2 is an illustration of the PACA NPs made at SINTEF with its potential loads and surface.

2.3.1 Emulsions and nanoemulsions

The NPs are produced through an emulsion and nanoemulsion process. Although an emulsion can be produced from almost any two immiscible liquids, the two liquids are most often oil and water. A pure mixture of oil and water will separate into two distinct phases that can easily be separated. An emulsion is produced by adding an emulsifying agent, also known as a surfactant. A surfactant is a molecule that spontaneously arranges itself at the oil-water interphase. This happens because the surfactant has two distinct regions; a polar part that is soluble in water, and a non-polar part that is soluble in oil. The surfactants used on the particles are described in section 2.3.2.

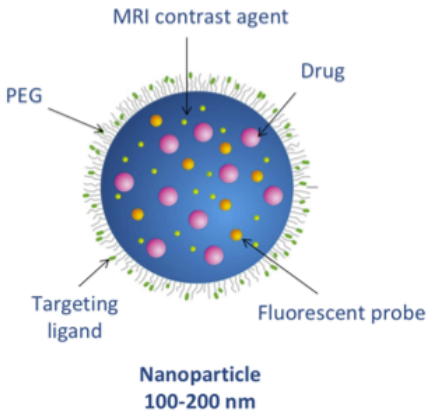

Figure 2.2: Illustration of the PACA NPs used in this project. Illustration adapted from a presentation by Yrr Mørch.

With the surfactant in place, the oil-water system may be mixed into an emulsion where one medium is dispersed (the inner phase) in the other (the continuous phase), with the surfactant at the interface. This system is only kinetically stable, this means that with enough time the system will separate back into two distinct phases. BCA and OCA, the monomers used in the NPs are hydrophobic, and are mixed in a neutral oil, water and a surfactant to create an oil in water emulsion. The hydrophobic oil is used as a co-stabilizer to avoid Oswald ripening, a destabilizing mechanism where large particles grow on expense of smaller ones[52]. Other molecules to be included in the NP must be mixed into the oil phase at this step. By radiating the solution with high power ultrasound, the droplet size can be reduce from micrometer to the nanometer regime and become a nanoemulsion. The nanoemulsion shares most of its properties with the standard emulsion, but while the emulsion contains polydisperse droplets and appear cloudy, the nanoemulsion contains droplets in the nanometer range and often appears translucent[53].

2.3.2 Polymerization and pegylation

While the motivations and effects of adding PEG to a particle surface are explored in section 2.3.3, the method for binding PEG to the surface is included here because it is a part of the polymerization step.

BCA (figure 2.3) and OCA (figure 2.4) are highly reactive and will generally polymerize easily. The polymerization happens through anionic polymerization. Anionic polymerization starts when a nucleophile (such as an amine or a hydroxide ion) carrying a free electron pair reacts with the BCA or OCA monomer. To avoid premature polymerization, the emulsion is prepared under acidic conditions. The excess of hydrogen ions in acidic solutions prevents formation of negative ions. The polymerization reaction of PBCA is illustrated and briefly explained in figure 2.5.

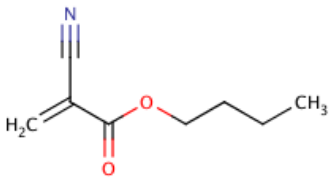

Figure 2.3: The chemical structure of butylcyanoacrylat, the monomer in PBCA.

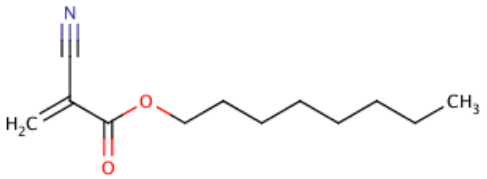

Figure 2.4: The chemical structure of octylcyanoacrylat, the monomer in POCA.

Pegylation means to cover the surface with polyethylene glycol(PEG) (figure 2.6). This is done to create an hydrophilic surface to an otherwise hydrophobic particle and will make the particle more biocompatible and lessen the chance of provoking an immune response[54]. Naked NPs are of little use in biological systems because they will rapidly bind proteins, both non-specifically and as a part of opsonization and removal by the RES system[55]. Most often, the PEG chain is part of a molecule that also has a non-polar part to make the molecule organize in the oil-water interphase and act as a surfactant. In this project, both covalently linked PEG and PEG held in place by hydrophobic interaction have been used. Because BCA polymerizes easily, surfactants with reactive groups can easily initiate polymerization. Described in the following paragraph are the surfactants and initiators used for the PBCA NPs in this project.

BRIJ 35 (figure 2.7) is a simple, non-reactive surfactant that will be attached to the oil water interphase by hydrophobic interaction. Compared to other sur-

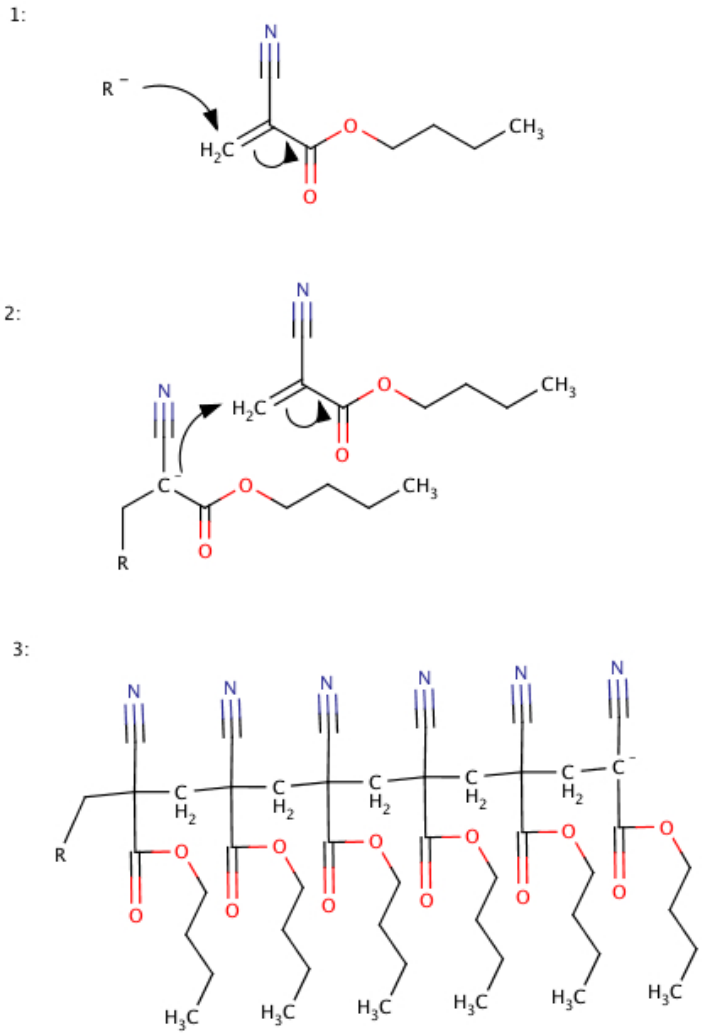

Figure 2.5: Anionic polymerization of butyl cyanoacrylat.
1. A group containing a free electron bind the CH_2 group, and the free electron is moved to the central C atom.
2.This C atom now has a free electron (negative charge) and can act on a neighbor BCA molecule.
3.The R group started a chain reaction leading to polymerization of the BCA molecules.

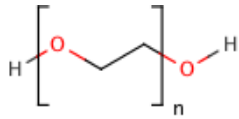

Figure 2.6: The chemical structure of polyethylene glycol (PEG).

factants, BRIJ 35 is easy to handle and is added to the particle because it simply organizes at the interphase without initiating polymerization. BRIJ 35 is attached to the surface of the NP because of the long alkyl chain that will be entangled into the polymer upon polymerization. The PEG chain in BRIJ is 23 units long (molecular weight$= 23 * 44g/mol = 1012g/mol$).

Jeffamin M2070 (figure 2.7) is an initiator containing PEG that has been attached to particles. Jeffamin has an amin group (NH_3) on the hydrophobic part of the molecule. This group is highly reactive and will initiate polymerization and be covalently linked to the NP. The PEG chain in Jeffamin is 19 units long (836 g/mol). Jeffamin is too reactive to use as a surfactant and is therefore added to the solution after the nanoemulsion has been made.

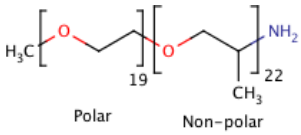

Jeffamin

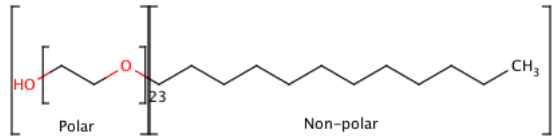

BRIJ 35

Figure 2.7: The chemical structure of Jeffamin and BRIJ 35, the two surfactants covering the PACA NP.

2.3.3 Particle stability and poly ethylene glycol (PEG)

Controlling the stability and surface properties of NPs is vital. The particles must have a sufficient shelf life in solution as well as controllable properties in biological environments. The life of a NP consists of multiple destabilizing mechanisms and forces. Both avoiding aggregation and premature degradation are important in order to maintain function and safety of the product. Injecting particles above $5\mu m$ into the vascular system will lead to blocked capillaries and embolism, while particle degradation may lead to drugs being leaked to the surrounding tissue or solution[56].

There are destabilizing mechanisms present in both solution and in biological environments. In solution, charged particles are generally effected primarily by two opposing forces; electrostatic repulsion and Van der Waals attractive forces[52]. Particles of similar charge will repel each other, but this surface charge is in solution screened by the electric double layer (EDL) of counter ions that build up on the particle surface. This phenomenon is described by the Gouy-Chapman model[52], where counter ions are divided into two layers. The inner layer is called the Stern layer, and is immobilized on the particle surface. The surface of the outer layer is called the slipping plane, here the ions move around, but are by electrostatic attraction bound to the proximity of the particle surface. This model is presented in figure 2.8. The effective surface potential is measured at the slipping plane and is called the zeta potential. A higher zeta potential will give more stable particles, and a value of $|\zeta| > 30mV$ is generally considered to give stable particles[52].

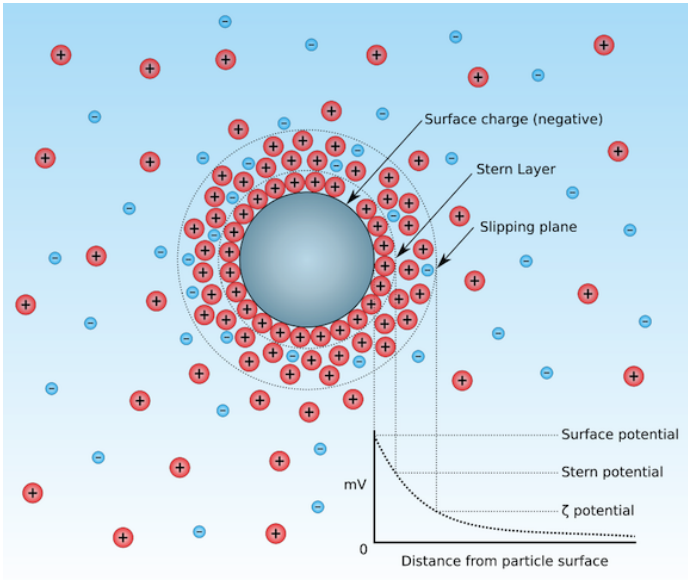

Figure 2.8: Illustration of the electric double layer. Adapted from [57].

In biological fluids, the particles will meet a high concentration of electrolytes as well as a variety of proteins. While a high electrolyte concentration will decrease the Stern layer and hence let other particles and proteins closer to the particle surface, proteins in for example blood serum will adsorb to anything unfamiliar[29]. The proteins on the particle surface will define the biological identity of the particle which is different to the synthetic identity. A NP might

change and become very different in terms of size, shape and surface properties once presented to biological environments[55]. Some proteins in blood are part of the innate immune system and are specifically designed to bind to foreign particles to help monocytes and macrophages performing phagocytosis[29].

Pegylation is a common strategy to avoid adsorption of proteins on the particle surface. In solution, this will also increase the stability by creating a steric repulsion but decrease the zetapotential. Decreasing the zetapotential is beneficial to avoid protein attaching to the NP[58]. A relatively recent study has shown that the rate of particle uptake by macrophages are indeed increased if the particles have adsorbed proteins to their surface, and also show that this effect can be limited by PEG (figure 2.9)[59]. The figure illustrates how the increasing density of PEG on the particle surface will limit the amount of proteins adsorbed. This will make the uptake in macrophages more dependent on serum-independent phagocytosis which is less effective than serum-dependent uptake. From the figure one can also see how the conformation of PEG changes with increasing concentration.

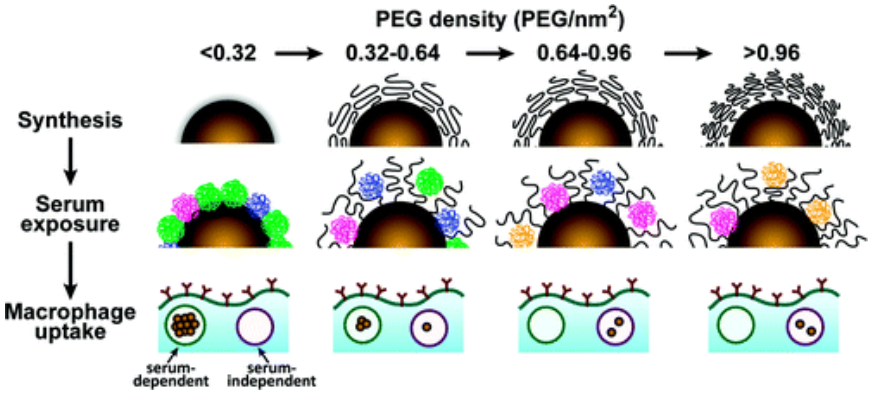

Figure 2.9: Illustration of protein adsorption and macrophage uptake dependent on PEG density. With high PEG density, the macrophage uptake is more driven by the less effective serum independent process, and the total particle uptake is reduced. Adapted from [59]

2.4 Cellular uptake of nanoparticles

2.4.1 Uptake mechanisms

Most cancer drugs works intracellularly, this means that the drug must be taken up by the cell to cause the desired effect[60]. To engineer the NP it is important to have detailed knowledge of the internalization mechanisms and the intracellular routing of the drug and NP. While ions, some small proteins and molecules such as glucose and amino acids are transported through the membrane by specialized transporter proteins[25], larger substances such as NPs are too big for the specialized transporter proteins, and are internalized through endocytosis[61][62][63]. Endocytosis is a number of mechanisms that involves folding the plasma membrane into vesicles that are released from the membrane, and transports it contents into the cell[25]. The opposite, where intracellular vesicles are fused with the cell membrane to release the contents extracellularly is termed exocytosis. Endo- and exocytosis are important for many of the cells vital processes such as uptake of nutrients, transcellular transport, signal transduction and phagocytosis. Also, this process is important for transporting membrane bound proteins such as receptors, transporter proteins and signaling molecules[64].

Endocytosis is divided into two subgroups, phagocytosis and pinocytosis. Phagocytosis is mainly performed by professional phagocytes; macrophages, monocytes neutrophils and dendritic cells. These are all part of the innate immune system where phagocytes can internalize whole bacteria and cells with a size up to tens of micrometers[62]. Phagocytosis occurs only after the object has been opsonized, that is the cell/bacteria/particle has been covered by proteins such has immunoglobulins and complement components. These proteins are recognized by the phagocytes prior to phagocytosis[65].

Cancer cells would internalize nanoparticles through pinocytosis. Pinocytosis can further be dived into subgroups, macropinocytosis, clathrin-mediated endocytosis (CME), caveolin-mediated endocytosis, and clathrin- and caveolin-independent endocytosis. The five different endocytotic pathways, phagocytosis included, are illustrated in figure 2.10.

Clathrin-mediated endocytosis

The best understood endocytosis mechanism is CME. This is also believed to be the most important mechanism for internalization of nutrients and macromolecules[25], and many of the principles involved in CME also apply to the other pinocytotic pathways[66]. CME is receptor mediated, meaning that the substrate to be internalized must bind to a surface receptor. Multiple receptors will bind to bigger objects and create an area concentrated with receptors. These areas will be covered by an adaptor complex AP2 and clathrin, a triskelia-shaped macromolecule,

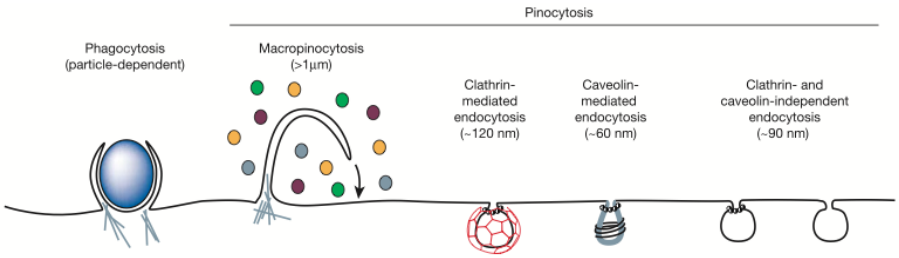

Figure 2.10: The different endocytotic pathways in a mammal cell. The pathways differ in size and mechanism of vesicle formation. Adapted from [66].

on the cytosolic side[67]. CME is illustrated in figure 2.11. Clathrin and AP2 will create curvature in the membrane, which continues as further clathrin and AP2 are connected. Eventually, a vesicle will be formed which is cut of from the membrane by a complex of dynamin proteins.

Caveolin mediated endocytosis

Caveolin mediated endocytosis is the main mechanisms of endocytosis after CME. Vesicles are formed by caveolin-oligomerization in the plasma membrane which creates an invagination and eventially, a flask-shaped vesicle. The vesicle is cut of from the membrane by dynamin 2. Caveosomes are vesicles with a neutral pH that can fuse with early endosomes or fuse directly with lysosomes[68].

This endocytosis mechanism is generally thought to capture smaller volumes and particles with a diameter around 60nm[66], and mainly work to internalize lipid rafts of cholesterol or sphingolipids, the actual endocytic capability is disputed[69]. However, it has been reported that for beeds above 200nm, caveolin is involved in a uptake superior to CME and also some pathogens enter cells through this mechanism[63]. Larger objects internalized through caveolin mediated endocytosis have been shown to have no colocalization with lysosomes, indicating that material taken up through this pathway escapes lysosomal degradation.

Clathrin- and caveolin independent endocytosis

Cellular uptake can also occur through macropinocytosis, which is large ruffles in the cell membrane folding over to create a vesicle. This mechanism is not selective, meaning that it does not depend on receptors or stimuli from the internalized material. Macropinocytosis also occurs at a relatively constant rate in most cells and serves as a method for sampling the environment[70].

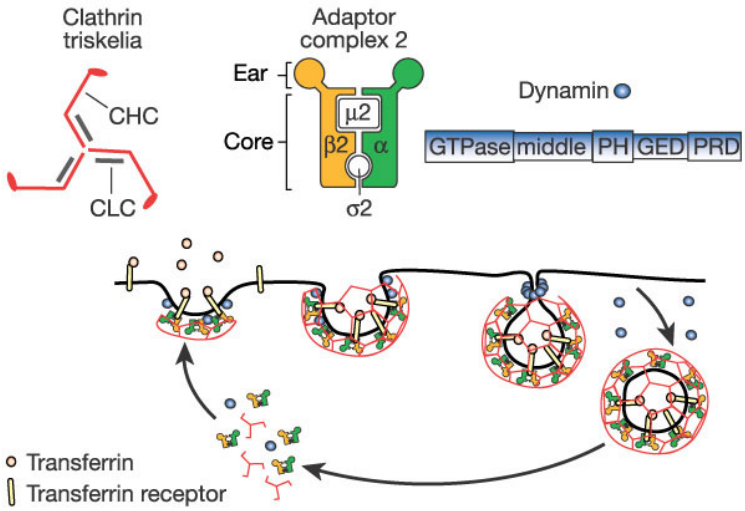

Figure 2.11: Illustration of CME. The internalization of receptor-bound molecules is exemplified by transferrin and the transferring receptor. AP2 and clathrin cover the cytosolic side of the cell membrane, and creates the invagination. A dynamin complex then assembles at the neck of the forming vesicle and cuts it of from the plasma membrane. Illustration adapted from[66].

Other endocytosis mechanism independent of both clathrin and caveolin have been discovered. Both dynamin- dependent and independent processes have been found, but they have in common a relatively limited size and often require the assembly of lipid rafts in the membrane[25].

Inhibitors of endocytosis

In order to study mechanisms of endocytosis, the different pathways can be selectively inhibited. This is achieved biologically by blocking one of the critical steps in vesicle formation. Chlorpromazine is such a pharmaceutical that selectively inhibits CME by blocking the recruitment of clathrin the plasma membrane hence limiting the formation of clathrin coated vesicles[71]. Genistein inhibits caveolin mediated endocytosis by disrupting the local actin network and limiting the recruitment of dynamin[72]. All forms of endocytosis can be inhibited by cultivating at 4°C[73].

Endocytosis inhibitors are effective tools for studying uptake mechanisms, but it is important to be aware of some limitations of the technique. The effect and also cytotoxicity of various inhibitors is cell line dependent, and many inhibitors

have selectivity issues[74][61].

2.4.2 Intracellular route

After internalization, the newly formed vesicle will fuse with hydrolase containing vesicles from the Golgi complex to create early endosomes[25]. This process is rapid, the vesicle is typically formed within 2 minutes and fusing with vesicles from Golgi will occur for approximately 10 minutes[75][64]. The early endosomes become late endosomes when the pH is dropped towards 5 and they loose the ability to fuse with endocytic vesicles. After 10-40 minutes, the late endosomes fuse with lysosomes[76]. After being degraded in the lysosomes, the material can either be removed from the cell by exocytosis, delivered to specific organelles or be released in cytosol. Possible routes for endocytosed NPs are illustrated in figure 2.12. Evaluating the possible lysosomal escape and drug delivery to cytosol using NPs is highlighted as a main challenge in a recent review article in ACS Nano[77]. A group studying delivery of siRNA using lipid NPs found that only 1-2% of the siRNA was able to escape endosomal vesicles[78].

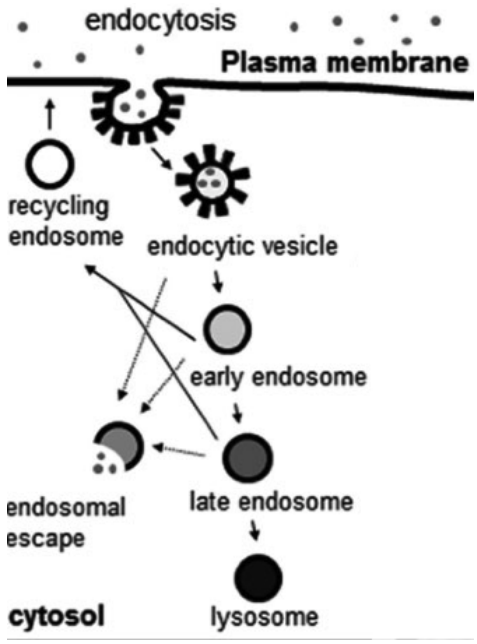

Figure 2.12: The uptake and possible intracellular routes of NPs, illustration adapted from [79].

2.4.3 Cellular uptake of nanoparticles

Characterizing the uptake of NPs is important in order to understand how NPs can help deliver drugs inside the cell. Due to the huge range of NPs with regards to size, material, shape, electric charge and surface modifications, this is a vast field of research, mainly the uptake of polymeric NPs will be described in this section. The study of uptake kinetics of polymeric particles is challenging due to the degradability of the particles. In a master thesis from spring 2013, Sofie Snipstad studied the same particles that are being studied in this master thesis, and found that the uptake was very high after only a few minutes. However, the thesis concluded that this was due to contact mediated uptake of the fluorescent dye that leaked from the NP[80]. In most polymeric particles, the fluorescent dye is spread in the polymer and can therefore either leak from the particle, or be gradually released as the particle is degraded. It is therefore important to separate uptake of free dye to the uptake of actual particles[81].

PBCA particles with sizes from below 60nm and up to 250nm were studied by Weiss et al.[82]. They found that particles around 60nm was taken up at a higher rate than those bigger, but also the largest particles (250nm) had a significant uptake after less than 10 minutes in both Jurkat and HeLa cells. The paper conclude that the two cell lines react differently to changing particle size and surface modifications. However, images presented in this paper suggest that also free dye is taken up by the cells. The dependency of surface molecules on uptake are also seen in other papers[83][84] where the surfactants polysorbate-80 and poloxamer 188 are seen to increase the uptake of polymeric NPs.

2.5 Experimental techniques

2.5.1 Fluorescence and fluorescent probes

Modern analysis methods such as flow cytometry (FCM) and fluorescence microscopy depends heavily on labeling structures with fluorescent molecules. This can assure selectivity to FCM measurements and specificity and high resolution in imaging. A fluorescent molecule will emit light at a longer wavelength than the wavelength used to excite the molecule. An exception is multi-photon excitation where multiple photons combine their energy to create an excited state with typically 2 or 3 times the energy of a single excitation photon[85]. The excitation and emission process is often illustrated with a Jablonski diagram as seen in figure 2.13. Within an energy band, the electron will rapidly decay to the lowest vibrational state within that band. The energy of the emitted photon will therefore be lower than the energy of the excitation photon. From the excited state there are multiple decay mechanisms back to the ground state, both radia-

tive (Γ) and non-radiative(κ) where only the radiative decay results in detectable photons emitted by the fluorophore [86]. The amount of light emitted from a fluorophore depends on the fraction of radiative decay termed the quantum yield Q defined in equation 2.1.

$$Q = \frac{\Gamma}{\Gamma + \kappa} \tag{2.1}$$

Fluophores with high quantum yield is desirable as the same signal intensity can be obtained at a lower laser intensity.

The wavelength λ of the photons are given from the photon energy through equation 2.2 where ν is the frequency, h is the Planck constant, and c is the speed of light.

$$E = h\nu = \frac{hc}{\lambda} \tag{2.2}$$

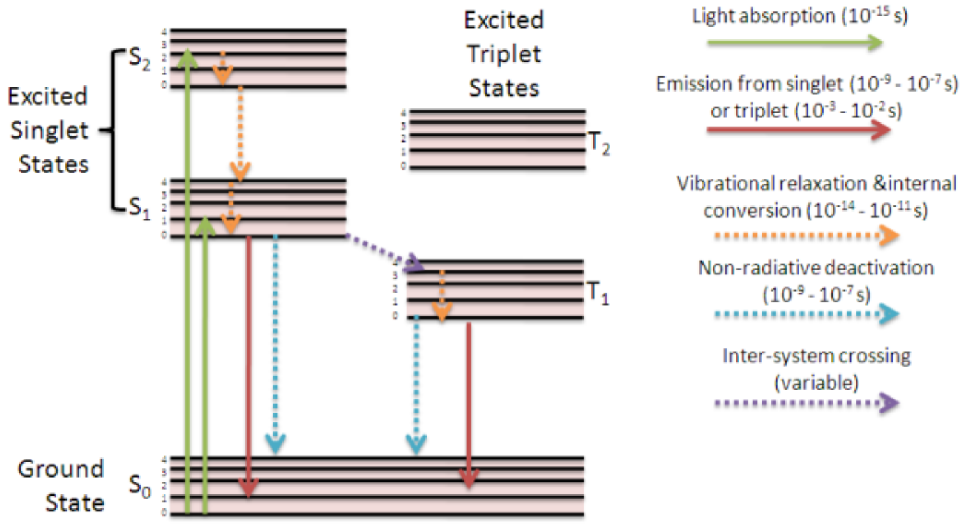

Figure 2.13: A Jablonski diagram describing the excitation from the S_0 state and possible relaxation mechanisms from the exited states. The horizontal lines within the states illustrate vibrational states. The lifetimes of the various relaxation mechanisms are indicated. Adapted from [87].

Another important property of the exited state that is used specifically for fluorescence lifetime imaging (FLIM) is the lifetime τ. Through the different decay mechanisms, the population of electrons in the exited state $N(t)$ will decay and in the simplest case follow an exponential decay from equation 2.3

$$N(t) = N_0 e^{-\frac{t}{\tau}} \tag{2.3}$$

where N_0 is the initial number of fluorophores in the exited state, t is time and τ is the fluorescent lifetime given by equation 2.4.

$$\tau = \frac{1}{\Gamma + \kappa} \tag{2.4}$$

Some fluorophores, including NR668 used in this thesis have a two-exponential decay where the fluorescent signal is given by equation 2.5[88][89].

$$F(t) = A_1 e^{-\frac{t}{\tau_1}} + A_2 e^{-\frac{t}{\tau_2}} \tag{2.5}$$

Here, A_1 and A_2 is the amplitude of the components, and τ_1 and τ_2 is the lifetimes of the corresponding excited states.

NR668-modified nile red

The fluorescent dye used in this thesis to detect the NPs is a novel form of nile red termed NR668[90]. Nile red is an old fluorescent dye, first developed by Greenspan et al to stain intracellular lipid droplets[91][92]. The chemical structure of conventional nile red and NR668 is seen in figure 2.14, where the modifications of NR668 from conventional nile red are the alkane chains making it more hydrophobic. Conventional nile red is hydrophobic, but it has been seen that it will leak from the particles[93][80].

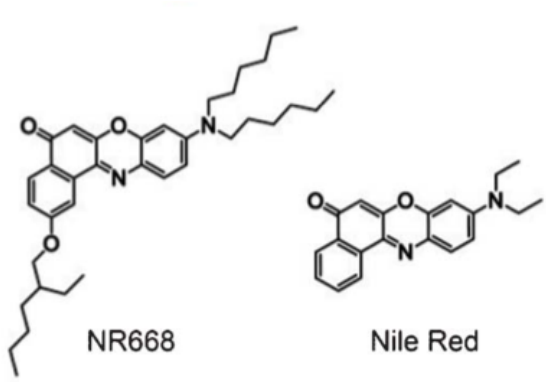

Figure 2.14: The chemical structure of nile red and NR668. Adapted from [90].

In FLIM, NR668 exhibits a double-exponential decay. The related physics is not fully understood, but it has been proposed that these double exponential

decays can occur due to the formation of either a twisted intramolecular charge transfer (TICT) state[94] or a solvent relaxed state[95]. The double exponential decay for conventional nile red is well documented [95][89], and due to the structural similarity, the explanation is most likely valid also for NR668. The TICT state is formed by conformational changes at a point where the fluorescent molecule has rotational freedom. NR668 has rotational freedom at the $-N(Hex)_2$ bond. It has been found that the fluorescence lifetime of conventional nile red encapsulated in various polymers depends on the elastic modulus of the polymer, but that two lifetimes are seen, a short lifetime varying from 0.55 ns to 1.4 ns and a long lifetime varying from 1.2 ns to 4 ns[89]. The short lifetime is from the initially excited state while the long lifetime results from either a TICT state or a solvent relaxed state[95].

2.5.2 Confocal laser scanning microscopy

Confocal laser scanning microscopy (CLSM) is the most popular technique for imaging of biological samples due to its high resolution both axially and radially and the limited invasion of the sample. The method is an evolution of wide field fluorescence microscopy where the resolution has been significantly improved by placing a pin hole at the conjugate plane in front of the detector and scanning the sample[96]. The pinhole removes signal from out of focus regions which is a limiting factor in wide field fluorescence microscopy where fluorescence occurs throughout the excited volume. CLSM uses lasers to selectively excite either endogenous fluorescence molecules in the sample, or fluorescent probes added[97].

A schematic illustration of the optical path in a CLSM is seen in figure 2.15. A modern CLSM is normally an integrated system offering multiple detectors, objective lenses and lasers. The sample is scanned by the scan head and a software is used to create and analyze the image. The general concept is that the laser beam is focused onto the sample by the objective lens. Light emitted by the sample then travels back trough the objective lens, is separated from the optical path of the excitation laser by a dichroic mirror, focused through either a square or a circular confocal pinhole, and often amplified by the detector, for example a photomultiplier tube[98]. In the illustration (figure 2.15) it is seen how signal from outside the focal plane is rejected by the pinhole.

The maximum resolution achievable, which will depend on the focal volume will depend on multiple parameters such as laser wavelength, scan speed, objective characteristics and eventually the sample[99]. The focal volume typically ranges from 0.25 to 0.8 μm laterally and 0.5 to 1.5 μm axially. The theoretical limit of resolution is set by the diffraction limit, which describes the smallest spot you can focus a laser. This is described by formula 2.6 where λ_{ex} is the wavelength of the excitation laser, NA is the numerical aperture and FWHM is the

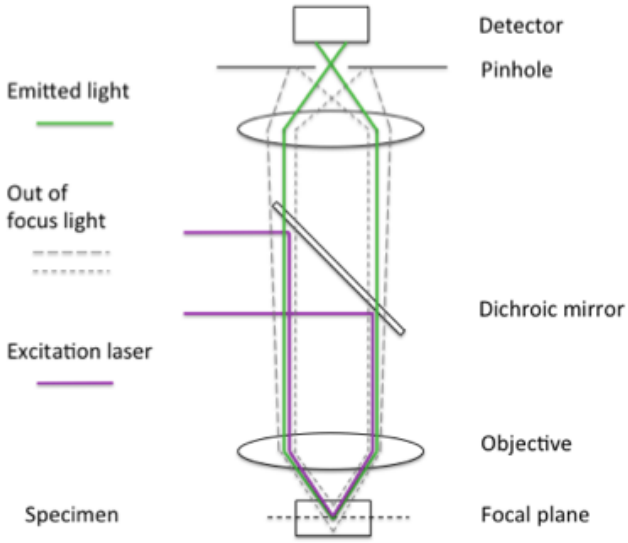

Figure 2.15: Illustration of the optical path in a CLSM. Adapted from [80].

width of the spot where the intensity is above half of maximum[100]. The NA is typically around 1.2 giving a maximum resolution of 212 nm. This is valid if the pinhole is equal to or bigger than one airy unit(AU), with a smaller pinhole, slightly better resolution is possible. With a pinhole smaller than 0.25 AU, the factor is 0.37 rather than 0.51

$$FWHM = \frac{0.51\lambda_{ex}}{NA} \tag{2.6}$$

With extra equipment connected to the CLSM, other imaging options are available. Non-linear imaging is possible, and describes a system where the fluorophore is excited by multiple photons where each have a lower energy than the emitted photon. For example two-photon excitation where a high intensity laser of $\lambda \approx 800nm$ can excite fluorophores with excitation peak around 400nm. Other analysis possible with CLSM is spectral analysis and fluorescence lifetime imaging (FLIM). Spectral analysis can include both varying the excitation wavelength, and measuring the fluorescence signal at different emitting wavelength. This can give valuable information if the specter from the emitter depends on the local environment. FLIM uses a separate set of detectors and software and is described in more detail in the following section.

2.5.3 Fluorescence lifetime imaging

Fluorescence lifetime imaging (FLIM) is based on an external system coupled to CLSM. The idea is to measure the lifetime of the excited state of the fluorophore. This can give valuable information because the lifetime will often depend on the local environment[101].

FLIM is normally divided into two categories, time domain (TD) and frequency domain (FD). Although these two approaches are theoretically equivalent and related through their Fourier transform, they offer different advantages. FD FLIM have the advantage of using a continuous light source which is generally cheaper. FD is also reported to obtain higher resolution for multi exponential decays[86]. TD has the advantage of being a more intuitive and flexible system and being capable of measuring a wide range of lifetimes. TD is the system offered at NTNU department of physics that was used during this thesis.

For TD FLIM, the sample is scanned using a pulsed laser source. A schematic of the setup is seen in figure 2.16. The beam is split in two parts, where one part is sent directly to the detector as a reference time point, the other part is used to excite the sample. The lifetimes are evaluated using time-correlated single photon counting (TCSPC). In TCSPC, only the first photon emitted after each excitation is detected. Depending on the time delay between the reference signal and the photon from the sample the photon will fall into an interval, by collecting many photons, a time correlated histogram is constructed[102].

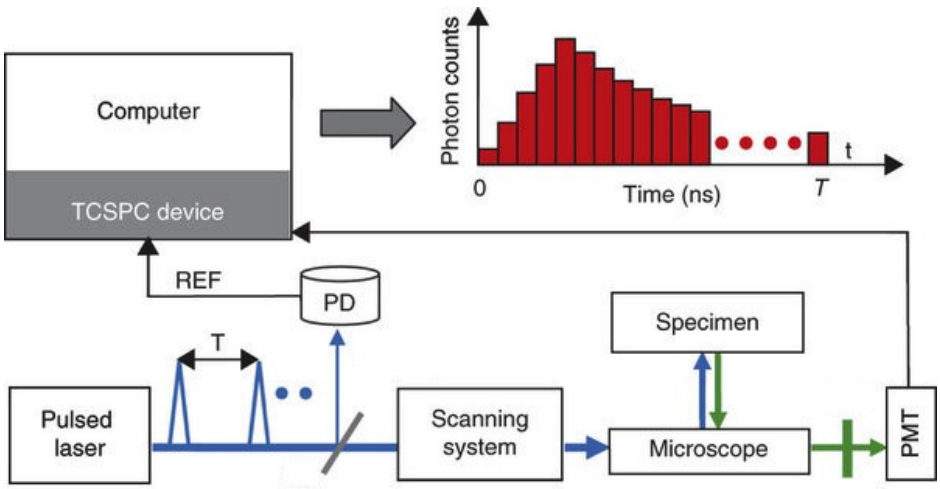

Figure 2.16: The setup of TD FLIM. PD = photodetector, PMT = photomultiplier tube. Illustration adapted from [103].

In an ideal case, the sample is excited by a delta (δ) pulse. In reality the excitation pulse has a curved intensity distribution, which gives rise to noise to the detected signal. This is corrected for using and instrument response function (IRF). This function is measured and the function describing the observed decay is a convolution of the IRF and the exponential decay. For a two-exponential system as seen with nile red in this thesis, the decay function $F(r,t)$ is given as[86]:

$$F(r,t) = E(t) * \sum_{i=1}^{2} A_i(r) e^{-\frac{t}{\tau_i(r)}} \tag{2.7}$$

Here, $E(t)$ is the IRF, A is the amplitude and τ is the fluorescence lifetime. To simplify calculations and graphical representations, the dual lifetime is often reduce to the average lifetime using

$$\tau_{ave} = \frac{\alpha_1 \tau_1^2 + \alpha_2 \tau_2^2}{\alpha_1 \tau_1 + \alpha_2 \tau_2} \tag{2.8}$$

where α_1 and α_2 are the amplitudes of the two lifetimes τ_1 and τ_2.

2.5.4 Flow cytometry

Flow cytometry (FCM) is a quantitative method used in this thesis to measure the amount of NR668 and by that the number of NPs inside the cells. Generally, FCM can be used to separate various cell types in a solution such as blood, perform live-dead assays in toxicity studies, or measure multiple dyes inside single cells. For FCM, the cells must be in solution. Using a mechanism termed hydrodynamic focusing where a jet stream of sheet fluid creates a focused stream with room for only one cell at the time, the stream of cells is directed through a laser beam orthogonal to the fluid stream, where the cells are illuminated and fluorophores are excited. The scattered light from the cells are detected both in front of the cell (forward scattering detector (FSD)) and to the side (side scatter detector (SSD)). The forward scatter will depend on the cell size where smaller cells will scatter less while the side scatter will measure the granularity of the cells. More granular cell content will result in more side scattering[104]. The emitted light from fluorophores is also detected, spatially separated from the excitation beam[105]. Using dichroic mirrors and multiple fluorescence detectors it is possible to quantify multiple fluorescent dyes for each cell.

Data obtained from FCM is relative, and control samples must be included in each analysis. In an uptake study, cells incubated under the same conditions but not incubated with NPs must be included to measure the autofluorescence of the cells. This way, it is possible to present data as histograms of the sample

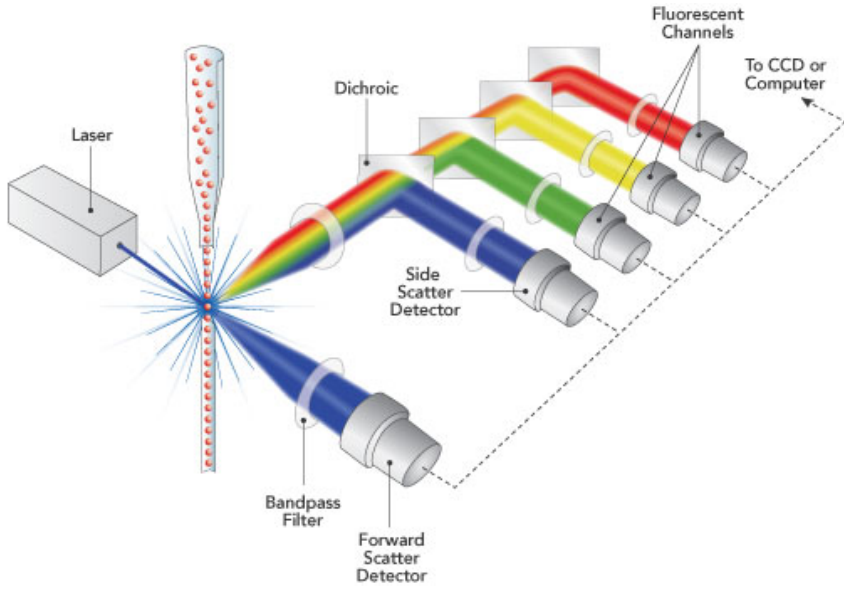

Figure 2.17: Illustration of the general setup of a flow cytometer. Adapted from [106].

and the control. In figure 2.18, FCM histograms showing the cellular uptake of POCA particles are shown. As the label in the right corner indicates, the red histogram presents the untreated cells (control). The two other histograms present are cells incubated with NPs for 3 hours (purple) and 24 hours (blue). The X-axis represents the fluorescence intensity. The gate labelled #1 indicates a selected area, and the percentage of cells from each sample found within this area can be red out from the numbers below.

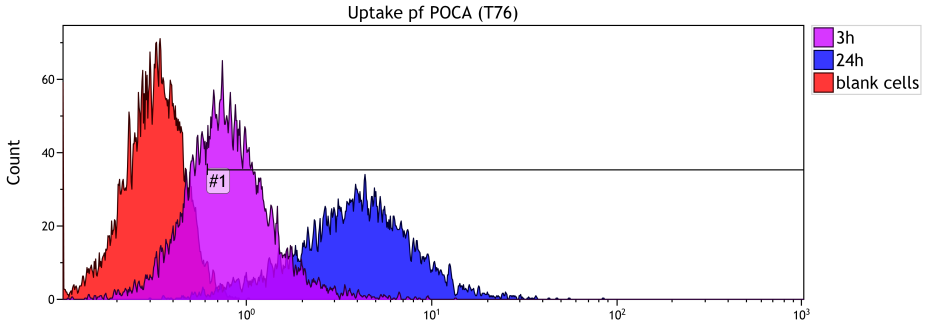

Marker	Number	%Total	%Gated	X-Med
All	6 624	66,24	100,00	0,77
All	4 956	49,56	100,00	3,92
All	6 045	60,45	100,00	0,32
#1	4 543	45,43	68,58	0,93
#1	4 903	49,03	98,93	3,95
#1	133	1,33	2,20	0,67

Figure 2.18: Example of histograms obtained from FCM. The figure shows the uptake of POCA NP's in PC3 cells after 3 hours(purple) and 24 hours(blue). The red histogram is from control cells not incubated with particles, but otherwise treated identically.

Chapter 3

Materials and methods

3.1 Cell cultivation

3.1.1 Cell medium

The medium used for cell cultivation was Dulbecco's modified eagle medium (DMEM, Gibco Life Technologies) supplemented with 10% fetal bovine serum (FBS, Sigma Aldrich). This will be referred to as DMEM 1. For long incubation times with NPs, DMEM with 10% FBS and 50mg streptomycin penicillin (Sigma Aldrich) was prepared, this will be referred to as DMEM 2.

3.1.2 Cell cultivation

In this master thesis, prostatic adenocarcinoma cells (PC3, American Type Culture Collection) were used for all experiments. The batch of cells was changed once (15th of march) to assure original properties.

The cells were cultivated in 75 cm^2 cell culturing flasks (Nunc) with 15mL DMEM 1, incubated at 37°C with 5% $C0_2$ and kept in the exponential growth phase. 1-2 million cells were transferred to the new flask, splitting was done every third or fourth day.

The cells were split by removing the medium and gently washed with 5 ml sterile phosphate buffered saline (PBS, Sigma Aldrich). PBS was then removed and 3 mL of 0.25% trypsin and 0.2% EDTA (Sigma Aldrich) was added to detach the cells from the incubation flask. The trypsin was allowed to work for 3 minutes at 37°C before the trypsination was stopped by adding 8 mL cell medium to the flask. 10 ml of this mix was added to a Falcon tube and centrifuged (Heraeus Megafuge 1.0) at 1500 rpm for 5 minutes. 10 μL of the solution remaining in the cell flask was mixed with 10 μL trypan blue (Molecular probe, Life Technologies).

The concentration of living cells was then analyzed using a cell counter (Countess, Invitrogen).

After centrifugation, the cells were resuspended in cell DMEM 1 to a concentration of 1E6 cells/mL. Then 1-2 million cells were passaged to a new flask. The remaining cells were either used for experiments or discarded. Back up of cells in case of infection was done either by cooperation with others working with the same cell line, or by keeping a second flask of cells. During the cultivation of cells, the medium was normally changed once during every passage.

3.2 Nanoparticles

The NPs used in this project are PBCA (poly(butylcyanoacrylat)) and POCA (poly(octylcyanoacrylate)) made by SINTEF materials and chemistry. The NPs are made through polymerization in a oil in water nanoemulsion. The general steps in this process are listed below while the general setup is shown in figure 3.1

1. The molecules that will end up in the NP are mixed in an oil in water emulsion. The droplets are stabilized by a surfactant (BRIJ-35). The oil phase consists of a monomer (butyl/octyl cyanoacrylate), a co-stabilizer (Miglyol 810N, a neutral, very hydrophobic oil), an initiator, and other molecules that you want in your particle (fluorescent molecules, cytotoxic drugs, etc.) The surfactant will organize at the oil-water interface, while the co-stabilizer will prevent Oswald ripening. The water phase is kept at acidic conditions to avoid premature polymerization.

2. An initiator (Jeffamin) is mixed into the solution and an ultrasound probe is used to make a nanoemulsion. The energy from the ultrasound creates nanometer droplets from the micrometer droplets in the emulsion.

3. The initiator starts the polymerization and the nano droplets polymerize.

The different NPs used, monomer, diameter, zetapotential and stability at pH 7.4 are listed in table 3.1.

Table 3.1: List of NPs used, adapted from [7] [8].

Particle	Monomer	Diameter	Load	Zeta potential (ζ)	Halflife at pH 7.4
Targ 67	BCA	177nm	NR688	-12	20 hours
Targ 76	OCA	151nm	NR688	-10	stable

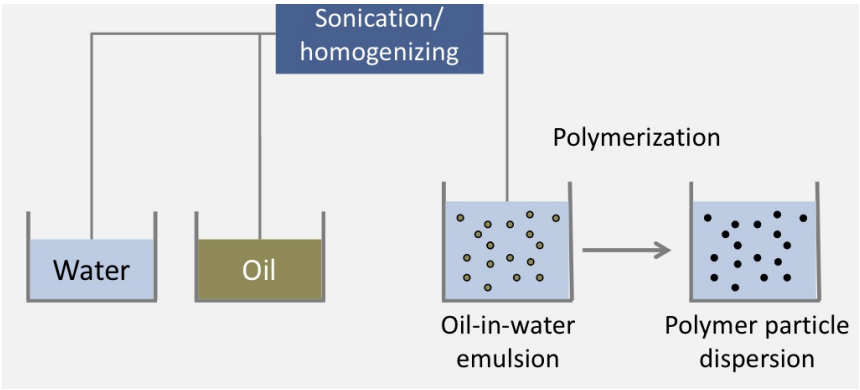

Figure 3.1: The general setup for making NPs through an oil in water emulsion. Adapted from a presentation by Yrr Mørch SINTEF Materials and chemistry.

3.3 Flow Cytometry analysis

The cellular uptake of NPs was quantified using FCM. PC3 cells were seeded in 12 well plates (COSTAR). The 1E6 cell/mL solution from splitting the cells (section 3.1) was diluted to a concentration of 125000 cells/mL. 1mL (125000 cells) was added to each well and the cells were cultivated at 37°C and 5% CO_2 for 2-4 days.

To incubate the cells with NPs, solutions of $20\mu g/mL$ of NPs in DMEM 1 was made prior to incubation. The cell medium in each well was then removed and either DMEM 1 (reference cells), or DMEM 1 with NPs was added to the wells. This was then cultivated at at 37°C and 5% CO_2 for the desired time.

After incubation with NPs, the cells were prepared for flow cytometry. The medium was removed from the wells, and the cells washed with $400\mu L$ PBS(Sigma Aldrich). This was removed, and $300\mu L$ of trypsin solution was added to the wells. The cells were left at 37°C for 3 minutes before the trypsination was stopped by adding $700\mu L$ DMEM 1 to each well. The solution from the wells was collected in separate falcon tubes and centrifuged at 1500 rpm for 3 minutes. The cells were then washed with cold PBS twice before they were resuspended in cold PBS and stored on ice. Before running flow cytometry, the cells were transferred to FCM tubes.

The cells were analyzed by FC (Gallios, Beckman Coulter). The dye in the particles used was modified nile red (NR688). A $\lambda = 561nm$ laser was used to excite the particles which was detected at $\lambda = 630nm$ using a 30nm bandpass filter. The voltage was set to place the unlabeled reference cells from 0-1 (first decade) on a log scale in terms of fluorescence intensity. Using a forward scatter

versus side scatter diagram, dead cells and aggregates were gated out and 10000 healthy cells were counted for each sample.

3.3.1 Endocytosis inhibitions

For inhibition studies, stock solutions of Chlorpromazin and Genistein were made;

- Chlorpromazin 5mg/mL in FBS.
- Genistein 10mM in DMSO.

Prior to each experiment, the solutions were diluted in DMEM 1 to a final concentration of 10μg/mL (Chlorpromazin) and 50μM (Genistein).

Cells were pre-incubated with the inhibitor for one hour before NP's were added. Inhibition experiments had three hours incubation with NP's. The protocols for inhibition with Chlorprozin[107] and Genistein[108] was found in the literature.

For the 4°C experiment, the cells were pre-incubated at 4°C for 10 minutes before cold particle solution was added. The cells were then stored at 4°C until the measurement.

3.4 Confocal laser scanning microscopy analysis

3.4.1 Preparation

Cells to be analyzed with CLSM were grown in 8-well imaging plates (Ibidi). The cells were diluted to 62500 cells/mL in DMEM 1, and 300 μL(18750 cells) were added to each well. The cells were cultivated at 37°C and 5% CO_2 for 3 days prior to imaging. Before imaging, the media was replaced with fresh DMEM 1.

3.4.2 Incubation with nanoparticles, free NR668 and staining for early endosomes and lysosomes

Solutions of 20 $\mu g/mL$ of NPs in DMEM 1 was made. After removing medium from the wells, 300 μL of this solution was added to each well at the required time point. The cells were then left 37°C and 5% CO_2 until imaging.

Cells were also labelled with free NR668. A stock solution was made by dissolving 2.6 mg NR668 in 10 ml DMSO (dimethyl sulfoxide). Before use, the solution was further diluted 1:10000 in DMEM 1 to a final concentration of 26 ng/mL.

Staining for early endosomes was done to study colocalization with NPs and early endosomes. The early endosomes were marked using CellLight®Early

Endosomes-GFP with excitation and emission maxima of 488nm and 510nm. A solution of 40 virus particles/cell was prepared in DMEM 1 and added to cells 24 hours before imaging.

Staining for lysosomes was done with Lysotracker®Blue (Life Technologies). Due to very weak staining, the concentration was increased from 75 nM as suggested in the manufacturers protocol to 2.5 μM. The dilution from Stock solution of 1mM was done in DMEM 1, and the solution added to the cells 1 hour before imaging. The excitation and emission maxima of Lysotracker®Blue is 373 nm and 422 nm.

3.4.3 Imaging

For imaging of the NPs and cells, the SP8 microscope was used with a 63x1.2 water objective with a motCorr coverslip. The pin hole was set to 1 airy unit. For excitation, a white light laser at 514nm was used and the signal detected from 580nm to 660nm using the HYD-3 detector. Bright field images was created using the 514nm laser and detecting with the PMT detector using a transmitted light filtercube.

3.4.4 Colocalization imaging

For colocalization, controls of cells incubated with either fluorescent stain (Lysotracker®Blue or CellLight®) or NP's were used to adjust laser and detector wavelengths to avoid cross-talk between channels. The images were recorded in a sequential scan, this also to reduce potential cross-talk.

Lysotracker®Blue was excited using a pulsed multiphoton laser at $\lambda = 746nm$, CellLight®was excited at 488nm.

3.4.5 Fluorescence lifetime imaging

For fluorescence imaging, the SP8-FLIM FCS APD SPADS mode was selected on the SP8 and the coverslip/Corring adjusted for minimal reflection, typically around 93-96. The sample was excited at 514nm at a 40MHz repetition rate and detected using the SPAD 2 detector (565-615nm). The FLIM was done with maximum resolution, 512x512 pixels. Pico Quant Sympho time was used to record and analyze the lifetimes.

Analysis of the lifetimes was done both by extracting the .dat file to Excel and in the PicoQuant software. In Excel, the maximum recorded intensity in the images was used to normalize the images, making them comparable. Averages from 5 FLIM images were then calculated to produce lifetime distributions.

In PicoQuant, the internally recorded IRF-function convoluted with a two-exponential decay function was used to fit the resulting decay curve. Regions of

interest (ROIs) were manually selected based on the color labeling in the original FLIM image. The areas were chosen large enough to obtain a peak value of approximately 1000 photons.

3.4.6 Spectral analysis

For spectral analysis, a 514nm laser was used as excitation light, and the emitted light detected in overlapping areas of 10nm starting from 550nm and running to 700nm. The areas had a 5nm overlap resulting in 30 areas for each sample. To analyze the data, the .csv files were extracted and analyzed in Excel.

3.4.7 Triton treatment

Triton X-100 (Tx100) was diluted to 10% in DMEM. $15\mu L$ of this solution was added to the Ibidi well during imaging. Prior to adding the Tx100 solution, the SP8 microscope was programmed to take an image every second using 514nm excitation and detecting from 600nm to 680. It was normally recorded approximately 10 seconds prior to adding Tx100 and 3 minutes after adding Tx100.

3.5 Statistical analysis

Statistical analysis was done using the t-test function in Excel. P-values below 0.05 are considered significant.

Chapter 4

Results

The results have been divided into two separate parts, one presenting the cellular uptake and the other presenting intracellular degradation of the PACA NPs. The particles used are described in table 3.1 in section 3.2, and will be referred to as PBCA (Targ 67) and POCA (Targ 76). The cells used were human prostate cancer cells (PC3).

4.1 Cellular uptake of nanoparticles

4.1.1 Initial uptake studies

Before uptake of POCA and PBCA particles can be compared, one have to measure the relative intensity of fluorescent emission from the two particles. This was done prior to this work by Eva von Haartman and Andreas Åslund, the result is presented in the appendix part A. It was found that at an emission wavelength of 561 nm, the wavelength used for FCM, PBCA NPs were more fluorescent than POCA particles by a factor of $1/0.52 = 1.923$. In studies were these two particles are compared quantitatively, the fluorescence of cells with POCA particles has been multiplied by this number.

Initially, uptake studies with FCM were performed. PC3 cells were incubated with PBCA and POCA NP for 3 and 24 hours at 37 °C. The resulting histogram from one of the parallels is seen in figure 4.1. The shift in mean fluorescence after 3 and 24 hours is presented in figure 4.2, both calculated from 3 different experiments (A), and calculated from 3 parallels within the same experiment (B). It can be seen that after 3 hours, the cellular uptake of POCA NPs is 3-10 times higher than the uptake of PBCA, after 24hours, there is no distinct difference. It can also be seen that the standard deviation between separate

experiments are generally higher than the standard deviation between parallels in one experiment. In FCM, 10000 healthy cells were recorded, but further gating reduces the effective amount to 7000-9000 cells.

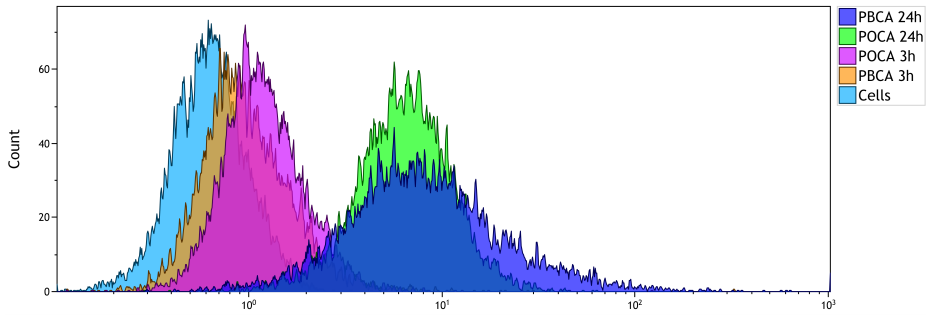

Figure 4.1: Representative logarithmic FCM histogram of uptake of POCA and PBCA NP by PC3 cells.

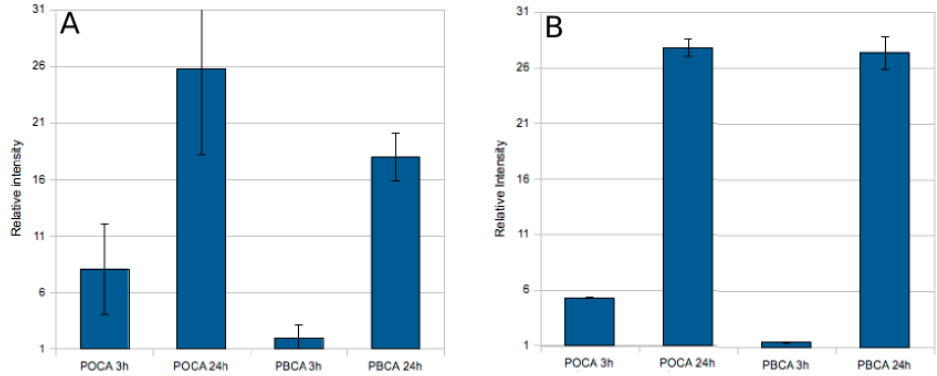

Figure 4.2: The relative change in mean fluorescence of PC3 cells incubated with POCA or PBCA NP for 3 and 24 hours. The values and standard deviations in A are calculated from 3 different biological experiments while B is from 3 parallels in one experiment. The difference in fluorescence intensity has been accounted by multiplying the the values from POCA by the normalization factor 1/0.52

It was confirmed that the particles where inside the cells using CLSM. Figure 4.3 shows three images from a z-stack of cells that has been incubated with POCA NP for 24 hours. The images show that the particles are found inside the cell, but generally not within the cell nuclei. The same thing was seen for the PBCA NP (not shown).

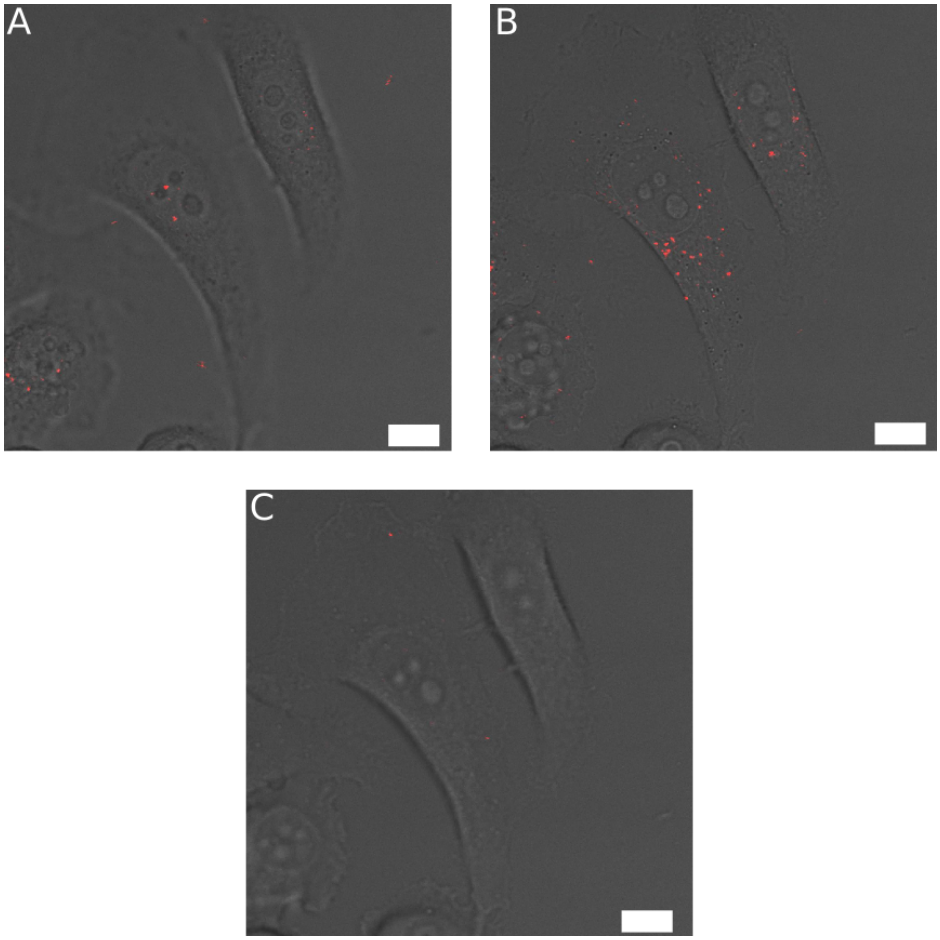

Figure 4.3: Three images from a Z-stack of PC3 cells and POCA NPs. NPs are colored red. A: top of the cells, B: the middle of the cells, C: the bottom of the cells. Scalebar: $10\mu m$

To gain more detailed information on the uptake of the NP, the uptake from 0-3hours was further evaluated, the result is seen in figure 4.4. The curve shows the that POCA is taken up more rapidly than PBCA.

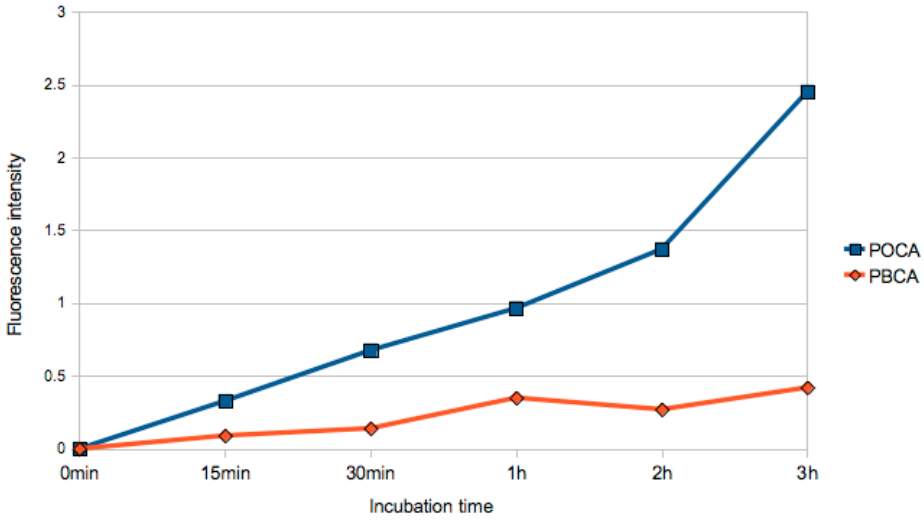

Figure 4.4: Cellular uptake of POCA and PBCA NP in 0 to 3 hours. The numbers are normalized to the different initial fluorescence intensity, autofluorescence has been subtracted.

Images were also taken of cells incubated with PBCA and POCA NPs for 24h to verify the amount of uptake, this is seen in figure 4.5. Here, it can be seen that after 24 hours, a large uptake of both POCA and PBCA particles has occurred. The amount of particles in the cells is relatively similar for the two images.

4.1.2 The effect of incubation conditions and pre-treatment of the nanoparticles on cellular uptake

The uptake of NPs presented in the results above was high compared to previous experiments performed fall 2013 by a visiting phd student, (unpublished results), and the difference between POCA and PBCA had not been previously observed. Further control experiments were therefore performed in order to better understand the parameters affecting the rate of uptake.

It was investigated if the cell medium or the cells affected the NP making them either more or less easy to internalize for the cells. POCA NPs were pre-incubated for 21 hours in two different environments:

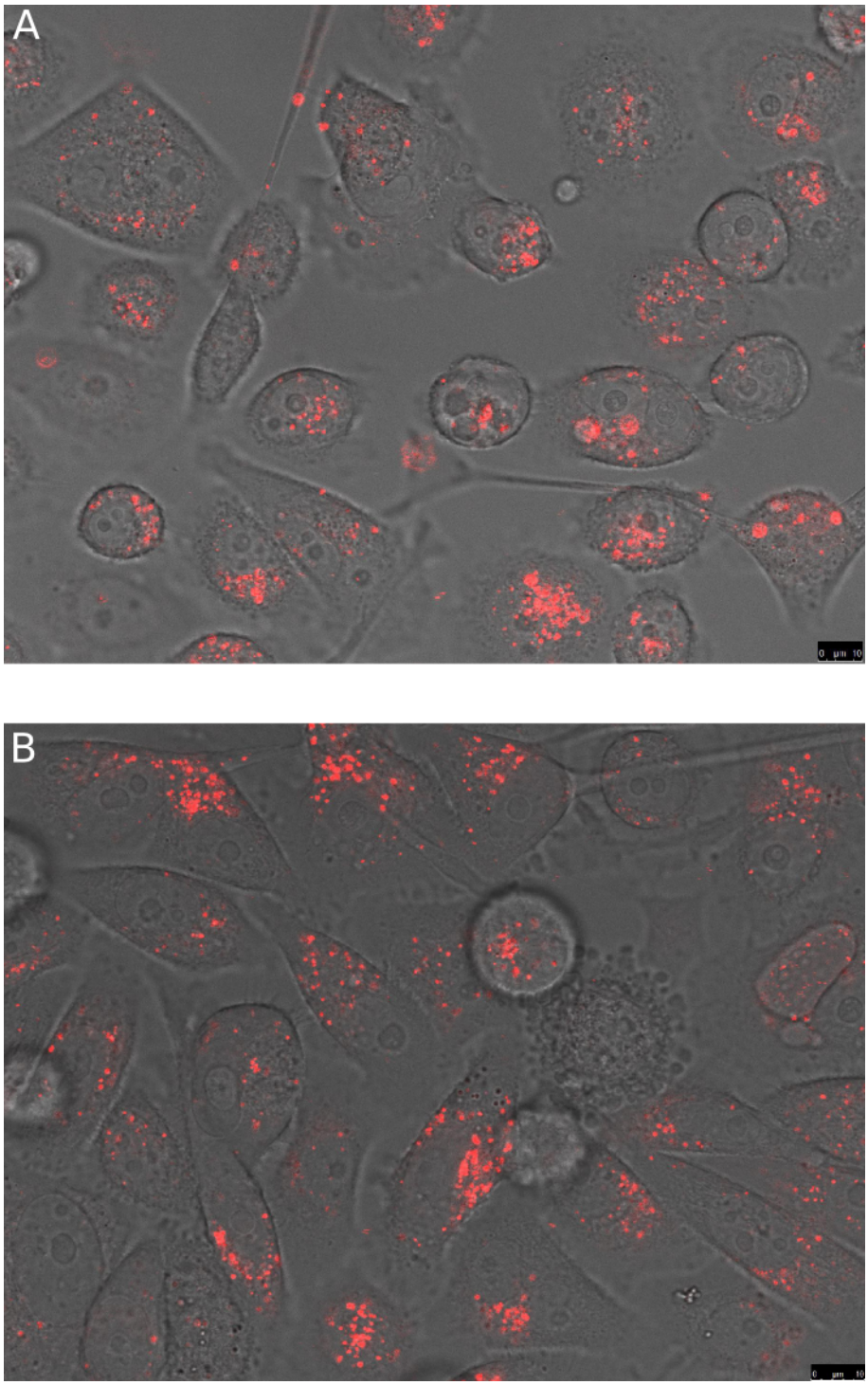

Figure 4.5: CLSM image of PC3 cells incubated for 24 hours with PBCA (A) and POCA (B) NPs. $I_{ex} = 514$ nm. Scale bar: 10 μm

- In DMEM 1
- In DMEM 1 and PC3 cells growing in a cell culturing in flask.

Thereafter, the solution solutions were transferred to wells with PC3 cells. Cells were also incubated with fresh POCA NP for 3 and 24 hours as control and reference value. Figure 4.6 shows the resulting histograms while figure 4.7 shows the mean fluorescence calculated from three parallels. An increased uptake of 63% is seen when the POCA particles have been incubated with other PC3 cells for 21 hours prior to incubation, compared to untreated particles. The effect of 21 hours in pure medium (DMEM 1) is only minor.

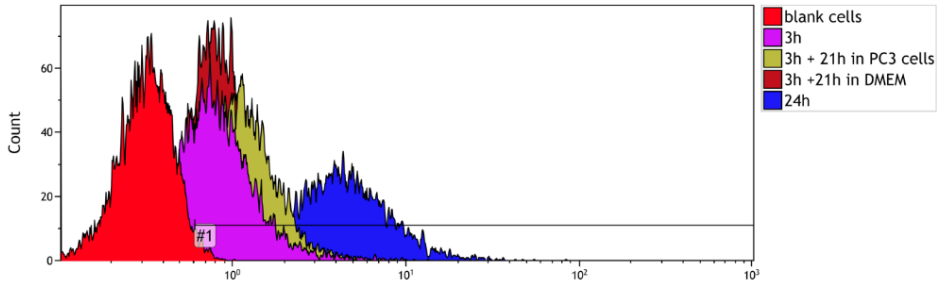

Figure 4.6: Histogram showing the fluorescence of cells after incubation with POCA NP stored under different conditions for 3 hours and cells incubated for 24 hours.

4.1.3 Effect of confluency/maturation of the cells

During the first set of experiments, it was observed that the cells would require multiple days to fully settle after seeding. The term maturation describes the time were the cells are cultivated after splitting, prior to measurements. It was observed that within the first 5-6 days of maturation the cells would spread more in the sample well and appear less rounded. It was therefore evaluated whether maturation would effect the uptake of NP and if this could explain the elevated uptake seen compared to previous experiments. Cells were seeded on day 0, and the uptake of POCA NP was measured on day 2, 3 and 4. The results seen in figure 4.8 show that the uptake increases with the number of days of maturation. The cells were seeded at the same density, so the confluency is also increased, approaching 95% on day 4. By gating the untreated cells at approximately 2% positive, the positive population on day 2, 3 and 4 is 43%, 66% and 82% respectively, with the shift in mean fluorescence being more than 4 times higher on day 4 than on day 2.

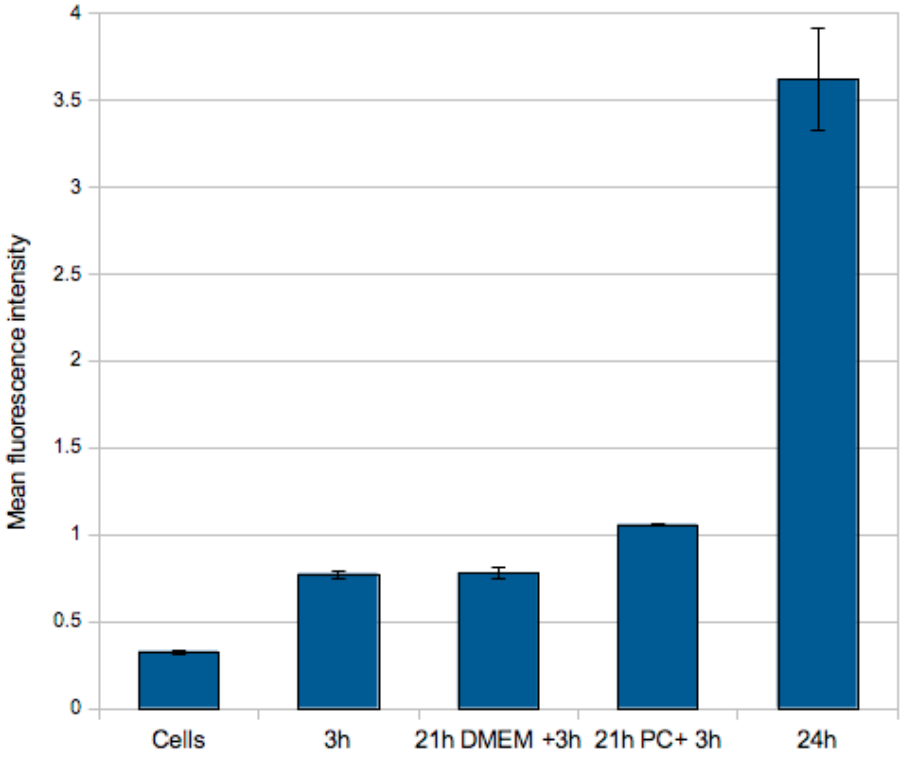

Figure 4.7: Mean fluorescence shift of cells incubated with POCA NP stored under different conditions for 21 hours prior to incubation and cells incubated with POCA NP for 24 hours as reference. Values are calculated from three parallels, error bars showing standard deviations.

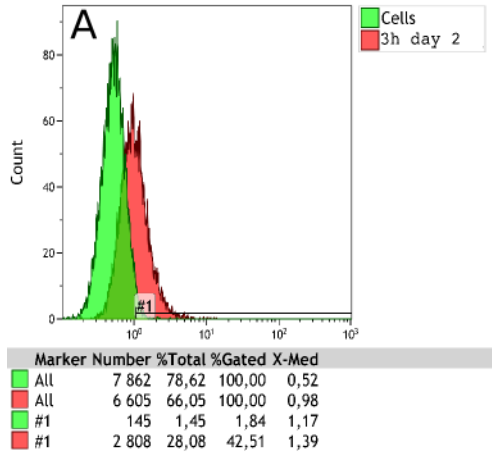

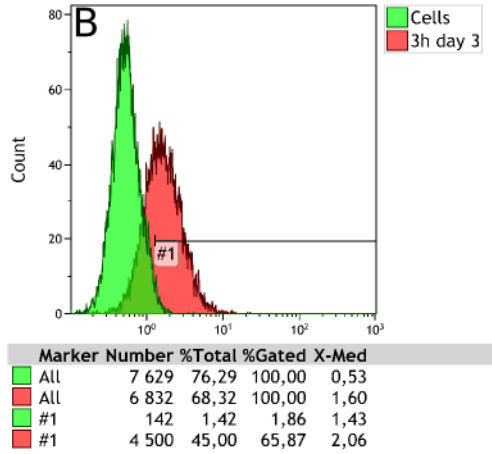

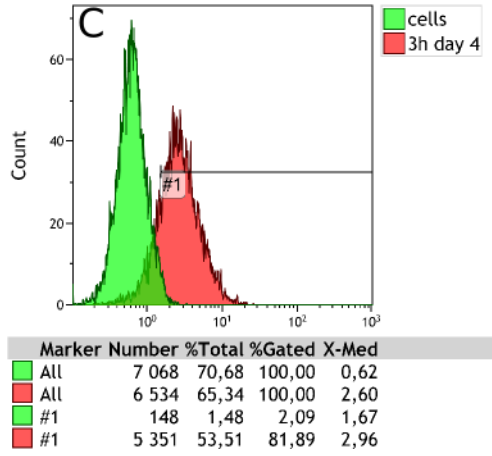

Figure 4.8: The uptake of POCA NP after 3 hours of incubation growing 2 (A), 3 (B) and 4 (C) days in the 12well plate. The gate (labelled #1) is set at approximately 1.8% false positive cells and captures 43.5%, 66% and 82% respectively of the cells.

4.1.4 Uptake mechanisms

To evaluate the uptake mechanism, cells were incubated with NP while suppressed by endocytosis inhibitors. Chlorpromazin was used to inhibit CME, Genistein to inhibit caveolin-mediated endocytosis. Also, cells were incubated with NP at 4°C to clarify that the uptake was an energy dependent process. Figure 4.9 shows the histograms of cells incubated at 4°C for 3 hours with POCA and PBCA, and control at both 4 and 37°C. The histograms are overlapping completely, indicating no uptake of NP. The uptake under suppression of inhibitors is seen in figure 4.10. 4.10A shows that the uptake of POCA is reduced equally by Chlorpromazin and Genistein indicating that both clathrin- and caveolin-mediated endocytosis plays an important role in the uptake. In 4.10B the uptake is reduced by Chlorpromazin, but hardly affected by Genistein. This indicates that caveolin mediated endocytosis is less important for the uptake of PBCA particles. This experiment was done twice to verify the result. The two experiments were done at different time points after seeding to see if length of cultivation also affected the mechanism. It was again found that the uptake was depending on time, but the effect of inhibitors was the same in the two experiments. The histograms obtained from the two experiments are found in the appendix part B. To make the two experiments contribute equally to the histograms in figure 4.10, the fluorescence shift from the experiment of low uptake was multiplied by the factor needed to gain a similar maximum uptake of NPs without inhibitors.

4.1.5 Intracellular location of nanoparticles

In order to understand the environment faced by the particles once inside the cell membrane, studies were done to look at the intracellular routing after entry. This could also cast light on the uptake mechanisms, if the particles are taken up by endocytosis, some colocalization with endosomes and lysosomes could be expected. The intracellular location was mainly evaluated using different methods available for CLSM. First, it was observed that the particles were inside the cell, but not inside the nuclei (figure 4.3). Using Cell light GFP for early endosomes, colocalization with this organelle was briefly assessed. It was found that the staining gave fluorescence signal from most of the intracellular compartment, making it hard to draw conclusions, this can be seen in the z-stack in figure 4.11 where green is GFP from early endosomes and red is NPs.

By carefully choosing suitable cells and reducing intensity post imaging the image shown in figure 4.12 could be created showing a cell expressing GFP and having POCA NP intracellularly. The white arrow points at possible colocalization between an early endosome and a POCA particle.

Lysotracker blue was used to label lysosomes. Images of cells stained with lysotracker and incubated with NPs were taken to look for colocalization. Figure

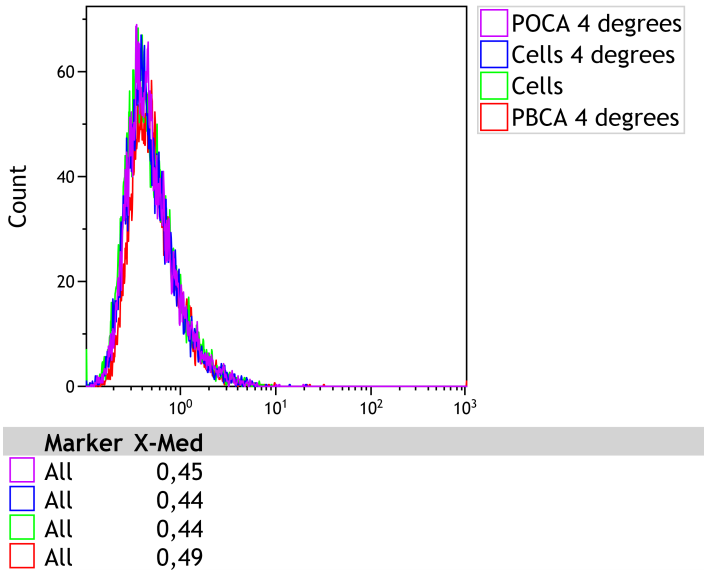

Figure 4.9: FCM histograms of PC3 cells incubated for 3 hours at 4°C with POCA and PBCA NP. Control both at 4 and 37°C are also shown.

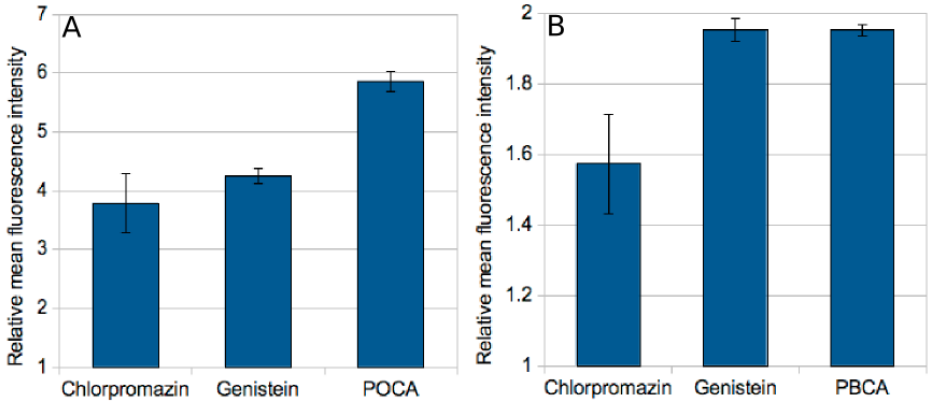

Figure 4.10: Bars showing the relative mean fluorescence of PC3 cells incubated for 3 hours with A: POCA and B: PBCA NP and suppressed by either Chlorpromazin or Genistein. Calculations based on doublets from two different experiments that has been normalized to the same maximum uptake of NPs and error bars showing standard deviation.

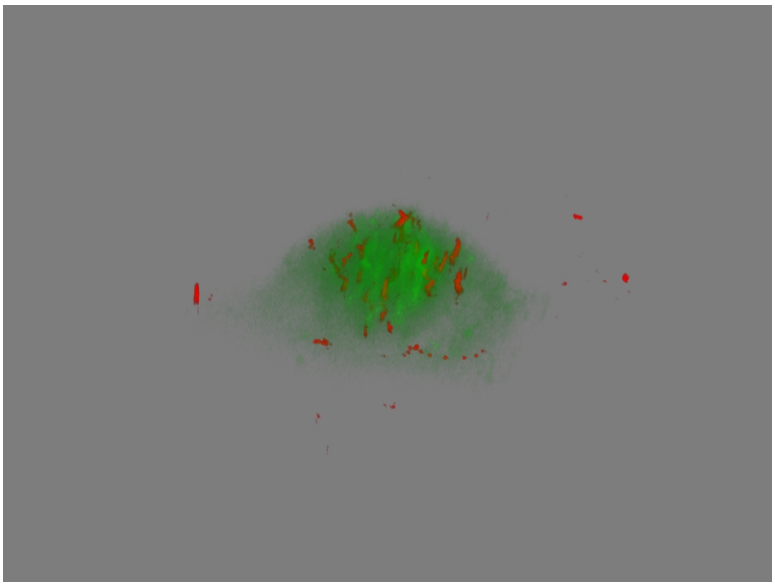

Figure 4.11: 3D model from a Z-stack of a PC3 cell transfected with Cell light GFP marker (green) for early endosomes, the problem of diffuse staining is clearly seen. Red spots are POCA NP .

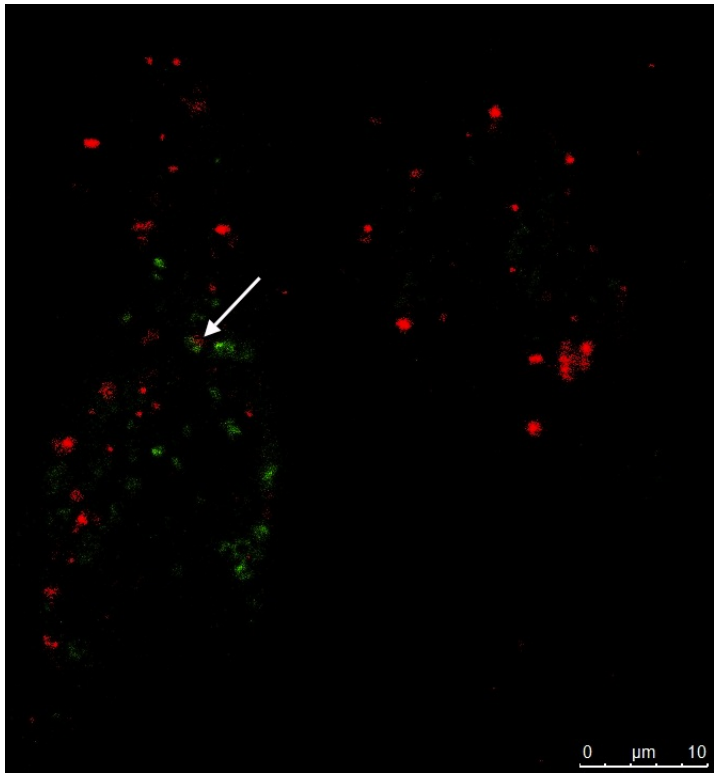

Figure 4.12: CLSM image of a PC3 cell expressing GFP on early endosomes after incubation with POCA NP for 3 hours. The white arrow points out a spot of possible colocalization between the particle and an early endosome. In the image, background has been subtracted reducing the intensity in the green channel.

4.13 shows a CLSM image of PC3 cells with lysosomes (green) POCA NPs (red) overlaid a BF image. Yellow indicates that green and red are expressed in the same pixel. The white arrows point at some of the yellow spots.

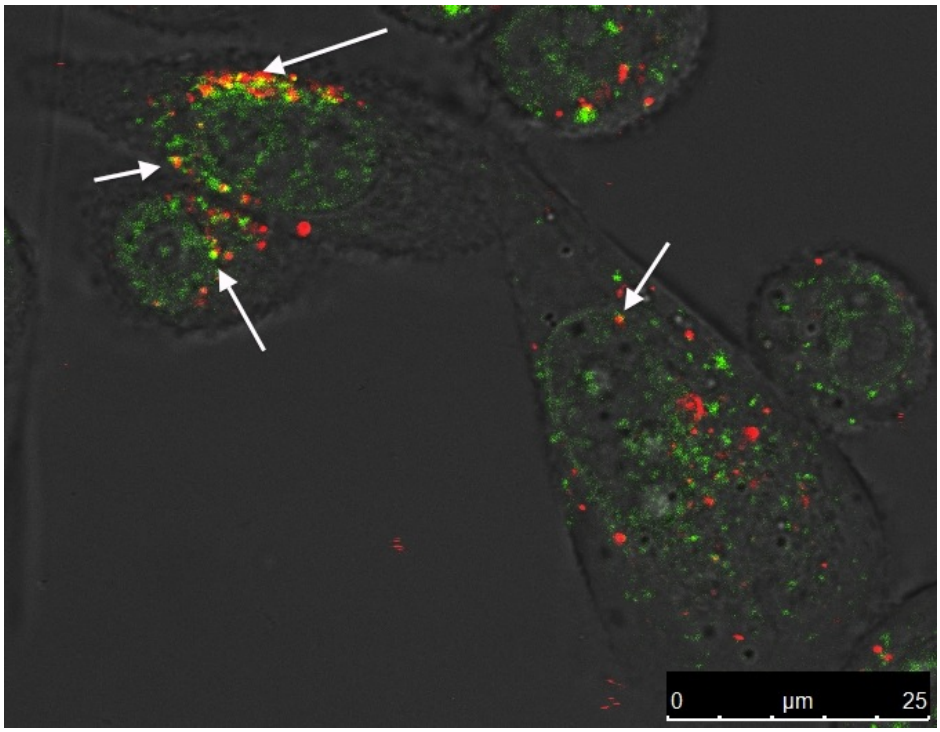

Figure 4.13: CLSM image of PC3 cells incubated with POCA NP (colored red) for 3 hours and stained with lysotracker blue (colored green). Yellow indicates that red and green are expressed in the same pixel, the white arrows points out examples of this.

It was verified that the particles and lysosomes were colocalized by scanning in the Z-direction. Figure 4.14 shows a Z stack of PC3 cells that has been sliced were green (lysosomes) and red (POCA NP) are expressed in the same area (white arrows). The bright field image has no transparency, so only particles and lysosomes at the rim of the Z-stack can be seen.

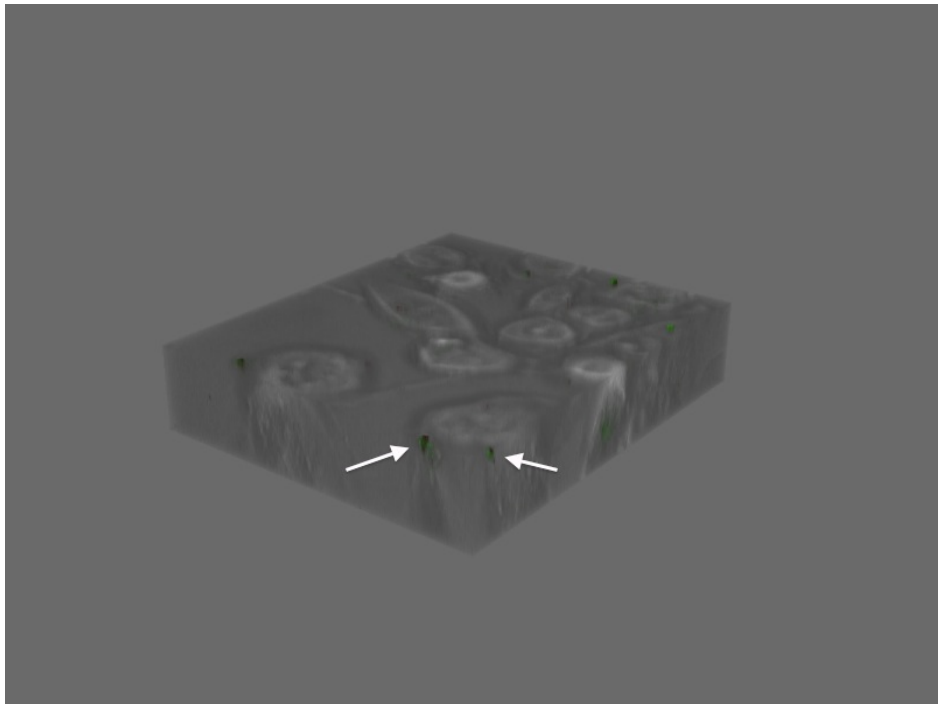

Figure 4.14: Z-stack of CLSM images of PC3 cells stained with Cell light GFP for lysosomes and incubated with POCA NP for 3 hours. The channels are set to have no transparency, so only the rim of the Z-stack is seen.

4.2 Intracellular degradation of nanoparticles

It was initially though that looking for diffuse staining would be a possible method of detecting intracellular degradation of NPs. However, as seen in figure 4.15, the different particles and free NR668 look very similar inside cells after 24 hours of incubation. Other methods were therefore tried in order to find ways of separating NPs to free dye.

4.2.1 Fluorescence lifetime imaging

Initially, work was done to establish whether FLIM would be a sensible way of detecting intracellular degradation. It would require that the fluorescence lifetime of NR668 was depending on the local environment of the dye, and that the differences were large enough the be readily measured. An initial literature study suggested a two-exponential decay for conventional nile red that would be different within for example different polymer materials[89]. Experiments were therefore started by measuring the lifetime of NR668 within the particles and finding a suitable protocol. The measurement conditions found are presented in materials and methods (section 3.4.5). One important discovery was that at some excitation wavelengths reflections from the sample well creates a devastating artifact to the lifetime measurement. This effect can be imaged, and is presented in figure 4.16 where (A) shows excitation at 488nm giving a bad case of ripples from the sample well, while (B) shows excitation at 514 giving the optimum imaging settings.

The first thing that was done was to measure the lifetime of NR668 inside POCA and PBCA particles in solutions of different pH. This in order to both look for potentially different lifetimes, and to see if the lifetime would change if the particles were intact. The measurement was done by adding the solution to an Ibidi well, and measuring the lifetime in the middle of the fluid volume. This was done on fresh particles within 30 minutes of mixing the solution. The lifetime measurement of fresh particles at different pH, measured in solution is seen in table 4.1, and shows that the fluorescent lifetime does not depend on pH, but is significantly different for the two particles with a P-value of 0.02 (short lifetime) and 0.04 (long lifetime).

When measuring lifetimes in solution, like what was done in table 4.1, a large contribution from the background limits the sensitivity of the measurement. When possible, the proceeding FLIM measurements were therefore done on particles either attached to the sample well or inside cells.

Particles were then stored in DMEM for 6 days. At this point the particles will stick to the sample well, likely due to degradation of the PEG layer. The measurement was done on a selection of particles in each image by choosing a suitable ROI (region of interest). This method removes the background noise,

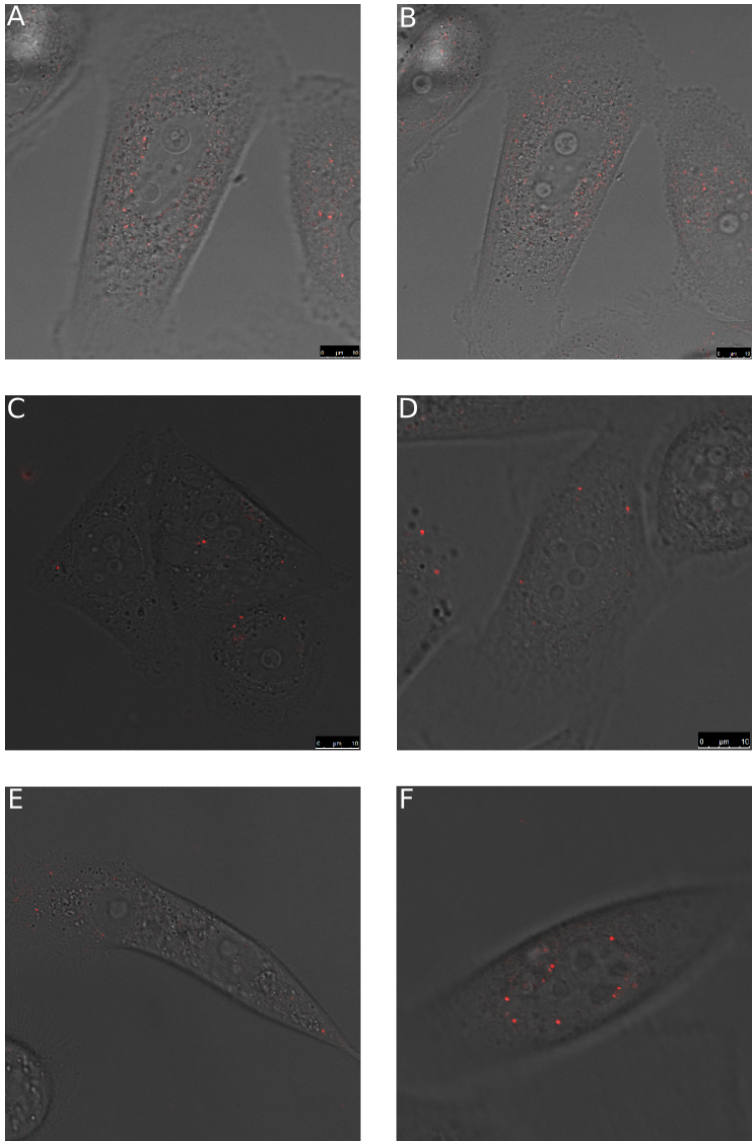

Figure 4.15: Images of PC3 cells incubated for 24 hours with free NR668 (A and B), PBCA NP (C and D), and POCA NP (E and F). NR668 and particles are colored red. The images show that free NR668 and NPs are visually similar.

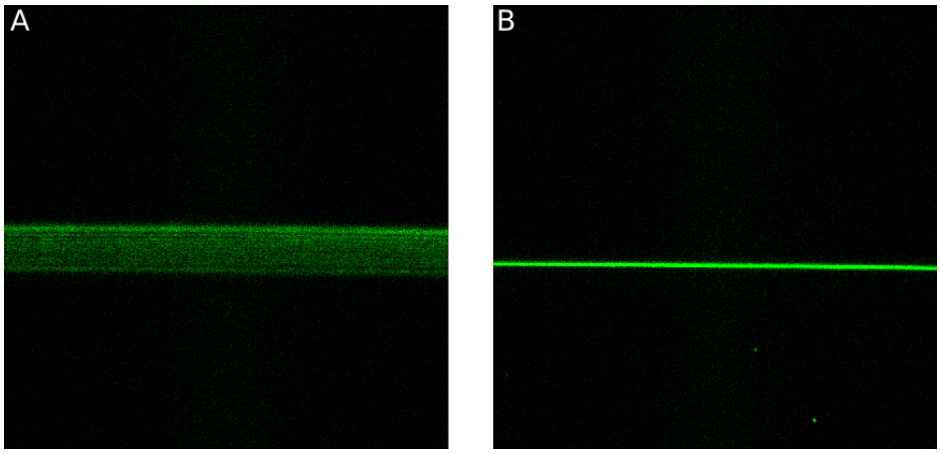

Figure 4.16: Image of the sample holder at good and bad imaging setup. In A, excitation wavelength is 488nm and in B the wavelength is 514nm, a wavelength that was used for all proceeding FLIM measurements. The image is a XZ scan, the green line is the sample holder. In image B, some NPs in the sample can be seen below the green line.

but captures fewer photons than when measuring in solution. The results were therefore calculated based on 6 images. FLIM images of particles attached to the glass well indicated that the PBCA especially had a different lifetime in the core of the particles compared to the shell, this is seen in figure 4.17. However, after spectral analysis (section 4.2.2) it was found that scattering from the sample well could be a problem when imaging the particles attached to the glass.

Figure 4.18 shows a CLSM image of PBCA NPs attached to the sample well (A), the corresponding FLIM image (B) and a FLIM image where a selection of particles has been chosen manually (C). The selected ROI's are still colored while the rest of the image is in black and white. The lifetimes collected from the particles stored in medium for 6 days prior to imaging in solutions of different pH are presented in table 4.2A. In table 4.2B, the significance calculated from a student t-test comparing the numbers to the measured lifetimes in DMEM is shown. These numbers can not be directly compared to those presented in table 4.1 due to different measurement conditions. The average numbers are also presented visually in figure 4.19. The results show that the lifetime of NR668 in POCA particles remains essentially unchanged after changes to the environment while inside PBCA particles, the lifetime changes.

A study was then started to look at the intracellular degradation of PBCA and POCA, and to see if lifetime measurements could cast some light upon this

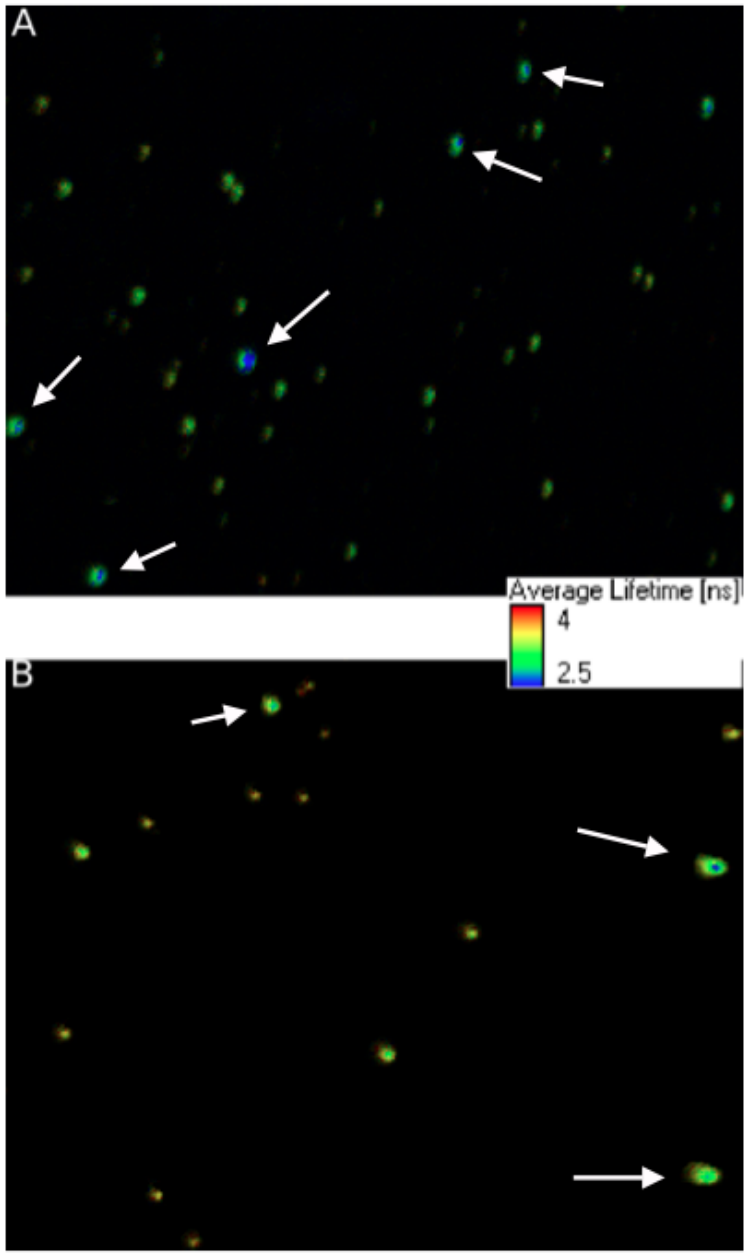

Figure 4.17: FLIM of PBCA (A) and POCA (B) attached to the sample well. Arrows point at particles where the core have a different, shorter lifetime than the shell of the particles.

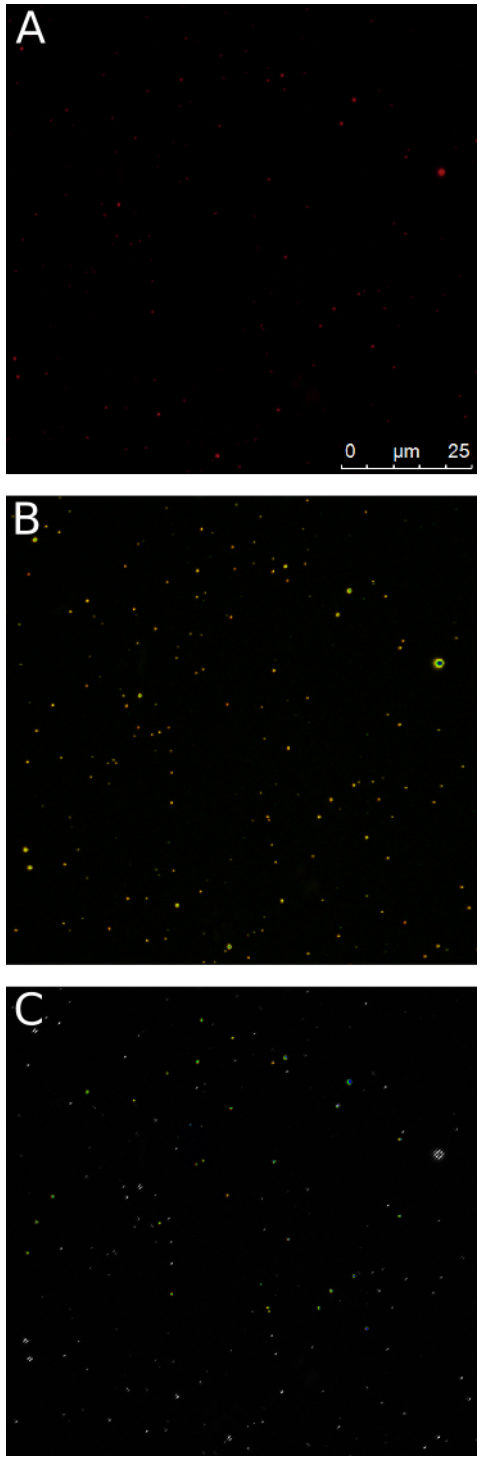

Figure 4.18: Images showing the processing step for each FLIM measurement. An image is taken in CLSM (A), the FLIM software creates an image showing the various lifetimes and total intensities (B), some of particles are manually circled in order to remove background noise, these are still colored in image C.

Table 4.1: Lifetimes of NR668 inside POCA and PBCA particles fresh from the particle solution measured in solution in various pH buffers.

	PBCA		POCA	
Medium	τ_1(ns)	τ_2(ns)	τ_1(ns)	τ_2(ns)
pH 7.2	1.4	4.0	1.6	4.1
pH 5.6	1.4	4.0	1.7	4.2
pH 4.0	1.4	4.0	1.7	4.2

process. PC3 cells were incubated with POCA and PBCA particles for 24 hours, before the medium was changed back to DMEM without any NP. It could therefore be assumed that all the particles inside the cells had been endocytosed within these 24 hours. Particles were also imaged after 5 hours of incubation, and on the bottom of the sample well immediately after incubation had started. Cells were also incubated with free NR668 solved in DMSO and diluted in DMEM to gain reference values and images of free nile red inside cells. Resulting FLIM images at varying time points are seen in figure 4.20, 4.21 and 4.22. The colors in the images depicts the average lifetime of each pixel, the color scale running from 2.5 ns to 4 ns. The images reveal that especially for NR668, but also for PBCA particles, areas of different lifetimes exists inside the cells. To calculate the lifetimes, 6 FLIM images were taken for each particle/dye and time point and ROI's were selected. When areas of different lifetimes existed in the same sample, areas of very long lifetime (red areas) were avoided. Scatter plots of all measurements are presented in figure 4.23.The corresponding numbers and standard deviations are found in table C.1 in the appendix part C. In figure 4.24, the average long and short lifetimes have been calculated for better visualization of the possible trend. For PBCA, a significant increase for both lifetimes is seen with P-values of 3.5E-5 (short lifetime) and 2.2E-4 (long lifetime) for the difference from the first to the last time point. For POCA, no clear trend is seen, the P-values from first to last time point is 0.41 (short lifetime) and 0.53 (long lifetime). The differences seen for POCA is therefore not significant. It is also worth noticing that for PBCA, the biggest change occurs between 5h and 24-48h after incubation.

While the images with average lifetimes for each pixel and the exact lifetimes observed in each case preserves a lot of information for analysis, it is for degradation purposes also interesting to look at general trends of the lifetimes captured on various time points. The overall lifetime distribution, where the two lifetimes have been averaged using formula 2.8, was collected for 5-8 images of each particle on the different time points to create lifetime distributions. The distribution of free NR668 is seen in figure 4.25, PBCA in figure 4.26 and POCA in figure 4.27. The distributions show that there is a shift towards shorter lifetimes for

Table 4.2: A: Lifetimes and standard deviation of NR668 inside POCA and PBCA particles after 6 days in cell medium, and left in various solutions for 1h prior to measurement. n=5. B: the P-value from t-test comparing the measured lifetimes in the different solutions to the lifetimes in DMEM.

A

	PBCA		POCA	
Medium	τ_1(ns)	τ_2(ns)	τ_1(ns)	τ_2(ns)
DMEM	1.07 (± 0.11)	3.47 (± 0.20)	1.09 (± 0.14)	3.70 (± 0.13)
pH 7.2	1.31 (± 0.08)	3.71 (± 0.11)	1.10 (± 0.15)	3.67 (± 0.08)
pH 5.6	1.09 (± 0.22)	3.51 (± 0.29)	1.04 (± 0.10)	3.62 (± 0.05)
pH 4.0	0.85 (± 0.07)	3.04 (± 0.07)	1.07 (± 0.08)	3.61 (± 0.12)

B

P-value from comparing the lifetime to the lifetime in DMEM

	PBCA		POCA	
Medium	Pτ_1	Pτ_2	Pτ_1	Pτ_2
pH 7.2	0.004	0.04	0.93	0.56
pH 5.6	0.86	0.76	0.41	0.16
pH 4.0	0.003	0.002	0.77	0.22

NR668 between 5 and 24 hours. For PBCA particles, there is an immediate shift towards shorter lifetimes from 0 to 5 hours, but from 5 to 48 hours, there is a large shift towards longer lifetimes that continues on the measurement after 6 days. For POCA NPs, only minor changes are seen.

4.2.2 Spectral analysis

To further analyze the possible intracellular degradation of particles, the emission spectra from cells with NPs and free NR668 were recorded. The measurements were done scanning for emission spectra, but the adsorption spectra were first measured to find the optimal excitation wavelength. It was found that $\lambda = 514nm$, the wavelength used for FLIM was suitable (not shown). The spectra were recorded for particles attached to the sample well immediately after incubation, inside cells after 24 hours of incubation, and inside cells after 6 days. In the 6th day sample, the cells were incubated with particles for the first 24 hours, the medium was then changed back to DMEM 2 (containing antibiotics) for the following 5 days. Cells were also incubated with free NR668 after 24 hours and after 6 days for reference spectra. 5 images were recorded for each sample, and each image normalized to the same maximum intensity.

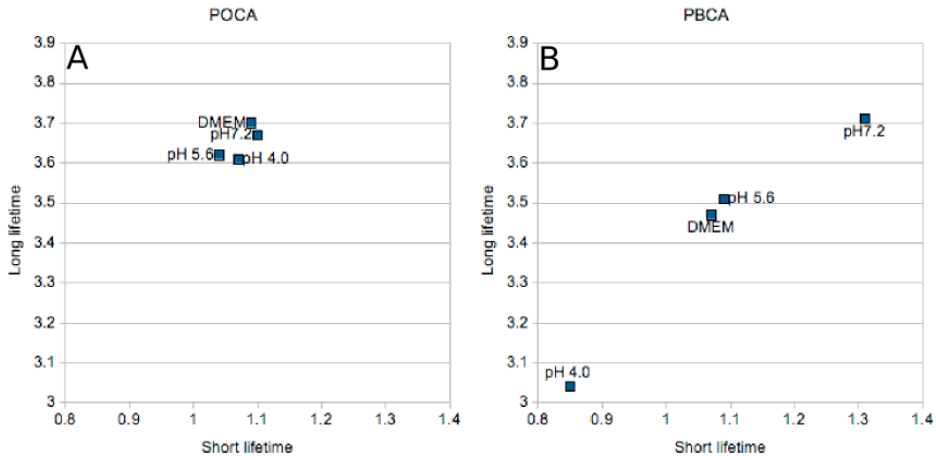

Figure 4.19: Scatter plots showing the average lifetime of NR668 encapsulated in POCA (A) and PBCA (B) NPs in different pH buffers after being stored 6 days in DMEM. It can be seen that for PBCA, the lifetime is now depending on the pH.

Figure 4.28 shows the spectra from PBCA(A) and POCA (B) evolving over time. It shows that from 0 to 24 hours, the spectra from PBCA particles is red-shifted, after 6 days it has shifted back towards shorter wavelengths again. For POCA, the spectra is very similar for all time points except for the shorter wavelengths in the first measurement. Figure 4.29 shows the comparison of PBCA, POCA and NR668 at each time point. Here it is shown that initially(A) the spectra from POCA and PBCA are similar, while after 24 hours (B) the specter from PBCA has shifted and is now similar to the specter from NR668 after 24 hours. On the last measurement(C), the spectra is more similar again because both spectra from NR668 and PBCA has shifted towards shorter wavelengths making them more similar to the spectra from POCA.

To control that the particles or free dye was still inside the cells after 6 days, the intensity at the maxima of each spectra was recorded prior to normalization. The intensities from NR668, PBCA and POCA is presented in figure 4.30. The intensity is a sum of the pixels in the entire frame and described the amount of fluorophores in the image rather than the intensity from a single point. It is seen that for POCA the maximum is reduced to 1/2 while for PBCA, the intensity is reduced to 1/4. The intensity from NR668 has increased in the same period.

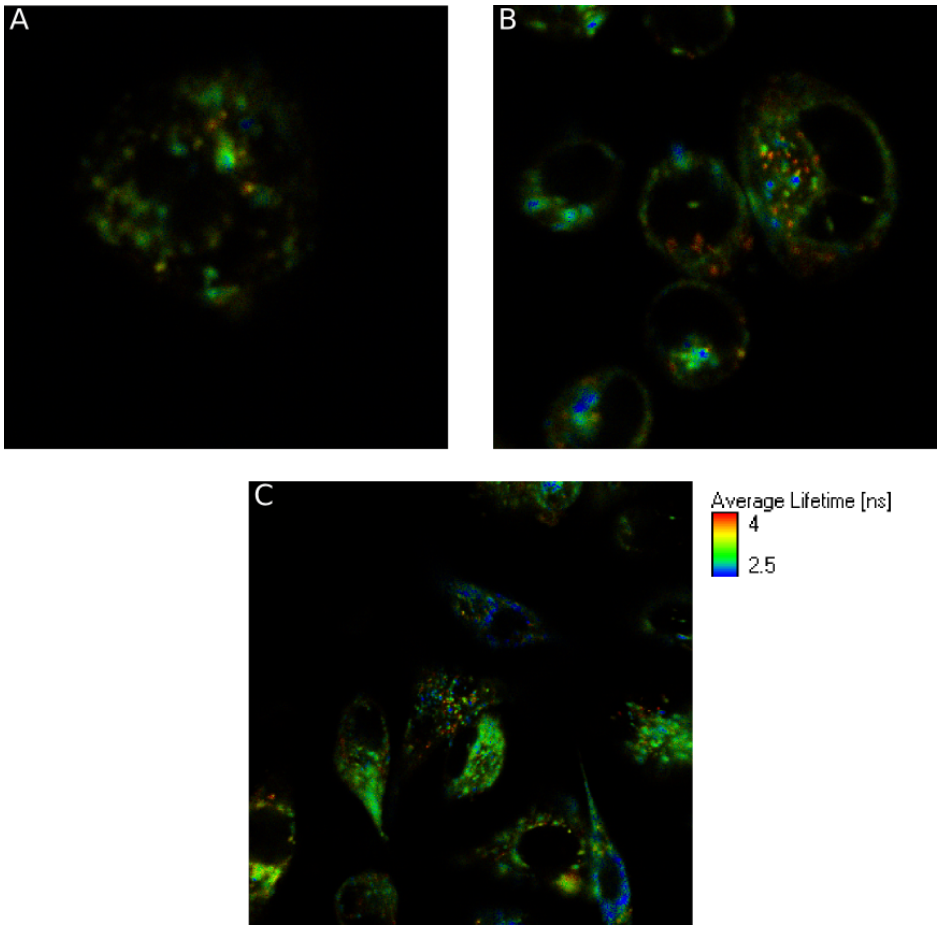

Figure 4.20: Images showing the lifetime of free NR668 inside PC3 cells after 5h (A), 24-48 hours(B) and 6-7 days (C). The colors depicts the average lifetime in each pixel adjusted to the scale attached.

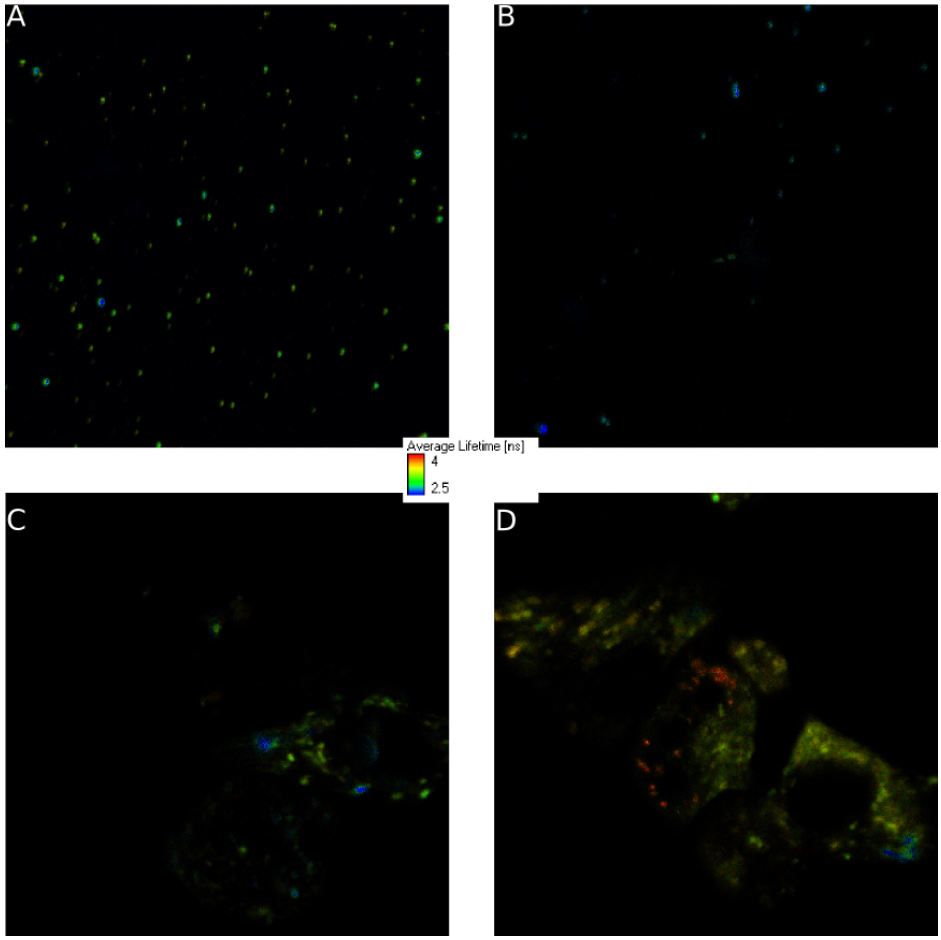

Figure 4.21: Images showing the lifetime of PBCA particles on the glass slides after 0h(A) inside PC3 cells after 5h (B), 24-48 hours(C) and 6-7 days (D). The colors depicts the average lifetime in each pixel adjusted to the scale attached.

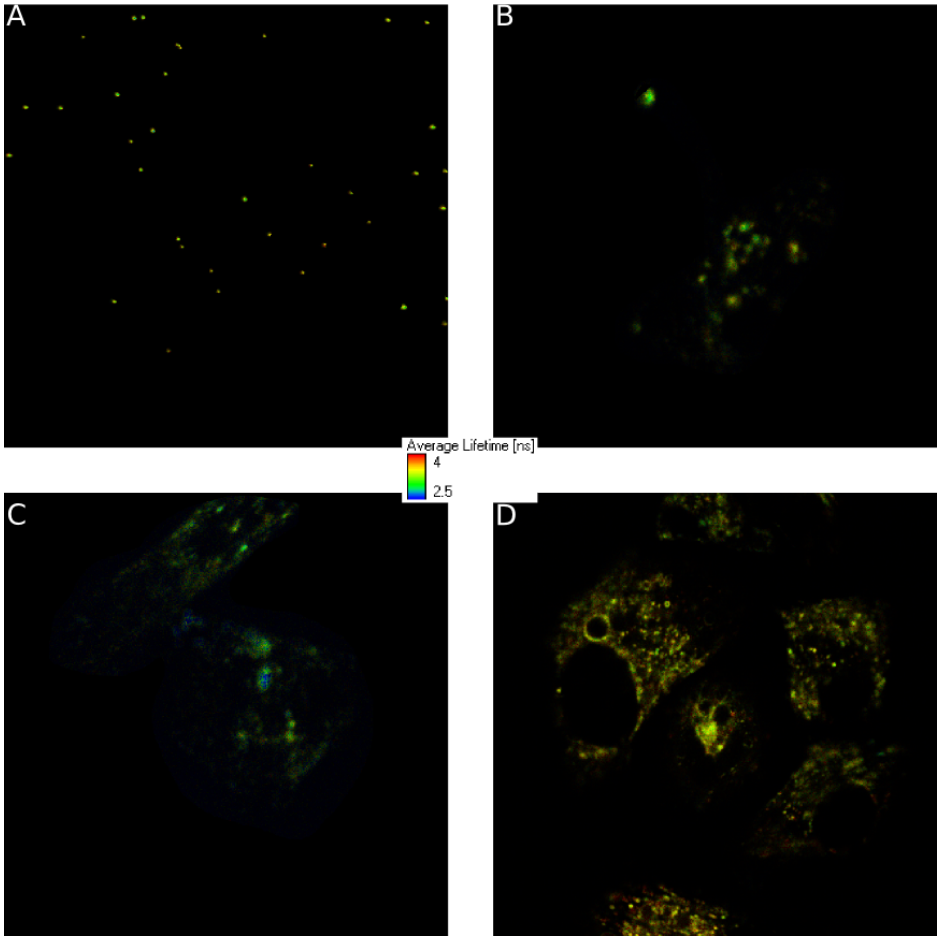

Figure 4.22: Images showing the lifetime of POCA particles on the glass slides after 0h(A) inside PC3 cells after 5h (B), 24-48 hours(C) and 6-7 days (D). The colors depicts the average lifetime in each pixel adjusted to the scale attached.

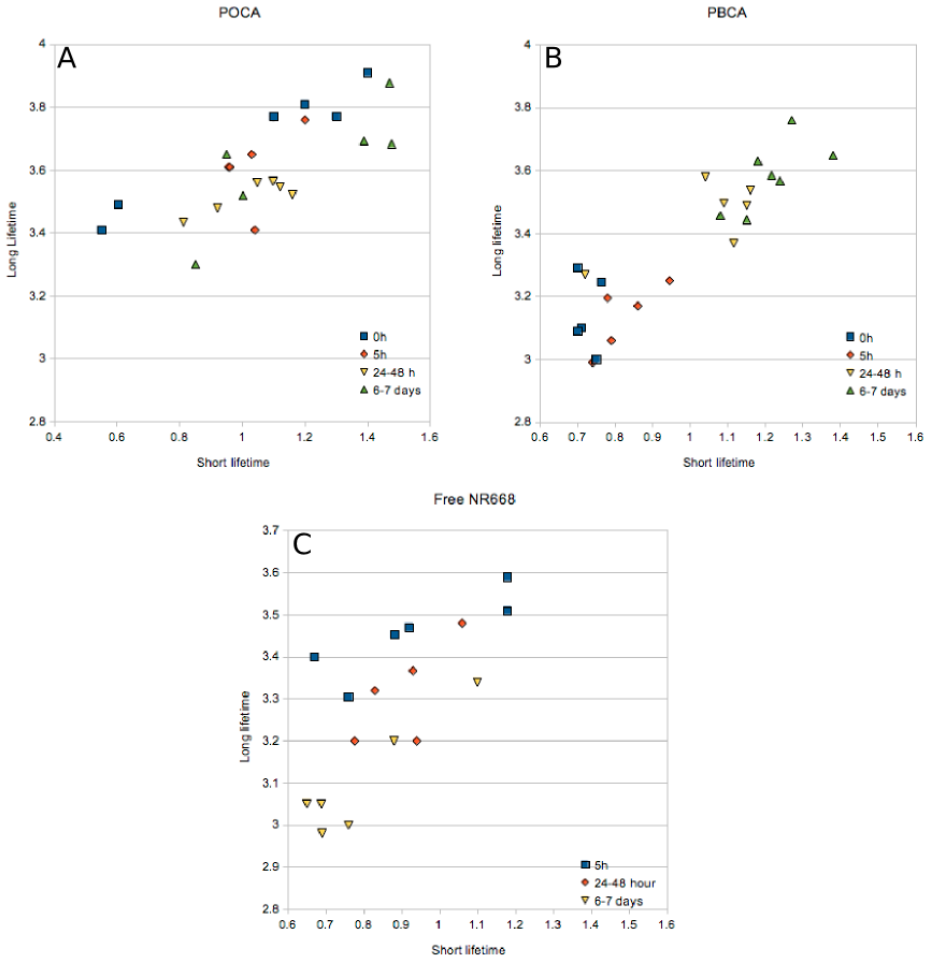

Figure 4.23: Scatter plots of lifetimes found when PC3 cells were incubated with POCA (A), PBCA(B) and free NR668(C) for various times.

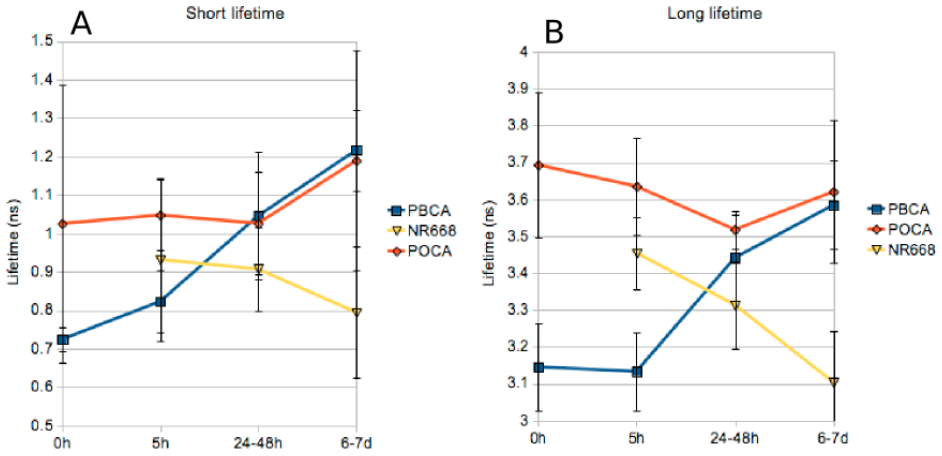

Figure 4.24: The average short (A) and long (B) lifetime on the various time points with standard deviation indicated (n=5).

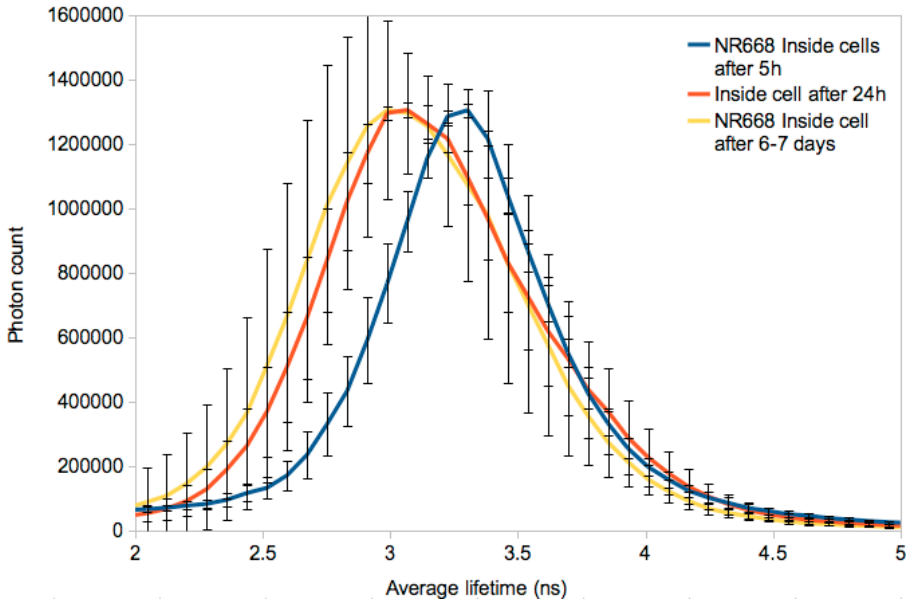

Figure 4.25: The lifetime distribution of free NR668 at different time points after incubation, error bars depicts standard deviation based on 5 samples for each curve. $\lambda_{ex} = 514nm$, error bars = SD, n=5.

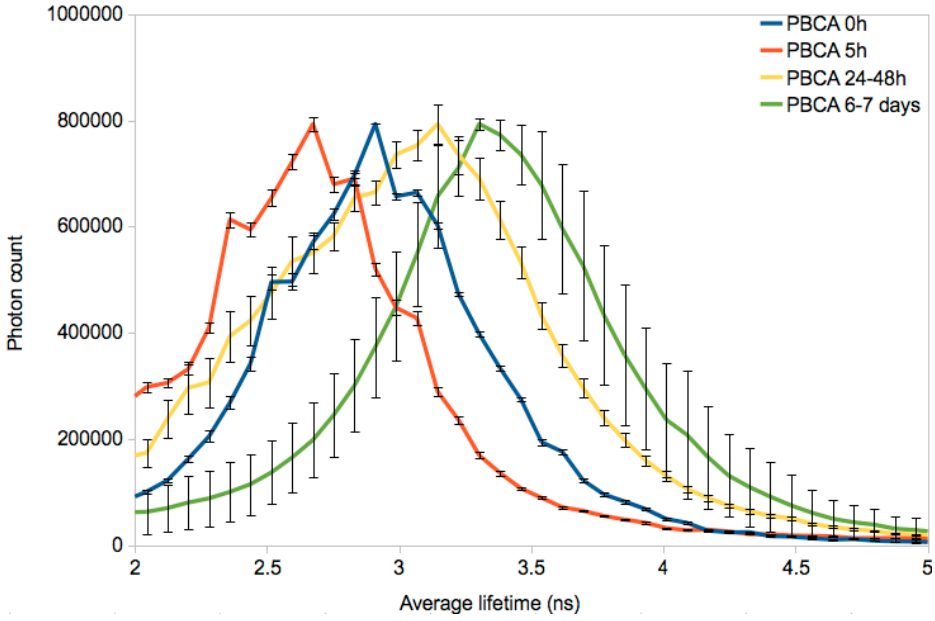

Figure 4.26: The lifetime distribution of PBCA particles at different time points after incubation, error bars depicts standard deviation based on 5 samples for each curve. $\lambda_{ex} = 514nm$, error bars = SD, n=5.

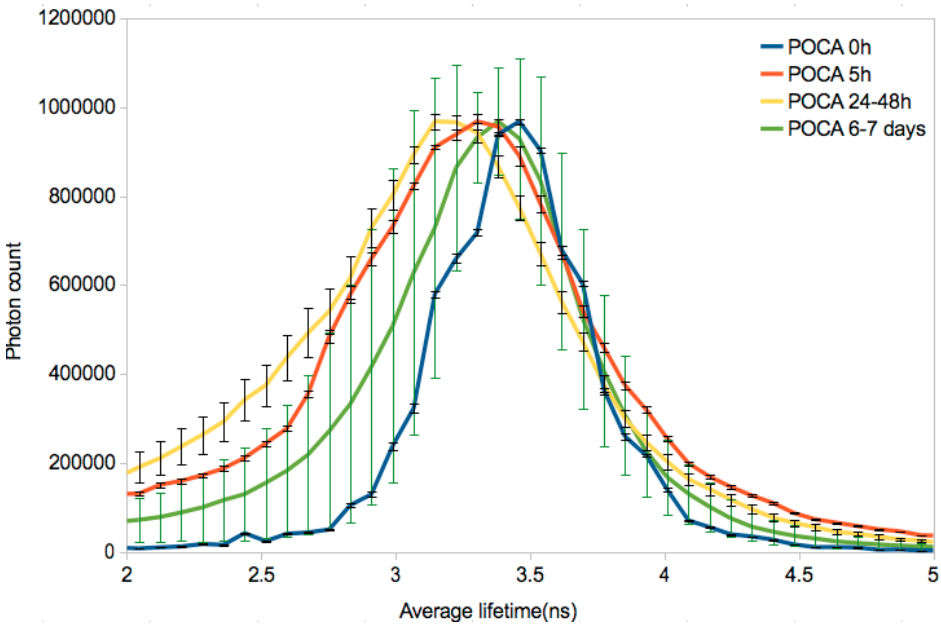

Figure 4.27: The lifetime distribution of POCA particles at different time points after incubation, error bars depicts standard deviation based on 5 samples for each curve. $\lambda_{ex} = 514nm$, error bars = SD, n=5.

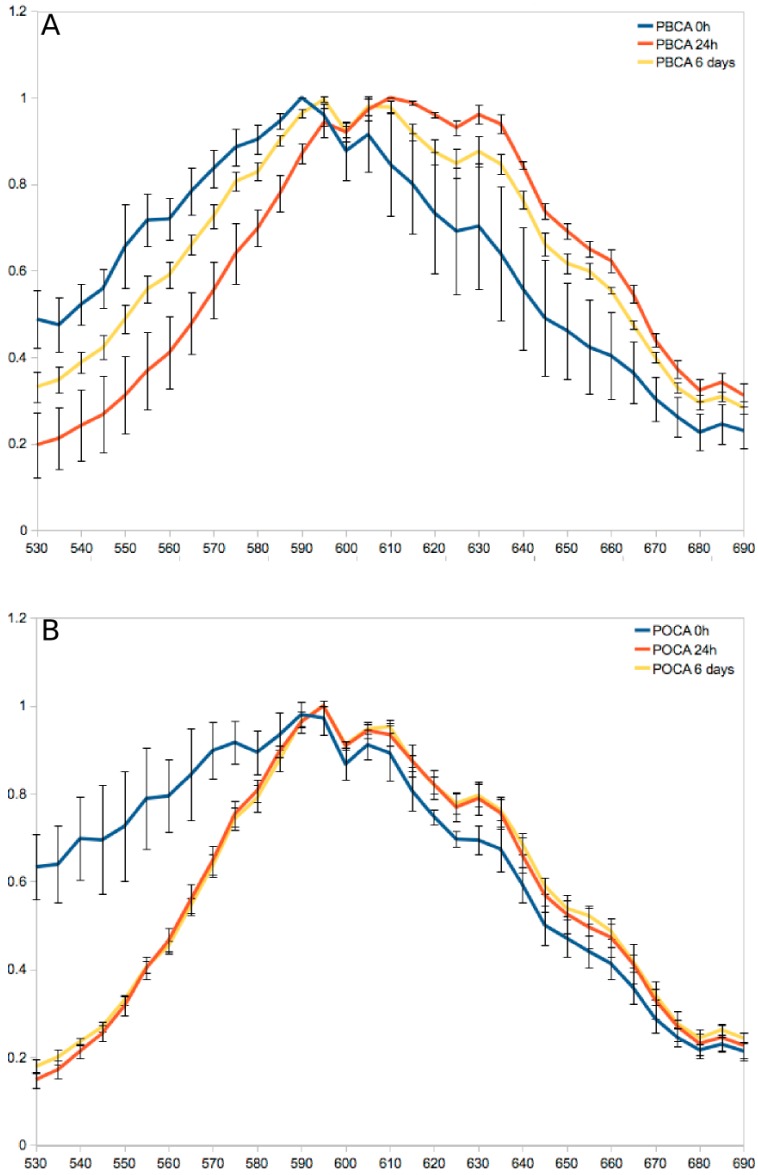

Figure 4.28: Emission spectra from PBCA (A) and POCA (B) after 0h, 24h and 6 days of incubation. In the 6 days sample, the medium containing NPs was removed after 24h. $\lambda_{ex} = 514nm$, Error bars = SD, n=5.

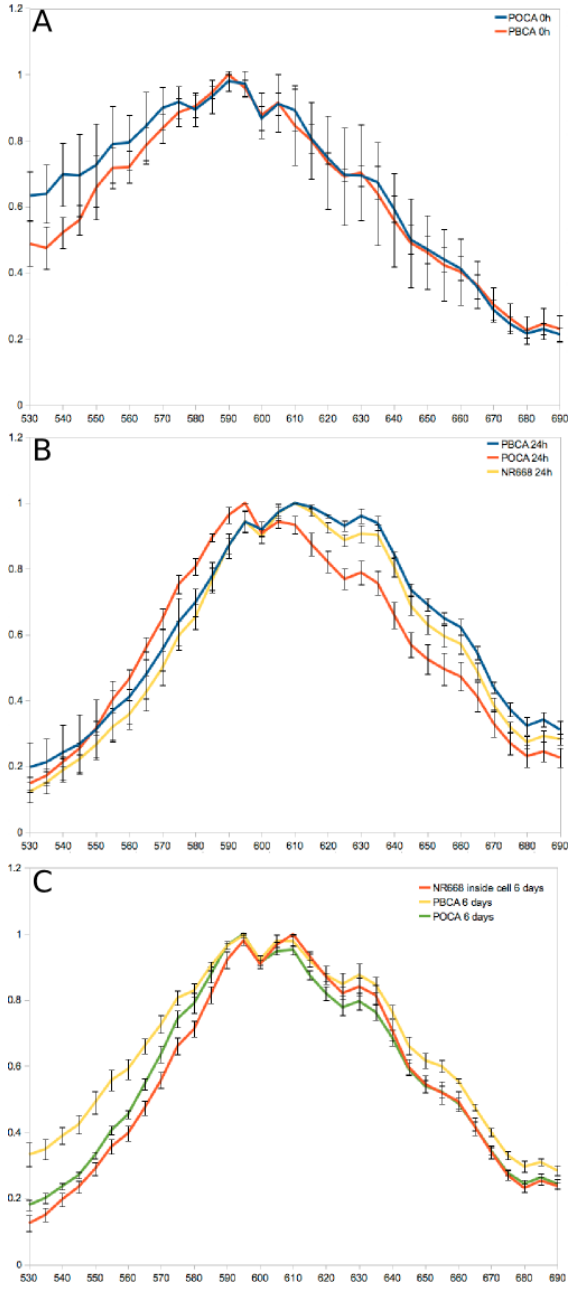

Figure 4.29: Emission spectra of PBCA, POCA and free NR668 at 0h (A)(PBCA and POCA), 24h (B) and 6 days(C). In the 6 days sample, the medium containing NPs was removed after 24h. $\lambda_{ex} = 514nm$, Error bars = SD, n=5.

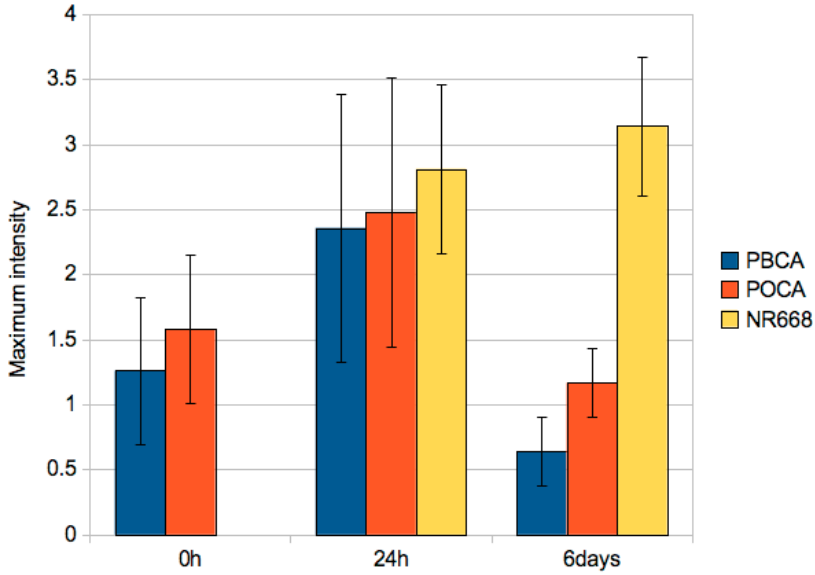

Figure 4.30: The intensity at the maximum excitation wavelength of NR668 after 24 hours and 6 days and PBCA and PACA after 0h, 24h and 6 days. Error bars = SD, n=5.

4.2.3 Triton treatment

In the preceding sections, it has been presented results describing the state of the particles based on the state of the fluorophore NR668. A method was sought for assessing whether the dye was actually fully released from the particle. PC3 cells were therefore incubated with POCA, PBCA and NR668 for 24 hours in CLSM imaging wells. While recording the cells 1 image/second with the SP8 confocal microscope, $15\mu L$ of 10% (Tx100) in DMEM was added to the well. The start point and effect with free NR668 is seen in figure 4.31, PBCA in figure 4.32 and on POCA in figure 4.33 . The staining is weak and challenging to present on paper, but it can be seen that the detergent has a different effect on the different particles and NR668. For NR668, Tx100 induced non specific, diffuse staining of the cellular compartment. A similar effect was seen with PBCA after 24 hours, but with slightly less intense staining. For POCA, many distinct points still remained after adding Tx100, essentially no diffuse staining was observed. The experiment was also performed after 6 days, with no observed differences to the results after 24 hours (data not shown).

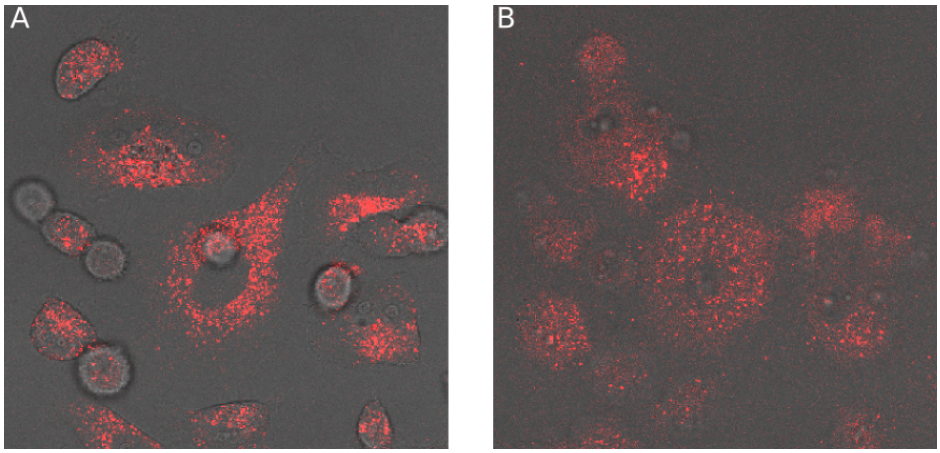

Figure 4.31: CLSM image of cells incubated with free NR668 for 24 hours before (A) and after (B) treatment with Tx100

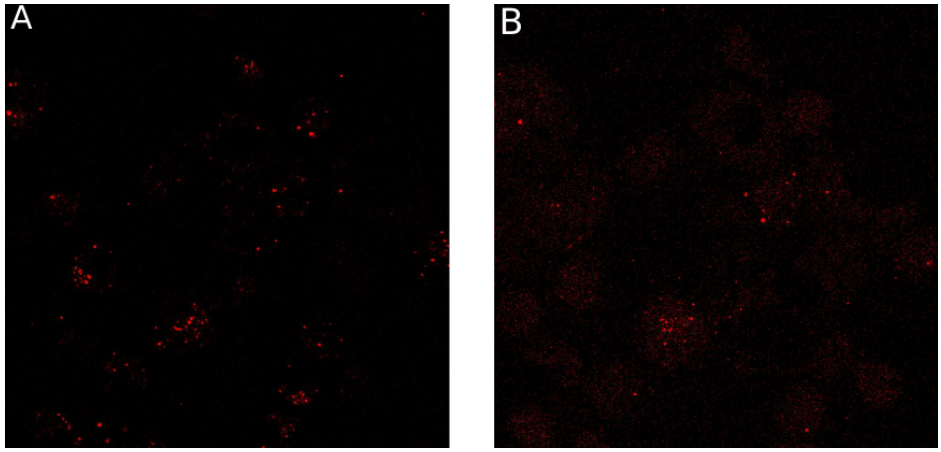

Figure 4.32: CLSM image of cells incubated with PBCA NPs for 24 hours before (A) and after (B) treatment with Tx100

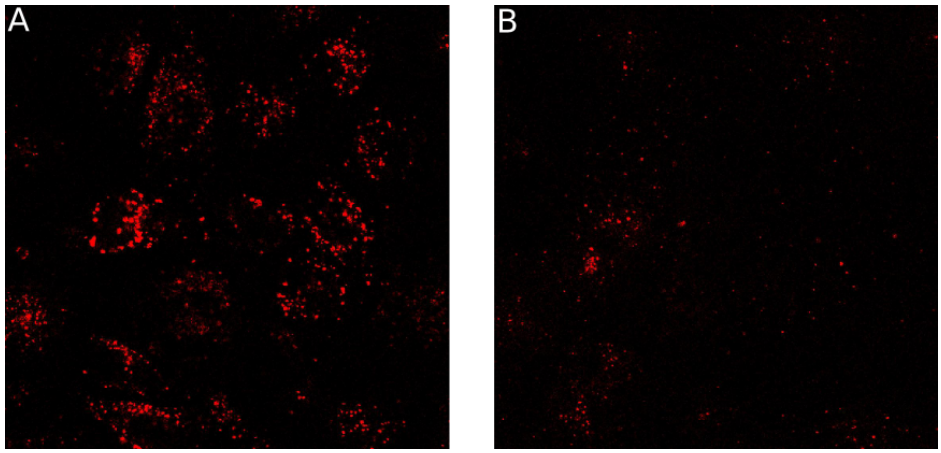

Figure 4.33: CLSM image of cells incubated with POCA NPs for 24 hours before (A) and after (B) treatment with Tx100

Chapter 5

Discussion

5.1 Initial remarks

This thesis describes the mechanisms involved in internalization and intracellular degradation of POCA and PBCA NPs. It was found that the particles are taken up through endocytosis and are probably degraded in cytosol, the route indicated by the results in this thesis is illustrated in figure 5.1. The figure illustrates 5 critical points that were evaluated in this thesis, the state of the NPs prior to cell contact (1), the uptake mechanism (2 and 3), the intracellular route (4) and the degradation (5). The discussion chapter has two main parts, cellular uptake (section 5.2) and intracellular degradation (section 5.3). Part 2 to 4 in the illustration are described in section 5.2 while 1 and 5 are described in section 5.3. Part 1 has been placed here because the methods used are the same as in the degradation study and because the results are important for comparison with the results after degradation. In both these sections, the quality and pitfalls of the experimental techniques are discussed before the results. In section 5.4, the overall consequences and impact of these results are discussed and future directions suggested.

5.2 Cellular uptake

5.2.1 Introduction

In previous work by Sofie Snipstad and Sara Westrøm, it was found that upon contact with cells, the fluorescent dye Nile red will leak out of the NPs and diffuse into the cells, eventually settling in intracellular lipid droplets. This made it impossible to assess the cellular uptake. It is worth mentioning that under CLSM,

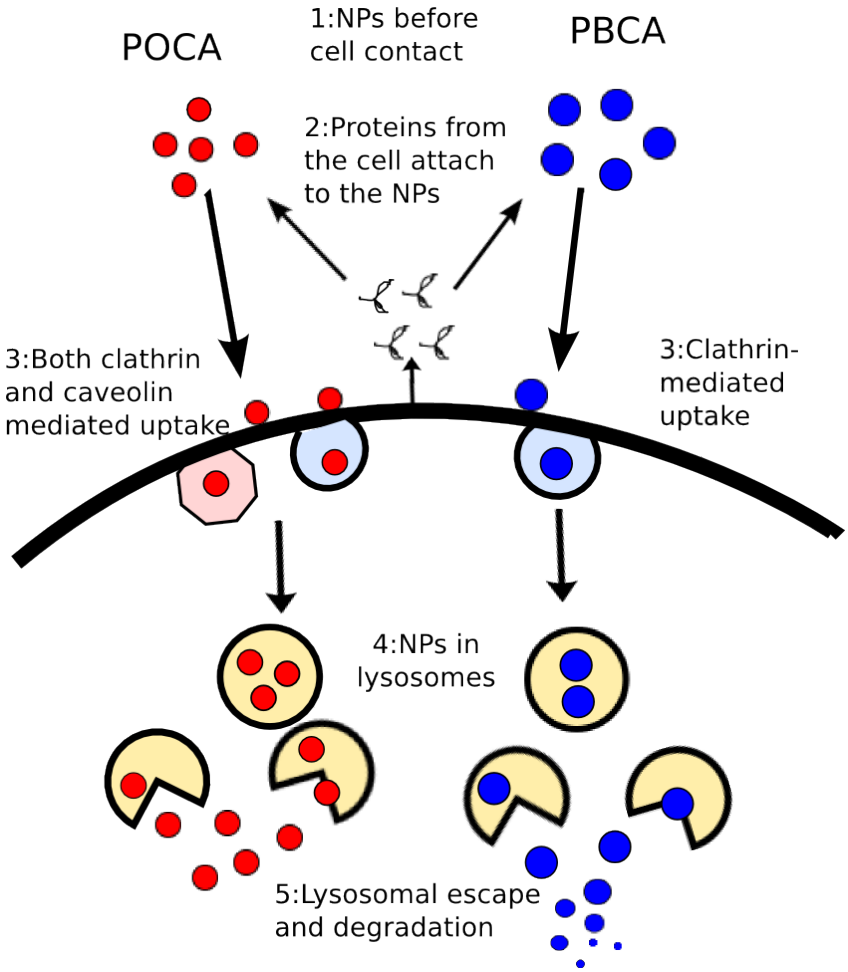

Figure 5.1: Illustration of the route taken by the NPs that was found in this thesis. Each point (number 1 to 5) shows a point that was evaluated and that is discussed in this chapter.

the lipid droplets and NPs have a striking similarity, separating them therefore calls for other methods than mere imaging. They found that the fluorescence could be taken up through contact mediated delivery that was not limited by endocytosis inhibitors nor incubation at 4°C.

This finding made it necessary to reassess the cellular uptake with a system where the fluorescent dye is tied to the particle. A collaborator of SINTEF Materials and Chemistry developed a modified edition of Nile red, NR668 with essentially the same spectral properties, but being a lot more hydrophobic allowing a stronger binding to the PACA NPs produced[90]. This work was started by Eva von Haartman, who was a visiting phd student fall 2013. It was then found that PC3 cells, a human cancer line chosen for this study, had essentially no uptake of the particles. The first part of the experimental work was therefore spent on unveiling why such variable degrees of uptake was observed in the first experiment of this thesis.

The cellular uptake was studied using conventional methods well described in literature and with significant expertise available in the research group at NTNU biophysics. The protocols for this part of the project was either found from previous work, or suggested by colleagues. The master theses by Sara Westrøm[93] and Sofie Snipstad[80] were frequently used.

5.2.2 Methods used

The uptake of NPs by PC3 cells was evaluated using FCM for quantitative analysis and CLSM for qualitative analysis. This is a well described method for evaluation cellular uptake kinetics uses by multiple groups in this field of research[82][109][110].

FCM offers high throughput analysis of cells, in this study, 10000 cells were analyzed in each run meaning that the collected population is huge. A question related to this topic is how to use controls and parallels to verify the different results. In figure 4.2 the uptake of POCA and PBCA NPs is presented in two diagrams. In A, the results and standard deviations have been calculated from 3 different experiments, in B, the results are calculated from 3 parallels in the same experiment. It can be seen that the measured uptake is relatively similar in A and B, but the standard deviation is far bigger in A. This is not too surprising given that the results from one measurement is an average of 10000 cells, as long as the wells in the sample holder are treated similarly, the exact same result can be expected to occur in two neighboring wells. The standard deviations measured in the two cases will reflect two different sources of uncertainty. The standard deviation from parallels in the same experiment originates from instrumental inaccuracy, while the standard deviation from different experiments reflects the biological variations.

For uptake studies, the important reason for doing CLSM is to validate the results from FCM by observing actually internalized NPs. FCM analysis will not distinguish between internalized material, and material bound to the plasma membrane. CLSM can help distinguish between these two scenarios.

A debatable issue is that many of the presented results have been normalized in some way, both due to prior knowledge and to make related results possible to compare. In figure 4.2, the actual uptake of POCA has been multiplied by 1/0.52 (see Appendix A) because POCA and PBCA have a different fluorescence. This could be dubious, or at least an important source of uncertainty to the results. Fluorescence intensity is not only a question of concentration of fluorescent dye, but also of the local environment. Nile red for example has a poor quantum yield in polar solvents and is essentially quenched in water[91]. Binding to low density lipoprotein, the intensity is more than 10 times higher than when binding to membranes and 2000 times higher than when bound to defatted albumin. The dye is highly fluorescent both in lipids and in organic solvents[92]. While the spectral properties will be throughly examined in section 5.3, the quantum yield of nile red is important when interpreting the uptake results. The uptake measured with FCM depends solely on fluorescence intensity. If, during the time inside cells, the dye is released from the particle and attaches to areas where the quantum yield or emission spectrum are different, this will affect the results. I therefore advice that trends and comparisons are emphasized more than exact values. One must also remember that NR668, the dye in focus, is not identical to conventional Nile red, the dye described in most of the literature[90].

In the experiment presented in figure 4.10, inhibition of endocytosis, another interesting normalization issue arises. The goal of that experiment was to asses the endocytosis mechanism, and the experiment was performed twice. In the two experiments, very different amount of uptake was seen, but the effect of inhibitors was exactly the same. When adding these two results together the experiment showing the highest uptake will dictate the overall result unless some normalization is done. Also, the different uptake will result in large standard deviations. This large standard deviation would easily be read as a large variability in the effect of inhibitors which would be a misassumption because the deviation seen would mainly be due to the change in absolute uptake of NPs. In the presented results, the two different experiments have been normalized to the maximum uptake in order to make the two results contribute equally and the make the standard deviation represent the actual uncertainty of the inhibition. The original histograms are found in the appendix part B.

5.2.3 Cellular uptake

Rate and variability of the cellular uptake of NPs

In order to study the interaction of NPs with cells, it is critical to understand and quantify the cellular uptake through endocytosis. For the degradation studies, it is also critical do first document that an actual uptake occurs. Figure 4.1 shows histograms of cells incubated with POCA and PBCA NPs for 3 and 24 hours compared to non-treated cells (light blue histogram). The control is needed to see the level of autofluorescence from the cells. Any increase from this value will indicate uptake or surface binding of fluorescent dye or fluorescently labelled NPs. Using CLSM and scanning in Z direction, it was confirmed that the source of fluorescence was inside the cells, this 3D information is challenging to present as images, figure 4.3 shows images from the top, center and bottom of the same cell where the particles are mainly seen in the middle one.

These results show that the particles are taken up by the cells and end up intracellularly. It was also found that the POCA particles were taken up more rapidly than PBCA cells, but that after 24 hours, the uptake of PBCA was equal or higher.

The uptake is relatively slow compared to other studies[110], but well within the expected range of endocytosis-dependent uptake. The rate of uptake varied heavily from different experiments. By observing the cells growing in the incubation flask it was found that the appearance of the cells changed every day from seeding until confluency was reached. At first the cells were rounded, and seemingly poorly attached to the bottom of the flask, it was therefore hypothesized that the cells required more time to fully attach than initially expected. It was found, as seen in figure 4.8 that the uptake depended heavily on days of culturing. It was seen that the shift in fluorescence intensity tripled if the experiment was performed 5 days after seeding, rather than 3 days which was initially suggested. From this result it is natural to hypothesize that the different state of the cells is the reason for the different uptake seen for POCA and PBCA NPs. However, no differences in state of the cells in PBCA and POCA sample wells were visually observed during the experiments.

This information is important to have when quantifying the cellular uptake, and probably also many other cellular processes. The rate depends on the state of the cells. Also, this information clearly limits the value of these results as a model for in vivo properties of this system. It must be expected that in a densely packed environment in tissue, the magnitude of uptake is different to that observed here. It was found that the mechanism of uptake was unchanged at different cell densities, indicating that the results on uptake mechanisms and intracellular routing could work as a model for in vivo properties. Similar observations were not found in the literature. This could be due to the effect being cell dependent, and more

important for slowly proliferating cells such as PC3 cells that fewer groups work with.

It is interesting that the POCA particles are taken up more rapidly than PBCA particles. These particles are very similar in physical parameters such as charge and size, and they are pegylated with the same molecules, details are found in table 3.1. Also, the difference is seen before significant degradation is expected to occur.

Effect of preincubation

This section explains point 2 in figure 5.1.

An increase in uptake was seen after preincubation with PC3 cells. Figure 4.6 and 4.7 shows the uptake of POCA particles, where the particle solution was either made fresh, made 21 hours in advance or made 21 hours in advanced and stored in an incubation flask with PC3 cells. This experiment was only done with POCA NPs, because after 24 hours, the PBCA particles will be partly degraded. It was seen that incubating with DMEM for 21 hours had no significant effect on the uptake, while incubating with PC3 cells for 21 hours increased the uptake by approximately 50%. This shows that there is no effect of degradation or leaking from the POCA NP, but that products from the PC3 cells increase the uptake. This could be proteins produced by the PC3 cells that bind to the particles and facilitates receptor mediated uptake. Either a protein that the cells secrete continuously, but most likely the production is triggered by the NP. To further evaluate these mechanisms would be interesting, but it was beyond the scope of this thesis. However, understanding this process is important and suggested for future studies.

Uptake mechanism

This section explains point 3 in figure 5.1.

The NPs are taken up by the PC3 cells through endocytosis. The control at 4°C shows essentially no uptake which means that the uptake is energy dependent. Inhibiting the two main endocytosis pathways also drastically reduced the uptake, this is seen in figure 4.10.

It is important that the 4°C cells show no uptake, otherwise, one would expect that the particles are still leaking fluorescent dye. For example in Sofie Snipstads master thesis, she found only a very limited reduction of uptake at 4°C [80]. At 4°C, the cells are unable to perform energy dependent processes. Some papers see only partly inhibition at 4 °C, which implies that also energy independent processes such as diffusion takes place[111][112][113]. It is not rare that only limited inhibition is seen at 4 °C, but full inhibition is also reported[114].

Inhibition of CME was done using Chlorpromazine with a protocol used by others studying endocytosis in PC3 cells[107]. Figure 4.10 shows that the uptake of both POCA and PBCA particles are reduced to approximately 50%. Chlorpromazine works by inhibiting a GTPase involved in formation of clathrin coated pits[71] and is reported to be very selective for CME, but not function properly in some cells[61].

Inhibition of caveolin-mediated endocytosis was done using a protocol for Genistein that had been shown effective for PC3 cells[108]. It was found that the uptake of PBCA particles was not inhibited by Genistein indicating that caveolin-mediated endocytosis is not an important mechanism for internalization of PBCA particles in PC3 cells. For POCA, Genistein had a significant effect reducing the uptake to 52%. This suggests that for POCA particles, clathrin- and caveolin-mediated endocytosis contributes equally to the uptake and that the entire uptake of POCA can be accounted for with these two mechanisms. Genistein is less selective than Chlorpromazin, and could possibly inhibit also other mechanisms than caveolin-mediated endocytosis[61]. Both tyrosine kinase and F-actin is blocked, which means that CME could also be inhibited either if tyrosine kinase receptors are involved[72], or if F-actin is blocked from the clathrin coated pits[115]. It is therefore possible that other mechanisms than caveolin-mediated endocytosis might be the reason for the different effect of Genistein on the uptake of POCA and PBCA.

While the exact mechanism inhibited by Genistein remains disputed, the results reveal that the POCA and PBCA particles are not as similar as the physical data and production method might suggest. These two particles are made using the same chemistry, where only the alkyl group on the monomer is different. Ideally though, the particles should be covered with a dense layer of PEG, making the core material invisible to the cells. There are two parameters that seem most likely the source of this difference, size and surface. From table 3.1 it is seen that the POCA particles have a diameter of 151 nm, PBCA 177 nm. The diameter is measured immediately after dilution from the particle solution and with dynamic light scattering (DLS), reporting the hydrodynamic diameter. However, it was found by Andreas Bøe[7] that in a buffer of pH of 7, the PBCA would swell by more than 25% within the first 10 hours while for POCA the swelling was limited to less than 5%. This means that the actual size difference seen by the cells might be bigger, and that the diameter of PBCA will exceed 200nm making the size difference between the two particles around 50nm within hours after dilution. In the experiments, the particle dilution was done within one hour prior to start of incubation. It has been documented that size is an important parameter for the amount of uptake. Rejman et al.[63] found that increasing the particle size from 50 to 100 nm would reduce the uptake 3-4 fold while increasing the size from 200 to 500nm would reduce the uptake 8-10 times. They also saw that the smaller

particles could be detected immediately after incubation while the particles at 500 nm were only detected in significant amounts after 2-3 hours. Interestingly, this same group also saw that CME had an upper size limit of approximately 200nm in the melanoma cell line studied. Larger particles (mainly 500nm) were internalized by a caveloae-dependent pathway. This is not caveloin-mediated endocytosis as originally described though, the flask shaped caveolin has been reported to be smaller than 100nm and often closer to 50nm[116][66]. In this study, the smaller particles (POCA) showed a connection to caveloae endocytosis, while for the larger, no such connection was found. Still, being far from the 500nm size studied, the cut off at 200nm is more relevant to this study. It is not unlikely that at least some of the differences seen is a result of the different size of the NPs.

Another option is that the surfaces of POCA and PBCA in reality are different and binds biological molecules with a different affinity. The particles are both pegylated using the same surfactants BRIJ 35 and Jeffamin. Also, the measured zeta potential is very similar (table 3.1) and recent results from nuclear magnetic resonance spectroscopy indicates that the amount of PEG on the NPs is essentially the same. The potential difference is then likely to be the homogeneity of the pegylated surface. Although there are many ways of measuring the amount of PEG, non of them are straightforward nor will they tell you the exact density of surface bound molecules[117]. The effect of PEG on the PBCA particles in this thesis was described in previous work[8], where it was found that the pegylation was important to avoid aggregation in certain media, but not sufficient to fully avoid the formation of a protein corona in protein-containing solutions. It has been shown that increasing the amount of PEG can decrease the uptake by cells especially particles that do not target specific receptors[114][118]. and that for PACA NPs the phagocytic uptake is decreased 10-fold with sufficient pegylation[110].

It was found that incubation the NPs with PC3 cells for 21 hours prior to the uptake study would increase the uptake significantly. This could indicate that the cells produce a protein that attaches to the particles and allows for receptor-mediated uptake. This secreted protein could have different affinity for the two particles. Given that the amount of PEG is the same, it is likely the monomer, BCA or OCA that lead to the difference in affinity something which indicates that the particles are not sufficiently pegylated. Interestingly, in rat brain endothelial (RBE4) cells that are being studied by a colleague (unpublished results), the uptake of PBCA is higher than for POCA, and it was found that PBCA is taken up through both clathrin and caveloin mediated endocytosis while POCA was only taken up through the clathrin-pathway. These results are opposite of those observed for the PC3 cells in this thesis. This observation can be explained by the different cells secreting different proteins that have affinity for different surfaces,

which is interesting because brain endothelial cells which constitute the blood brain barrier are known to specifically endocytose PBCA NPs[119][120]. These results implies that secreted proteins might be the reason for this affinity.

If differences in pegylation is the reason behind the different uptake of POCA and PBCA, heterogeneity in the pegylation is likely the reason which implies that POCA is more heterogeneously pegylated than PBCA. POCA is the particle that was shown to be endocytosed through caveolin-mediated endocytosis. One could therefore argue that the difference seen is due to POCA being compatible with caveolin-mediated endocytosis while PBCA could be incompatible with this endocytosis mechanism. A closer look at the numbers however will show that even the amount of POCA uptake inhibited by Chlorpromazine is bigger than the total uptake of PBCA, showing that the different magnitude of uptake is not solely due to caveolin mediated uptake of POCA NPs.

Caveolin is used to internalize membrane lipid rafts, mobile areas in the plasma membranes densely packed with lipids such as cholesterol[116][121]. These lipid-rich areas are more hydrophobic, and might show some affinity towards hydrophobic, poorly pegylated areas of the NP. For the internalization of these lipid rafts, the tyrosine kinases inhibited by Genistein are important[61]. One could hypothesize that POCA NPs attach to lipid rafts and are endocytosed through a tyrosine kinase dependent mechanism.

This theory is far more speculative than the explanation based on particle size or protein affinity, but it can not be ruled out that heterogeneous pegylation is involved in the uptake difference.

After 24hours, the uptake of PBCA has reached that of POCA in terms of mean fluorescence intensity from the cells. To draw conclusions based on this information is challenging because at 24 hours, parameters such as degradability of the particles and properties of the fluorescent dye comes into play. However, the results are quite striking, after 3 hours, POCA is endocytosed 3-10 times more than PBCA, while at 24 hours, the uptake is similar. The possible explanations to this observation can be grouped in two. Either the PBCA particles are actually taken up more effectively than POCA after some hours, or the result is due to an artifact possibly created by the fluorescent dye.

The PBCA particles will be partly degraded after 24 hours, this means that the particle will release hydrophobic dye, and some of this increased uptake might be due to this effect, the control at 4°C also showed a minor uptake of NR668 for the sample with PBCA particles. The degradation is limited though, in Bøes master thesis[7], it was found that the PBCA particles were a lot more stable in cell medium than in a pH 7.4 buffer. It is not unrealistic though to expect increased uptake as the particles are becoming slightly degraded and less pegylated. It is likely that the increased uptake of PBCA seen with time is due to degradation and internalization of either degraded particles or released NR668.

It is also possible that the measured high uptake of PBCA after 24 hours is an artifact caused by the interaction between the particle, cell and the hydrophobic dye NR668. From the results presented in this thesis and in work by Andreas Bøe[7] one can assume that the PBCA particles are, at least to some degree, degraded after 24 hours intracellularly. This will release fluorescent dye an allow it to diffuse to other locations. NR668 is a very hydrophobic molecule and will if degraded from the particle, diffuse to other hydrophobic regions such as intracellular lipid droplets. Nile red was originally developed as a stain for these droplets[91]. In the original paper describing NR668, they found that auto-quenching occurs if the dye is too concentrated. In 40nm oil droplets, Klymchenko et al.[90] found that 5%wt. of NR668 in the droplet would have a quantum yield of 13%, while 1%wt. NR668 had a quantum yield of 60%. This lead to somehow surprising result that the particle can be equally fluorescent even if 4/5 of the dye has leaked out. However, spectral measurements presented in figure 4.28A do not show the blue-shift that would be expected with increased quantum yield. Also, the theoretical amount of NR668 in the particle is only approximately 0.2%, far below the concentrations used in the referred article. There is no guarantee though, that the dye is uniformly distributed in the NP and that higher concentrations can not be found locally.

Intracellular routing

This section explains part 4 in figure 5.1.

Colocalization with lysosomes was found, less so for early endosomes. Uptake through endocytosis should lead to the particles being routed through early endosomes, late endosomes and lysosomes[122], colocalization with these organelles would therefore be expected. Figure 4.11 and 4.12 shows PC3 cells transfected with Cell Light GFP transfection agent for staining early endosomes. It was found that transfected cells had a high expression of GFP making colocalization difficult. This is probably due to deficient staining protocol and could be improved in future studies. In figure 4.12, the intensity has been reduced, making only the brightest areas visible, a possible colocalization is seen under the white arrow. Early endosomes has a very short lifetime and will normally become a late endosomes within 10 minutes after internalization[75]. Although some colocalization with early endosomes would be expected, it is not too surprising that this is difficult to observe given the slow rate of uptake and the limited time spent on perfecting the staining protocol.

The particles were found to colocalize with lysosomes. Figure 4.13 shows a PC3 cell incubated with POCA NPs for 24 hours and stained for lysosomes. In the image, pixels will be colored yellow if roughly equal intensity is detected in the two channels. The image shows that many particles are found inside lysosomes, but also that many particles were found to not be inside lysosomes at this time

point. The colocalized lysosomes and NPs were found in close proximity of the cell nucleus. The image is consistent with images taken by other groups who have looked for colocalization with lysosomes and NPs[123][61][124], where the lysosomes are also found in proximity of the nuclei.

Finding the NPs colocalized with lysosomes verify that that the particles are going through endocytotic uptake and intracellular routing. It is interesting however, that these particles do not seem to remain in the lysosome. The degradation studies showed a rate of degradation for the PBCA particle that is much more rapid than what would be expected if the particle remained in lysosomes. Also, in image 4.13, only a fraction of the NPs are colocalized with lysosomes. The mechanism for lysosomal escape is not understood nor described in the literature[77], but should be the goal of future studies.

5.3 Intracellular degradation

5.3.1 Introduction

In previous work, Andreas Bøe evaluated the degradation by measuring decrease in the particle concentration in different solutions and at various time points using Nanosight[7]. He found that the POCA NPs were essentially stable under a biological relevant range of pH, but some degradation was seen at pH 7.4 in combination with esterase. The PBCA particles were stable at pH 4, relatively stable in cell medium and pH 5.6, but would degrade quite rapidly at pH 7.4 with a half life of less than 24 hours. No effect of esterase was seen for the PBCA particles. He also found that the particles would increase in size in cell medium, likely due to swelling, and that this occurred more for PBCA than POCA. In the study and discussion of intracellular degradation, his results are highly relevant.

For measuring intracellular degradation of NPs, no established method was available. In the literature, Förster resonance energy transfer (FRET) is often presented as the golden standard for detecting degradation. For this technique, two dyes with a suitable excitation and emission spectra must be in close proximity to get a FRET signal indicating that the particle is still intact[125]. Unfortunately, the PACA particles produced at SINTEF are very sensitive to properties of the load and loading two dyes functioning as a FRET-pair to the same particle has not yet been accomplished. A lot of effort was therefore put in to exploiting properties of NR668 to detect changes in the local environment of the fluorescent dye and to draw some conclusions based on that information. However, NR668 being a new dye, no literature is available as reference. Therefore articles describing conventional nile red are used, but with great care as reference and comparison to understand the observed results.

5.3.2 Methods used

Finding unambiguous signs of the intracellular degradation of the NPs was difficult and conclusion are based on results from multiple techniques which all gave some clues, but neither offered the full solution. In the literature, similar systems have been evaluated using self-quenching[126], FRET[127], and often the degradation is measured in solutions and assumed to be the same intracellularly[128]. These systems were either not available or desirable in this situation, and other methods were sought. Snipstad[80] had shown that free nile red would appear both as bright spots and diffuse staining inside cells, this could be easily observed. Greenspan et al.[91] have described the spectral footprint of Nile red and a method for spectral separation of nile red in lipid droplets and diffuse nile red in cytosol. However, this diffuse staining was never observed nor imaged for NR668 except when artificially induced by adding detergent to the cells (section 4.2.3). The main property of NR668 compared to nile red is the increased hydrophobicity[90]. It is likely that this increase limits the amount of nile red binding to proteins in cytosol because NR668 has a stronger attraction towards the lipid droplets. Intracellular free NR668 was visually similar to POCA or PBCA particles, imaging did therefore not offer any knowledge of the intracellular degradation.

FLIM

The fluorescence lifetime of the fluorescent dye is a property related but not similar to the emission spectrum. If a suitable dye is found, FLIM is described as a potentially ideal tool to observe intracellular processes because the lifetime depends on excited state reactions, but is independent of fluorophore concentration and light-path length[129]. For nile red, a selection of properties have been explored for lifetime measurements such as elastic modulus of the encapsulation material [89], solvent polarity[95], hydrogen bonding strength[130] and concentration of cholesterol[131] in the local environment. To my knowledge, no studies on the lifetime properties of NR668 are published.

From the referred literature and from experience during the work in this thesis, it is found that the fluorescence lifetime of the excited state of NR668/Nile red is very sensitive to the surrounding environment. This, and the lack of comparable studies made it challenging to interpret the results. The number of variables inside the cell is vast, and the intracellular behavior and location of the NP and NR668 is not fully characterized. The results from FLIM did offer some clear trends that could support conclusions, but also results opening up for discussion and further investigation. Given the limited time available, further investigations had to be postponed to future studies. One concrete case that could be studied in the future is the possibility to find a distinct lifetime of NR668 in lysosomes

by measuring the lifetime of spots colocalized with labelled lysosomes. A theory would be that NR668 has a clear signature from inside a lysosome given the low pH[132], it was found that for degraded/slightly degraded particles, the pH would have a significant effect on the measured lifetime (figure 4.19 and table 4.2). A drawback of FLIM is that it might be too sensitive for some applications and for doing quick and easy measurements. Some variability within the results from each sample was found (table 4.2), this makes it necessary to do multiple measurements for each sample if one wants to record and compare lifetimes numerically. Each measurement is also time consuming and requires manually selecting suitable ROIs. Also, some work was required to find suitable imaging conditions that minimized the noise and reflections from the sample holder (figure 4.16).

It was found that NR668 holds a great potential for monitoring intracellular processes. If cause and effect of various parameters are further analyzed, NR668 could provide information on state of the particles and possibly colocalization with endocytic vesicles.

It was not clear how to best present the results from FLIM. Figure 4.23 show scatter plots of exact lifetimes, while 4.25, 4.26 and 4.27 shows the distribution of lifetimes in the same images. The images in figure 4.20, 4.21 and 4.22 resemble fluorescence microscopy images, but each pixel has been given a color related to the average lifetime in that pixel. Although calculated from the same set of images, these different ways of presenting and reading the data each holds some specific information.

Spectral analysis

The measurement of lifetimes and spectral analysis of particles outside cells was done in the proximity of the sample well. It is important to be aware that this imaging condition is suboptimal and different from the images and measurements of particles inside cells. An example of this is the emission spectra presented in figure 4.28. It can be seen in the measurements on the first time point, high intensity is seen in the blue(short wavelength) side of the spectra. This intensity could possibly be due to the scattering from the glass. The excitation laser at 514nm is relatively close to the detector range of FLIM (565-615 nm) and the lowest detected wavelengths in spectral analysis (530 nm) and could therefore lead to detected light that is scattered from the glass and not emitted by the fluorophores.

The reason for doing spectral analysis was to confirm the observations from the FLIM measurements. Compared to FLIM, spectral analysis has the advantage of being fast and well described in the literature. It was also found that the emission specter is less sensitive to the environment than FLIM making it easier to separate noise and randomness from true differences. This is seen as a generally lower standard deviation in the results from spectral analysis than in the results

from FLIM. A major drawback of spectral analysis is that it is depending on fluorophore concentration, adding a variable that is difficult to control to the equation.

Triton

Triton is a detergent that will solve lipids and lipid membranes. The reason for using it in this thesis was to see if some red dots would be dissolved (lipid droplets) and others would remain (intact NP) upon addition of Triton. The idea came from an article by Bjørkøy et al.[133].

It was found that the experiment had a low reproducibility, the magnitude of the effect was different from time to time. Sometimes the cell in focus would immediately disrupt and all fluorescence stain leak out to the environment, and sometimes hardly any effect was seen. Separating lipid droplets from intact NP was therefore difficult due to this. However, in cases were the effect was relatively low, a diffuse staining of the cell would occur within 45 seconds after addition of Triton. This was observed for free NR668 and PBCA, but not for POCA.

5.3.3 Degradation

Nanoparticles before cell contact

This section explains point 1 in figure 5.1.

FLIM images suggest that especially the PBCA particles are not all fully polymerized towards the core of the particle, this is seen in figure 4.17. This has not been documented previously, but transmission electron microscope (TEM) images taken in an ongoing study indicate the same (unpublished results). With both imaging systems (TEM and FLIM), this is especially evident for the larger particles. With FLIM, it was found that with fresh particles, the lifetime did not depend on the pH in the solution (table 4.1) while after 6 days in cell medium (table 4.2) the lifetime from PBCA particles varied significantly with pH. No change was found for the POCA particles. The lifetime in PBCA was found to be shorter with low pH ranging from 0.85/3.04 at pH 4 to 1.31/3.71 at pH 7.2 (short lifetime/long lifetime). It has previously been documented that the PBCA particles are relatively stable in cell medium with more than 2/3 of the particles left after 4 days incubation[7].

The result of pH variations could support the theory that the particles have a liquid or poorly polymerized core. It is hard to imagine the fluorophores encapsulated within a solid NP changing with the pH because the fluorophore is protected inside the particle. For the POCA particles, very little change in lifetime was observed intracellularly although many of the NPs were found to colocalize with lysosomes. Also, when the particles are imaged directly after being mixed with

cell medium, no effect was seen. This indicates that the lifetimes presented for PBCA NPs in table 4.2 are not intact NPs. Here it was found that the lifetimes varied significantly with pH in the buffer solution. The NPs are attaching to the sample well more readily after 6 days than immediately after mixing. Especially at low pH, no particles were found on the sample well from freshly made particle solutions. This suggests that the particles have become less pegylated during the time in DMEM and the same effect was observed for both POCA and PBCA particles. The lifetime from POCA NPs however does not depend on pH, and the particles are therefore still solid. For PBCA, the result suggests that the material stuck to the sample well is not solid NPs, but might be degraded or slightly degraded polymer material in an oil droplet.

The initial lifetime from NR668 in POCA and PBCA NPs is different due to either different elastic modulus of PBCA and POCA or due to different hydrophobicity. It has been established that the fluorescence lifetime in polymer material is highly dependent on the modulus of elasticity[89]. POCA is a harder material than PBCA and a longer initial lifetime was found (table 4.1). With the limited amount of literature available for comparison, it is an important confirmation of the technique that the finding is in compliance with one of the few available references[89]. The numerical values match the expected values from similar materials examined in the referred article, if one consider the expected value for solid particles rather than particles with a liquid core. An important source of error that comes into play here is that the population of particles stuck to the sample holder might not fully mirror the complete population of particles. If the imaged particles are bigger and poorly polymerized, this might also affect the pegylation and stability in solution. This result lead to the conclusion that the initial measurement of particles at 0h should be handled with some care. This also suggests that a liquid core might not be an important property for most particles in the solution.

The most important conclusion from this experiment is that the information obtained at 0h for both lifetime measurements and spectral analysis is not from intact particles and should be handled with care. For example in figure 4.26, where the distribution of lifetimes from PBCA NPs at different time points is seen, the distribution from 0 hours does not fall into the trend seen at the other time points. This could be because the 0h measurement is done on the subpopulation of particles that stick to the sample well that are poorly polymerized and degrades faster.

Intracellular degradation

This section explains point 5 in figure 5.1.

It was found that the PBCA NPs degrade significantly during 24 hours intracellularly while the POCA particles remain essentially unchanged. This rate of

degradation is in compliance with previous work[7].

This is not as obvious as it might seem. In lysosomes the pH is close to 4[25] and it has been documented that both these particles are highly stable at this pH. In endocytosis, the internalized material is normally degraded in lysosomes, where enzymes and low pH is effective to most biological material[134]. Different pathways can be taken from the lysosomes, but degraded material is often released in cytosol, or trafficked out of the cell through autophagy/exocytosis[25]. The PACA particles are poorly degraded in the lysosomes, this could make exocytosis a likely outcome. It has been observed by others that NPs that are covered in albumin from cell medium is rapidly cleared by exocytosis[135]. For the drug delivery, this is a challenge. The goal is to create particles that can release the drug inside cells in a controllable manner. Exocytosis or continuous habitation of lysosomes would be devastating to the potential of these NPs as platforms for drug delivery. In this thesis it is shown that the NPs are still inside the cell after 7 days. It is also shown only partly colocalization with lysosomes, and a degradation rate incompatible with storage in lysosomes has been found for the PBCA particles. Together, this is a clear sign that the particles are able to escape the lysosomes and degrade in cytosol. If this is the case, this is an important discovery making the particles very promising for drug delivery.

Figure 4.15 shows the first attempt to observe intracellular degradation after 24 hours. It can be seen that the distribution of free NR668, PBCA and POCA NPs are visually very similar inside the cell. Conventional nile red is a stain for lipid droplets and NR668 is even more hydrophobic which makes it very unlikely to observe the dye bound to a protein or membrane. Lipid droplets/lipid bodies are intracellular storages of fat with a size ranging down to 100nm[136].

The degradation was documented using FLIM, spectral analysis and cell lysis with Triton. The images in figure 4.20, 4.21 and 4.22 shows the distribution of average lifetimes from 2.5 ns to 4 ns inside cells that have been incubated with NPs or free NR668 for various times. The images show that for free NR668, defined areas of different colors are visible after only 5 hours and very distinct after 24-48h. For PBCA NPs, the same tendency can be seen after 24-48 hours, and after 6-7 days also areas of lifetimes close to 4 have started occurring. For POCA NPs, even after 6-7 days, the lifetimes is essentially the same ranging only between yellow and faint green. Intuitively, this result suggest that PBCA NPs will eventually express the same distribution of lifetimes as free NR668, suggesting that the dye inside the particle has been released to the surroundings.

To get more quantitative knowledge, ROI's were selected in each image, and the decay was approximated to a two exponential decay. The two-exponential decay was used because of the observation that single-exponential decay gave a large residual and based on existing literature[89]. The lifetimes that were found are seen in figure 4.23. Of the three dot plots, 4.23 B, showing the lifetime from

cells with PBCA particles is the only one suggesting a clear trend. Through the four time points, it can be seen that the lifetimes are continuously increasing. Also, they are grouped with the lifetimes after 0h and 5h in the lower left corner and the lifetimes from the two later time points located close together in the upper right part of the diagram. This is highlighted in figure 4.24 where the trend of the average short (A) and long (B) lifetimes are seen. In Bøes master thesis [7], it was found that after 48 hours the PBCA particles would be highly degraded unless stored at low pH. The results here also indicate that the main difference is seen in the time from 5h post incubation until 48 h post incubation. In figure 4.24 it is seen that the lifetimes of NR668 are reduced through the measurements, the reason for this is not clear, but is is possible that with time NR668 will diffuse to areas of increasing hydrophobicity resulting in shorter lifetimes.

Figure 4.23 A and C shows the lifetimes of POCA NPs and free NR668. Especially for POCA particles, no trend is seen. This indicates that very little happen to the particles within the first 7 days of incubation. This was also seen measuring the effect of pH outside cells (figure 4.19).

It is a challenging task to understand and explain why the lifetimes change the way they do. The literature offers very few general guidelines for interpreting, and changing one condition can have an opposite effect on the lifetime of two different dyes. Also, one can not be certain that what is found for Nile Red is also valid for NR668, the original article describing NR668[90], report different excitation and emission maxima of Nile red and NR668 in various solutions.

To help interpret the results, the emission spectra on the various time points are valuable. The spectral properties of NR668 has been found to depend on concentration and polarity/hydrophobicity while the effect of pH and material elasticity is not described[90]. In figure 4.28, the spectra of PBCA(A) and POCA(B) are presented. It can be seen that there is a clear red-shift in the emission spectra from PBCA, while the emission spectra from POCA is very similar on the three time points. The high intensity seen in the shorter wavelengths on the measurement at 0 hours could possibly be an artifact from measuring on the glass as discussed in the previous section. Figure 4.29 compares the emission spectra from PBCA and POCA at 0h (A), and the emission spectra of PBCA, POCA and free NR668 after 24 hours (B) and 6 days (C). It is seen that the spectra of PBCA and POCA are very similar on the measurement after 0h. This is an important validation of the method. When neither particles are degraded, the local hydrophobicity and concentration are relatively similar, and the spectra should hence be the same. This also indicates that different variables are important for the fluorescence lifetime and the emission spectra because the initial lifetimes of PBCA and POCA are not similar. In 4.29 B, it can be seen that within the first 24hours, the spectra from PBCA has changed and is now similar to the spectra of free NR668 after 24 hours intracellularly. Surprisingly, after 6 days, a significant

blue shift is observed both for PBCA and free NR668 making them more similar to the emission spectra of POCA. This is probably due to the dye diffusing to more hydrophobic domains.

The maximum intensity from the emission spectra was also recorded. Figure 4.30 shows that the average intensity over 5 images is reduced for POCA and PBCA from 24 hours to 6 days, while the intensity from free NR668 is maintained at the same level. The reduction in POCA particles is reduced to roughly 50% while PBCA is reduced to 25%. The most important reason for this shift is that the cells have undergone multiple cell cycles within these days without NPs in the solutions. This means that the particles that were encapsulated by one cell after 24 hours will after 6 days have been distributed to multiple daughter cells. The difference between POCA or PBCA could indicate one of two things. Either POCA has a more toxic effect than PBCA, reducing the rate of cell proliferation, or the intensity of PBCA is reduced because in these samples, NR668 has diffused to less hydrophobic domains where the quantum yield is lower or has been removed from the cell. The first option is improbable because the medium containing NPs is removed after 24 hours, meaning that the amount of NPs per cell decreases from this point. The second option is in compliance with other results in this thesis showing that the particle is degraded. It is not clear why intensity has not been decreased for free NR668, it is possible that the concentration of free Nile red in the solution is above the maximum that can be solved in the lipid droplets and that significant amounts of quenched NR668 are also present in the cells.

Lysing the cells with Triton was only partly successful because the effect varied from experiment to experiment. The observations from those experiments are difficult to present on paper, but the attempt is presented in figure 4.31, 4.32 and 4.33. It was seen that upon addition of Triton a faint staining of the entire cell, except the nuclei, was observed both for free NR668 and PBCA, but not for POCA. This is interpreted as the detergent making the lipid droplets solvable in the intracellular compartment, intact NPs however would not be affected by addition of the detergent.

Comparing the results from FLIM and from emission specter analysis it is possible to conclude on the degradation of the NPs. For POCA particles, the general trend is that the change with time is insignificant. This is also in compliance with the FLIM images in figure 4.22, where a narrow distribution of lifetimes is seen compared to free NR668 and PBCA. Adding Triton to the cells incubated with POCA particles also support the conclusion that the intracellular degradation of POCA particles is very limited after 6 days.

The lifetime measured from PBCA particles increases with time over the four measurements and it can be considered very likely that these particles are either degraded or has delivered a significant amount of free NR668 to the cell. Both

from FLIM and spectral analysis, the initial values measured for the PBCA NP are different for the endpoints, and the lifetimes are also different to those found for free NR668, which is also an important piece of information. If the fluorescent dye was released from the particle, without the particle degrading, one should expect to find lifetimes identical to those found in cells incubated with free dye only. The scatter plots in figure 4.23 show that the longer lifetimes measured in cells incubated with PBCA particles is higher than the lifetimes found for free NR668, this suggests that the remaining material from the particle still plays a role. This is not surprising though, BCA is a highly hydrophobic molecule and once degraded from the particle is likely to end up in hydrophobic domains along with the fluorescent dye. FLIM, being highly sensitive to the local environment can be expected to react to this.

The red-shift seen in the emission spectra from PBCA particles is likely to result from NR668 occupying less hydrophobic domains than the particle. This effect is well documented in the literature[90][91]. When the particle is degraded and NR668 is released to the surroundings, NR668 will bind to hydrophobic areas. If the molecules here have a higher polarity than the polymer, the emission spectra will be red shifted as seen in figure 4.29A. The quantum yield will also decrease, suggesting that the magnitude of released dye could actually be bigger than what is seen in the result. The slight blue-shift seen from 24 hours to 6 days in the same figure can occur because the degraded monomer and free NR668 will slowly be drawn towards the most hydrophobic domains, creating lipid droplets consisting of both particle residuals and NR668 in an environment not too different from that of the intact particle. This means that after 24 hours intracellularly, many of the red dots seen in CLSM images is in reality lipid droplets stained with NR668 that has been released from the PBCA particles.

5.4 Concluding remarks

Throughout this thesis, the uptake in PC3 cells and intracellular degradation of POCA and PBCA particles has been evaluated. PACA NPs for drug delivery is promising amongst other due to the controllable degradability, this has been stated in numerous research articles and reviews[137][138][139][140]. To assess the overall potential of the particles evaluated in this thesis, a quick review of the necessary properties of a drug carrier is needed. The NP must be biodegradable to reduce toxic effects and accumulation in healthy tissue. The particles must either be small enough to exploit the EPR-effect, exploit active targeting or be subject to external stimuli. At the same time the particle must be large enough to carry the drug load. The rate of degradation should allow the particles to be within the tumor or ideally inside the tumor cells before the drug is delivered, but at the same time the particle must degrade fast enough to allow a sufficient

local concentration of released drug.

The particles in this thesis are made from either PBCA or POCA, both materials that have previously been shown to be relatively biocompatible[141][142], and the effect of the particle pegylation was assessed in previous work[8]. Mechanisms for targeting the tumor is currently being developed by my colleagues, (mainly unpublished data). Within the research group related to this project, the EPR effect, focused ultrasound, focused ultrasound and microbubbles, active targeting with RGD and efflux pump inhibition are all being tested or developed for use with these particles[21][5][143]. The goal of this thesis was to evaluate the mechanisms after the particles have reached the tumor.

It was found that both PBCA and POCA particles are taken up in PC3 cells by endocytosis. The uptake of POCA was found to be higher in the short term, with 4-10 times higher uptake than PBCA after 3 hours. It was found that both clathrin- and caveolin-mediated uptake were important for the uptake of POCA, while PBCA is insensitive to selectively inhibiting caveolin-mediated endocytosis. This difference can explain some of the differences in uptake. The reason for this difference is not fully identified, but it has previously been found that the PBCA particles in cell medium quickly swell to a diameter well above 200 nm, and this might lead to the slower uptake of this particle. Also the amount and homogeneity of PEG should be evaluated as a possible explanation for the slightly deviating uptake of POCA and PBCA NPs. Importantly, it was found beyond any reasonable doubt that particles were internalized, and not free dye as seen in previous studies. This shows that the chemistry for encapsulating hydrophobic molecules is functional and that the particles can be used for degradation dependent drug delivery. Also, documented endocytosis is vital for the analysis of the intracellular degradation.

Inside the cell, the PBCA particle is degraded and the drug released in cytosol. The result in this thesis and knowledge of the degradation at lysosomal pH makes it possible to conclude that the particles do not remain in lysosomes. Results both from FLIM, spectral analysis and Triton experiments show that after 24 hours intracellularly, a large part of the fluorescence molecules are in a similar environment as free NR668. This shows that the fluorescent dye is no longer within the particle, but released and diffused to liquid droplets in cytosol. This study also show that after 6 days, a significant part of the remaining particles and free NR668 is still inside the cell showing that if exocytosis occurs, it is to a very limited degree. This rate of degradation and delivery is well suited, and possibly faster than extracellular degradation. Although Bøe in his Master thesis found that the PBCA particles had a half life of less than 24 hours, the same was not the case for particles at lower pH or in cell medium. As described in the theory section, tumors often have a lower pH than healthy tissue due to anaerobe energy consumption[26]. Release of drug will therefore be postponed

until the particles are internalized. The particle will protect healthy tissue from the effects of the cytotoxic drug until the particle has either reached its target or been removed from circulation by the RES system. It has been found in related systems, that even with extensive pegylation, less than 30% of the particles are found circulating after 4 hours[144]. For the PBCA particles in this thesis it was found that after 5 hours, the lifetime from PBCA is still more similar to the initial lifetime than the lifetime of free NR668. From the results in this thesis PBCA NPs can be regarded a promising platform for drug delivery.

POCA particles are much less degraded, and is in those terms less promising for drug delivery. Still, there are potential applications for these particles as well. First of all, it shows that using PACA chemistry, it is possible to create also stable particles. It is possible to mix OCA and BCA to create new particles, and the POCA particles represent the lower boundary in terms of degradation rate for this family of NPs[48]. One could imagine creating a cancer therapy protocol where particles of different variations of POCA and PBCA are used to create a continuous release of drug that lasts for weeks. This could be favorable because many cancer drugs target specific step in the cell cycle, and is only functional towards actively proliferating cells[15]. Temporary quiescent cancer cells will not be affected by most of the drugs available. Another potential application for the POCA particles is for imaging purposes, where you want to monitor the location of the particle.

5.4.1 Future directions

This thesis follows two years of projects and master theses that have been focused on PACA NPs encapsulating a fluorescent dye as a model drug. It has now been documented that hydrophobic drugs can be delivered intracellularly, either through contact mediated delivery[80] or through endocytosis and intracellular degradation. What remains unknown is the intracellular distribution and effect of the delivered drug. It would therefore be suggested that future studies revolves around NPs encapsulating a true drug. This way it is possible to assess whether the drug loading capabilities and rate of degradation is sufficient to have an impact on treatment of cancer.

There are also some loose ends from this work that should be subject to continuous study. The uptake mechanism was not completely described, and it was not fully understood why POCA had an increased uptake compared to PBCA. It was found that particles incubated with cells for 21 hours and then re-incubated with another population of cells had a significantly increased uptake compared to the reference particles. There are mechanisms there that if understood could be important for manufacturing particles with properties that are ideal for maximum cellular uptake. It is also important to understand and quantify the escape

from lysosomes that was indicated in this thesis. A specific suggestion would be do a thorough colocalization study with the NPs and early endosomes, late endosomes and lysosomes. It would be essential and also novel knowledge if this process was understood and if lysosomal escape could be demonstrated.

It is also suggested that continued work is done to utilize FLIM and NR668 for potentially new applications. The effect of various parameters was not fully understood. However, it was found that FLIM is far more sensitive than spectral measurements and that in combination with NR668, it can be used to evaluate intracellular properties. One specific suggestion is that co-localization with organelles such as lysosomes and endosomes is combined with FLIM measurements both on endocytosed NPs and on free NR668. It is hypothesized that a clear footprint of lysosomal pH and free NR668 can be seen in FLIM images.

Chapter 6

Conclusion

In this thesis the cellular uptake and degradation of PBCA and POCA particles has been evaluated. CLSM and FC was used in combination with various organelle staining and endocytosis inhibitors to assess the cellular uptake. The degradation was measured using FLIM, emission specter analysis and cell lysis with Triton. This led to the following conclusions:

- The PBCA particles were endocytosed primarily through clathrin-mediated endocytosis. The uptake was relatively low compared to POCA after 3 hours, but highly dependent on cell confluency and maturation, with a 4 fold higher uptake after 5 days of incubation compared to 3 days. It is therefore questionable how relevant the measured uptake is to evaluated in vivo properties of the particles. The PBCA particles were found to be degraded mainly within the first 24-48 hours after incubation, this is a favorable rate for drug delivery.

- The POCA particles were endocytosed 3-fold more than the PBCA particles after 3 hours, with the same dependency on confluency and maturation. The particles were not found to degrade readily within the first week of incubation, making them too stable for most drug delivery. This rate might be better suited for imaging applications.

- Both colocalization with lysosomes and the rate of degradation suggest that these particles are able to escape the lysosomes and degrade in cytosol. This process should be further analyzed and quantified.

- It was found that FLIM and spectral analysis can both be used to evaluate intracellular degradation. FLIM is more sensitive and holds potentially a lot

more information than spectral analysis, but is also far more complicated and the results have a higher standard deviation and are harder to interpret.

Bibliography

[1] H. Maeda, J. Wu, T. Sawa, Y. Matsumura, and K. Hori, "Tumor vascular permeability and the EPR effect in macromolecular therapeutics: a review," *Journal of controlled release*, vol. 65, no. 1, pp. 271–284, 2000.

[2] J. Fang, H. Nakamura, and H. Maeda, "The EPR effect: unique features of tumor blood vessels for drug delivery, factors involved, and limitations and augmentation of the effect," *Advanced drug delivery reviews*, vol. 63, no. 3, pp. 136–151, 2011.

[3] J. D. Byrne, T. Betancourt, and L. Brannon-Peppas, "Active targeting schemes for nanoparticle systems in cancer therapeutics," *Advanced drug delivery reviews*, vol. 60, no. 15, pp. 1615–1626, 2008.

[4] S. Ganta, H. Devalapally, A. Shahiwala, and M. Amiji, "A review of stimuli-responsive nanocarriers for drug and gene delivery," *Journal of Controlled Release*, vol. 126, no. 3, pp. 187–204, 2008.

[5] M. Afadzi, S. Eggen, Y. Morch, P. Stenstad, R. Hansen, B. Angelsen, and C. de Lange Davies, "Multifunctional nanoparticles for drug delivery and imaging: Effect of ultrasound on cellular uptake and tumor tissue distribution," in *Ultrasonics Symposium (IUS), 2012 IEEE International*, pp. 421–424, IEEE, 2012.

[6] C. Vauthier, C. Dubernet, E. Fattal, H. Pinto-Alphandary, and P. Couvreur, "Poly(alkylcyanoacrylates) as biodegradable materials for biomedical applications," *Adv Drug Deliv Rev*, vol. 55, pp. 519–48, Apr 2003.

[7] A. Bøe, "Degradation and Stability of PBCA and POCA Nanoparticles," *Master*, 2013.

[8] E. Sulheim, "Analysis of PACA nanoparticles and NP-stabilized microbubbles with qNano," *Project thesis dep.physics NUTS/NTNU*, 2013.

[9] J. Ferlay, H.-R. Shin, F. Bray, D. Forman, C. Mathers, and D. M. Parkin, "Estimates of worldwide burden of cancer in 2008: Globocan 2008," *International journal of cancer*, vol. 127, no. 12, pp. 2893–2917, 2010.

[10] C. registrary of Norway, "Cancer in norway 2011," tech. rep., 2011.

[11] R. J. King and M. W. Robins, *Cancer biology*. Pearson Education, 2006.

[12] A. Garcia-Bennett, M. Nees, and B. Fadeel, "In search of the holy grail: folate-targeted nanoparticles for cancer therapy," *Biochemical pharmacology*, vol. 81, no. 8, pp. 976–984, 2011.

[13] W. C. Dewey, C. C. Ling, and R. E. Meyn, "Radiation-induced apoptosis: relevance to radiotherapy," *International Journal of Radiation Oncology* Biology* Physics*, vol. 33, no. 4, pp. 781–796, 1995.

[14] L. K. Mell, A. K. Mehrotra, and A. J. Mundt, "Intensity-modulated radiation therapy use in the US, 2004," *Cancer*, vol. 104, no. 6, pp. 1296–1303, 2005.

[15] L. Stewart, "Chemotherapy in adult high-grade glioma: a systematic review and meta-analysis of individual patient data from 12 randomised trials.," *Lancet*, vol. 359, no. 9311, pp. 1011–1018, 2002.

[16] S. Ugurel, D. Schadendorf, C. Pföhler, K. Neuber, A. Thoelke, J. Ulrich, A. Hauschild, K. Spieth, M. Kaatz, W. Rittgen, *et al.*, "In vitro drug sensitivity predicts response and survival after individualized sensitivity-directed chemotherapy in metastatic melanoma: a multicenter phase ii trial of the dermatologic cooperative oncology group," *Clinical cancer research*, vol. 12, no. 18, pp. 5454–5463, 2006.

[17] B. Haley and E. Frenkel, "Nanoparticles for drug delivery in cancer treatment," in *Urologic Oncology: Seminars and original investigations*, vol. 26, pp. 57–64, Elsevier, 2008.

[18] R. A. Gatenby and R. J. Gillies, "Why do cancers have high aerobic glycolysis?," *Nature Reviews Cancer*, vol. 4, no. 11, pp. 891–899, 2004.

[19] S. K. Hobbs, W. L. Monsky, F. Yuan, W. G. Roberts, L. Griffith, V. P. Torchilin, and R. K. Jain, "Regulation of transport pathways in tumor vessels: role of tumor type and microenvironment," *Proceedings of the National Academy of Sciences*, vol. 95, no. 8, pp. 4607–4612, 1998.

[20] A. Eberhard, S. Kahlert, V. Goede, B. Hemmerlein, K. H. Plate, and H. G. Augustin, "Heterogeneity of angiogenesis and blood vessel maturation in

human tumors: implications for antiangiogenic tumor therapies," *Cancer research*, vol. 60, no. 5, pp. 1388–1393, 2000.

[21] S. Eggen, M. Afadzi, E. A. Nilssen, S. B. Haugstad, B. Angelsen, and C. d. L. Davies, "Ultrasound improves the uptake and distribution of liposomal doxorubicin in prostate cancer xenografts," *Ultrasound in medicine & biology*, vol. 39, no. 7, pp. 1255–1266, 2013.

[22] H. Maeda, G. Bharate, and J. Daruwalla, "Polymeric drugs for efficient tumor-targeted drug delivery based on EPR-effect," *European Journal of Pharmaceutics and Biopharmaceutics*, vol. 71, no. 3, pp. 409–419, 2009.

[23] A. K. Iyer, G. Khaled, J. Fang, and H. Maeda, "Exploiting the enhanced permeability and retention effect for tumor targeting," *Drug discovery today*, vol. 11, no. 17, pp. 812–818, 2006.

[24] K. Hori, M. Suzuki, S. Tanda, and S. Saito, "Characterization of heterogeneous distribution of tumor blood flow in the rat," *Cancer Science*, vol. 82, no. 1, pp. 109–117, 1991.

[25] W. M. Becker, L. Kleinsmith, J. Hardin, and G. Bertoni, *The world of the cell*. Pearson/Benjamin Cummings, 2009.

[26] I. F. Tannock and D. Rotin, "Acid pH in tumors and its potential for therapeutic exploitation," *Cancer research*, vol. 49, no. 16, pp. 4373–4384, 1989.

[27] L. T. Baxter and R. K. Jain, "Transport of fluid and macromolecules in tumors. i. role of interstitial pressure and convection," *Microvascular research*, vol. 37, no. 1, pp. 77–104, 1989.

[28] Y. Boucher, L. T. Baxter, and R. K. Jain, "Interstitial pressure gradients in tissue-isolated and subcutaneous tumors: implications for therapy," *Cancer research*, vol. 50, no. 15, pp. 4478–4484, 1990.

[29] P. Parham and C. A. Janeway, *The immune system*, vol. 250. Garland Science New York, NY, 2005.

[30] K. Cho, X. Wang, S. Nie, D. M. Shin, *et al.*, "Therapeutic nanoparticles for drug delivery in cancer," *Clinical cancer research*, vol. 14, no. 5, pp. 1310–1316, 2008.

[31] I. Brigger, C. Dubernet, and P. Couvreur, "Nanoparticles in cancer therapy and diagnosis," *Advanced drug delivery reviews*, vol. 54, no. 5, pp. 631–651, 2002.

[32] D. Peer, J. M. Karp, S. Hong, O. C. Farokhzad, R. Margalit, and R. Langer, "Nanocarriers as an emerging platform for cancer therapy," *Nature nanotechnology*, vol. 2, no. 12, pp. 751–760, 2007.

[33] T. Lammers, F. Kiessling, W. E. Hennink, and G. Storm, "Drug targeting to tumors: principles, pitfalls and (pre-) clinical progress," *Journal of controlled release*, vol. 161, no. 2, pp. 175–187, 2012.

[34] E. A. Nance, G. F. Woodworth, K. A. Sailor, T.-Y. Shih, Q. Xu, G. Swaminathan, D. Xiang, C. Eberhart, and J. Hanes, "A dense poly (ethylene glycol) coating improves penetration of large polymeric nanoparticles within brain tissue," *Science translational medicine*, vol. 4, no. 149, pp. 149ra119–149ra119, 2012.

[35] M. E. Davis, D. M. Shin, *et al.*, "Nanoparticle therapeutics: an emerging treatment modality for cancer," *Nature Reviews Drug Discovery*, vol. 7, no. 9, pp. 771–782, 2008.

[36] J. C. Morris and T. A. Waldmann, "Advances in interleukin 2 receptor targeted treatment," *Annals of the rheumatic diseases*, vol. 59, no. suppl 1, pp. i109–i114, 2000.

[37] H. Thomas, H. M. Coley, *et al.*, "Overcoming multidrug resistance in cancer: an update on the clinical strategy of inhibiting p-glycoprotein," *Cancer control*, vol. 10, no. 2, pp. 159–159, 2003.

[38] D. Schmaljohann, "Thermo-and pH-responsive polymers in drug delivery," *Advanced drug delivery reviews*, vol. 58, no. 15, pp. 1655–1670, 2006.

[39] J.-H. Park, G. von Maltzahn, L. L. Ong, A. Centrone, T. A. Hatton, E. Ruoslahti, S. N. Bhatia, and M. J. Sailor, "Cooperative nanoparticles for tumor detection and photothermally triggered drug delivery," *Advanced Materials*, vol. 22, no. 8, pp. 880–885, 2010.

[40] S. Mitragotri, "Healing sound: the use of ultrasound in drug delivery and other therapeutic applications," *Nature Reviews Drug Discovery*, vol. 4, no. 3, pp. 255–260, 2005.

[41] S. Hernot and A. L. Klibanov, "Microbubbles in ultrasound-triggered drug and gene delivery," *Advanced drug delivery reviews*, vol. 60, no. 10, pp. 1153–1166, 2008.

[42] X. Ma, Y. Zhao, and X.-J. Liang, "Theranostic nanoparticles engineered for clinic and pharmaceutics," *Accounts of chemical research*, vol. 44, no. 10, pp. 1114–1122, 2011.

[43] B. Mishra, B. B. Patel, and S. Tiwari, "Colloidal nanocarriers: a review on formulation technology, types and applications toward targeted drug delivery," *Nanomedicine: Nanotechnology, biology and medicine*, vol. 6, no. 1, pp. 9–24, 2010.

[44] B. Y. Kim, J. T. Rutka, and W. C. Chan, "Nanomedicine," *New England Journal of Medicine*, vol. 363, no. 25, pp. 2434–2443, 2010.

[45] S. V. Vinogradov, T. K. Bronich, and A. V. Kabanov, "Nanosized cationic hydrogels for drug delivery: preparation, properties and interactions with cells," *Advanced drug delivery reviews*, vol. 54, no. 1, pp. 135–147, 2002.

[46] H. Hillaireau and P. Couvreur, "Nanocarriers' entry into the cell: relevance to drug delivery," *Cellular and Molecular Life Sciences*, vol. 66, no. 17, pp. 2873–2896, 2009.

[47] N. Kamaly, Z. Xiao, P. M. Valencia, A. F. Radovic-Moreno, and O. C. Farokhzad, "Targeted polymeric therapeutic nanoparticles: design, development and clinical translation," *Chemical Society Reviews*, vol. 41, no. 7, pp. 2971–3010, 2012.

[48] C.-Y. Huang and Y.-D. Lee, "Core-shell type of nanoparticles composed of poly (-butyl cyanoacrylate)-(2-octyl cyanoacrylate) copolymers for drug delivery application: Synthesis, characterization and in vitro degradation," *International journal of pharmaceutics*, vol. 325, no. 1, pp. 132–139, 2006.

[49] N. Behan, C. Birkinshaw, and N. Clarke, "Poly-butyl cyanoacrylate nanoparticles: a mechanistic study of polymerisation and particle formation," *Biomaterials*, vol. 22, no. 11, pp. 1335–1344, 2001.

[50] R. Arshady, "Suspension, emulsion, and dispersion polymerization: a methodological survey," *Colloid and polymer science*, vol. 270, no. 8, pp. 717–732, 1992.

[51] D. E. Owens III and N. A. Peppas, "Opsonization, biodistribution, and pharmacokinetics of polymeric nanoparticles," *International journal of pharmaceutics*, vol. 307, no. 1, pp. 93–102, 2006.

[52] P. C. Hiemenz and R. Rajagopalan, *Principles of Colloid and Surface Chemistry, revised and expanded*, vol. 14. CRC Press, 1997.

[53] T. G. Mason, J. Wilking, K. Meleson, C. Chang, and S. Graves, "Nanoemulsions: formation, structure, and physical properties," *Journal of Physics: Condensed Matter*, vol. 18, no. 41, p. R635, 2006.

[54] M. A. Dobrovolskaia, P. Aggarwal, J. B. Hall, and S. E. McNeil, "Preclinical studies to understand nanoparticle interaction with the immune system and its potential effects on nanoparticle biodistribution," *Molecular pharmaceutics*, vol. 5, no. 4, pp. 487–495, 2008.

[55] C. D. Walkey and W. C. Chan, "Understanding and controlling the interaction of nanomaterials with proteins in a physiological environment," *Chemical Society Reviews*, vol. 41, no. 7, pp. 2780–2799, 2012.

[56] V. Patravale, R. Kulkarni, *et al.*, "Nanosuspensions: a promising drug delivery strategy," *Journal of pharmacy and pharmacology*, vol. 56, no. 7, pp. 827–840, 2004.

[57] "www.zetawest.com."

[58] A. Vila, A. Sanchez, M. Tobıo, P. Calvo, and M. Alonso, "Design of biodegradable particles for protein delivery," *Journal of Controlled Release*, vol. 78, no. 1, pp. 15–24, 2002.

[59] C. D. Walkey, J. B. Olsen, H. Guo, A. Emili, and W. C. Chan, "Nanoparticle size and surface chemistry determine serum protein adsorption and macrophage uptake," *Journal of the American Chemical Society*, vol. 134, no. 4, pp. 2139–2147, 2012.

[60] L. H. Hurley, "DNA and its associated processes as targets for cancer therapy," *Nature Reviews Cancer*, vol. 2, no. 3, pp. 188–200, 2002.

[61] T.-G. Iversen, T. Skotland, and K. Sandvig, "Endocytosis and intracellular transport of nanoparticles: present knowledge and need for future studies," *Nano Today*, vol. 6, no. 2, pp. 176–185, 2011.

[62] G. Sahay, D. Y. Alakhova, and A. V. Kabanov, "Endocytosis of nanomedicines," *Journal of controlled release*, vol. 145, no. 3, pp. 182–195, 2010.

[63] J. Rejman, V. Oberle, I. Zuhorn, and D. Hoekstra, "Size-dependent internalization of particles via the pathways of clathrin-and caveolae-mediated endocytosis," *Biochem. J*, vol. 377, pp. 159–169, 2004.

[64] F. R. Maxfield and T. E. McGraw, "Endocytic recycling," *Nature reviews Molecular cell biology*, vol. 5, no. 2, pp. 121–132, 2004.

[65] A. Aderem and D. M. Underhill, "Mechanisms of phagocytosis in macrophages," *Annual review of immunology*, vol. 17, no. 1, pp. 593–623, 1999.

[66] S. D. Conner and S. L. Schmid, "Regulated portals of entry into the cell," *Nature*, vol. 422, no. 6927, pp. 37–44, 2003.

[67] F. M. Brodsky, C.-Y. Chen, C. Knuehl, M. C. Towler, and D. E. Wakeham, "Biological basket weaving: formation and function of clathrin-coated vesicles," *Annual review of cell and developmental biology*, vol. 17, no. 1, pp. 517–568, 2001.

[68] P. Lajoie and I. R. Nabi, "Lipid rafts, caveolae, and their endocytosis," *International review of cell and molecular biology*, vol. 282, pp. 135–163, 2010.

[69] L. Pelkmans and A. Helenius, "Endocytosis via caveolae," *Traffic*, vol. 3, no. 5, pp. 311–320, 2002.

[70] G. J. Doherty and H. T. McMahon, "Mechanisms of endocytosis," *Annual review of biochemistry*, vol. 78, pp. 857–902, 2009.

[71] L.-H. Wang, K. G. Rothberg, and R. Anderson, "Mis-assembly of clathrin lattices on endosomes reveals a regulatory switch for coated pit formation.," *The Journal of cell biology*, vol. 123, no. 5, pp. 1107–1117, 1993.

[72] L. Pelkmans, D. Püntener, and A. Helenius, "Local actin polymerization and dynamin recruitment in sv40-induced internalization of caveolae," *Science*, vol. 296, no. 5567, pp. 535–539, 2002.

[73] R. J. Lee and P. S. Low, "Delivery of liposomes into cultured kb cells via folate receptor-mediated endocytosis.," *Journal of Biological Chemistry*, vol. 269, no. 5, pp. 3198–3204, 1994.

[74] A. I. Ivanov, "Pharmacological inhibition of endocytic pathways: is it specific enough to be useful?," in *Exocytosis and Endocytosis*, pp. 15–33, Springer, 2008.

[75] D. Perrais and C. J. Merrifield, "Dynamics of endocytic vesicle creation," *Developmental cell*, vol. 9, no. 5, pp. 581–592, 2005.

[76] J. Huotari and A. Helenius, "Endosome maturation," *The EMBO journal*, vol. 30, no. 17, pp. 3481–3500, 2011.

[77] L. K. Bogart, G. Pourroy, C. J. Murphy, V. Puntes, T. Pellegrino, D. Rosenblum, D. Peer, and R. Lévy, "Nanoparticles for imaging, sensing, and therapeutic intervention," *ACS nano*, vol. 8, no. 4, pp. 3107–3122, 2014.

[78] J. Gilleron, W. Querbes, A. Zeigerer, A. Borodovsky, G. Marsico, U. Schubert, K. Manygoats, S. Seifert, C. Andree, M. Stöter, *et al.*, "Image-based analysis of lipid nanoparticle-mediated sirna delivery, intracellular trafficking and endosomal escape," *Nature biotechnology*, vol. 31, no. 7, pp. 638–646, 2013.

[79] S. A. Ferreira, A. Correia, P. Madureira, M. Vilanova, and F. M. Gama, "Unraveling the uptake mechanisms of mannan nanogel in bone-marrow-derived macrophages," *Macromolecular bioscience*, vol. 12, no. 9, pp. 1172–1180, 2012.

[80] S. Snipstad, "Mechanisms for delivery of hydrophobic drugs from polymeric nanoparticles to cancer cells," *Master thesis dep.physics NUTS/NTNU*, 2013.

[81] S. Snipstad, S. Westrøm, Y. Mørch, M. Afadzi, A. Åslund, and C. deL Davies, "Contact-mediated intracellular delivery of hydrophobic drugs from polymeric nanoparticles," *(Manuscript not yet accepted)*, 2014.

[82] C. K. Weiss, M. R. Lorenz, K. Landfester, and V. Mailänder, "Cellular uptake behavior of unfunctionalized and functionalized pbca particles prepared in a miniemulsion," *Macromolecular bioscience*, vol. 7, no. 7, pp. 883–896, 2007.

[83] P. Ramge, R. E. Unger, J. B. Oltrogge, D. Zenker, D. Begley, J. Kreuter, and H. Von Briesen, "Polysorbate-80 coating enhances uptake of polybutylcyanoacrylate (pbca)-nanoparticles by human and bovine primary brain capillary endothelial cells," *European Journal of Neuroscience*, vol. 12, no. 6, pp. 1931–1940, 2000.

[84] F. Yan, C. Zhang, Y. Zheng, L. Mei, L. Tang, C. Song, H. Sun, and L. Huang, "The effect of poloxamer 188 on nanoparticle morphology, size, cancer cell uptake, and cytotoxicity," *Nanomedicine: Nanotechnology, Biology and Medicine*, vol. 6, no. 1, pp. 170–178, 2010.

[85] W. R. Zipfel, R. M. Williams, and W. W. Webb, "Nonlinear magic: multiphoton microscopy in the biosciences," *Nature biotechnology*, vol. 21, no. 11, pp. 1369–1377, 2003.

[86] C. Chang, D. Sud, and M. Mycek, "Fluorescence lifetime imaging microscopy," *Methods in cell biology*, vol. 81, p. 495, 2007.

[87] "www.photochemistry.files.wordpress.com/2009/08/jablonski," 08 2009.

[88] R. Cubeddu, D. Comelli, C. D'Andrea, P. Taroni, and G. Valentini, "Time-resolved fluorescence imaging in biology and medicine," *Journal of Physics D: Applied Physics*, vol. 35, no. 9, p. R61, 2002.

[89] A.-Y. Jee, S. Park, H. Kwon, and M. Lee, "Excited state dynamics of nile red in polymers," *Chemical Physics Letters*, vol. 477, no. 1, pp. 112–115, 2009.

[90] A. S. Klymchenko, E. Roger, N. Anton, H. Anton, I. Shulov, J. Vermot, Y. Mely, and T. F. Vandamme, "Highly lipophilic fluorescent dyes in nano-emulsions: towards bright non-leaking nano-droplets," *RSC Advances*, vol. 2, no. 31, pp. 11876–11886, 2012.

[91] P. Greenspan, E. P. Mayer, and S. D. Fowler, "Nile red: a selective fluorescent stain for intracellular lipid droplets.," *The Journal of cell biology*, vol. 100, no. 3, pp. 965–973, 1985.

[92] P. Greenspan and S. D. Fowler, "Spectrofluorometric studies of the lipid probe, nile red.," *Journal of lipid research*, vol. 26, no. 7, pp. 781–789, 1985.

[93] S. Westrøm, "Master thesis," *NUTS/NTNU*, 2013.

[94] Z. R. Grabowski, K. Rotkiewicz, and A. Siemiarczuk, "Dual fluorescence of donor-acceptor molecules and the twisted intramolecular charge transfer (tict) states," *Journal of Luminescence*, vol. 18, pp. 420–424, 1979.

[95] M. Krishna, "Excited-state kinetics of the hydrophobic probe nile red in membranes and micelles," *The Journal of Physical Chemistry A*, vol. 103, no. 19, pp. 3589–3595, 1999.

[96] J. Pawley, *Handbook of biological confocal microscopy*. Springer, 2010.

[97] S. W. Paddock, "Principles and practices of laser scanning confocal microscopy," *Molecular biotechnology*, vol. 16, no. 2, pp. 127–149, 2000.

[98] L. microsystems, "Leica tcs sp8," *Leica SP8 user manual*, 2014.

[99] S. J. Wright and D. J. Wright, "Introduction to confocal microscopy," *Cell Biological Applications of Confocal Microscopy, in Methods in Cell Biology*, vol. 70, pp. 1–85, 2002.

[100] E. Abbe, "Beiträge zur theorie des mikroskops und der mikroskopischen wahrnehmung," *Archiv für mikroskopische Anatomie*, vol. 9, no. 1, pp. 413–418, 1873.

[101] D. Elson, J. Requejo-Isidro, I. Munro, F. Reavell, J. Siegel, K. Suhling, P. Tadrous, R. Benninger, P. Lanigan, J. McGinty, *et al.*, "Time-domain fluorescence lifetime imaging applied to biological tissue," *Photochemical & Photobiological Sciences*, vol. 3, no. 8, pp. 795–801, 2004.

[102] D. O'Connor, *Time-correlated single photon counting*. Academic Press, 1984.

[103] Y. Sun, R. N. Day, and A. Periasamy, "Investigating protein-protein interactions in living cells using fluorescence lifetime imaging microscopy," *Nature protocols*, vol. 6, no. 9, pp. 1324–1340, 2011.

[104] H. M. Shapiro, *Practical flow cytometry*. John Wiley & Sons, 2005.

[105] J. V. Watson, *Introduction to flow cytometry*. Cambridge University Press, 2004.

[106] "www.semrock.com," 2014.

[107] S. Barua and K. Rege, "Cancer-cell-phenotype-dependent differential intracellular trafficking of unconjugated quantum dots," *Small*, vol. 5, no. 3, pp. 370–376, 2009.

[108] J. N. Davis, O. Kucuk, and F. H. Sarkar, "Genistein inhibits nf-kb activation in prostate cancer cells," *Nutrition and cancer*, vol. 35, no. 2, pp. 167–174, 1999.

[109] K. T. Thurn, H. Arora, T. Paunesku, A. Wu, E. Brown, C. Doty, J. Kremer, and G. Woloschak, "Endocytosis of titanium dioxide nanoparticles in prostate cancer pc-3m cells," *Nanomedicine: Nanotechnology, Biology and Medicine*, vol. 7, no. 2, pp. 123–130, 2011.

[110] K. R. Chaudhari, M. Ukawala, A. S. Manjappa, A. Kumar, P. K. Mundada, A. K. Mishra, R. Mathur, J. Mönkkönen, and R. S. R. Murthy, "Opsonization, biodistribution, cellular uptake and apoptosis study of PEGylated PBCA nanoparticle as potential drug delivery carrier," *Pharmaceutical research*, vol. 29, no. 1, pp. 53–68, 2012.

[111] M. S. Cartiera, K. M. Johnson, V. Rajendran, M. J. Caplan, and W. M. Saltzman, "The uptake and intracellular fate of PLGA nanoparticles in epithelial cells," *Biomaterials*, vol. 30, no. 14, pp. 2790–2798, 2009.

[112] K. Yin Win and S.-S. Feng, "Effects of particle size and surface coating on cellular uptake of polymeric nanoparticles for oral delivery of anticancer drugs," *Biomaterials*, vol. 26, no. 15, pp. 2713–2722, 2005.

[113] J. Dausend, A. Musyanovych, M. Dass, P. Walther, H. Schrezenmeier, K. Landfester, and V. Mailänder, "Uptake mechanism of oppositely charged fluorescent nanoparticles in HeLa cells," *Macromolecular bioscience*, vol. 8, no. 12, pp. 1135–1143, 2008.

[114] M. Ogris, P. Steinlein, S. Carotta, S. Brunner, and E. Wagner, "DNA/polyethylenimine transfection particles: influence of ligands, polymer size, and PEGylation on internalization and gene expression," *Aaps Pharmsci*, vol. 3, no. 3, pp. 43–53, 2001.

[115] L. W. Zhang and N. A. Monteiro-Riviere, "Mechanisms of quantum dot nanoparticle cellular uptake," *Toxicological Sciences*, vol. 110, no. 1, pp. 138–155, 2009.

[116] R. G. Parton and A. A. Richards, "Lipid rafts and caveolae as portals for endocytosis: new insights and common mechanisms," *Traffic*, vol. 4, no. 11, pp. 724–738, 2003.

[117] J. C. Zillies, K. Zwiorek, G. Winter, and C. Coester, "Method for quantifying the pegylation of gelatin nanoparticle drug carrier systems using asymmetrical flow field-flow fractionation and refractive index detection," *Analytical chemistry*, vol. 79, no. 12, pp. 4574–4580, 2007.

[118] H. Mok, K. H. Bae, C.-H. Ahn, and T. G. Park, "PEGylated and MMP-2 specifically dePEGylated quantum dots: comparative evaluation of cellular uptake," *Langmuir*, vol. 25, no. 3, pp. 1645–1650, 2008.

[119] R. N. Alyaudtin, A. Reichel, R. Löbenberg, P. Ramge, J. Kreuter, and D. J. Begley, "Interaction of poly (butylcyanoacrylate) nanoparticles with the blood-brain barrier in vivo and in vitro," *Journal of drug targeting*, vol. 9, no. 3, pp. 209–221, 2001.

[120] J. Kreuter, P. Ramge, V. Petrov, S. Hamm, S. E. Gelperina, B. Engelhardt, R. Alyautdin, H. Von Briesen, and D. J. Begley, "Direct evidence that polysorbate-80-coated poly (butylcyanoacrylate) nanoparticles deliver drugs to the cns via specific mechanisms requiring prior binding of drug to the nanoparticles," *Pharmaceutical research*, vol. 20, no. 3, pp. 409–416, 2003.

[121] B. Nichols, "Caveosomes and endocytosis of lipid rafts," *Journal of cell science*, vol. 116, no. 23, pp. 4707–4714, 2003.

[122] B. Alberts, A. Johnson, J. Lewis, M. Raff, K. Roberts, and P. Walter, "Molecular biology of the cell," *New York: Garland Science*, vol. 1, 2008.

[123] N. Zhang, C. Chittasupho, C. Duangrat, T. J. Siahaan, and C. Berkland, "Plga nanoparticle- peptide conjugate effectively targets intercellular cell-adhesion molecule-1," *Bioconjugate chemistry*, vol. 19, no. 1, pp. 145–152, 2007.

[124] H. Shi, X. He, Y. Yuan, K. Wang, and D. Liu, "Nanoparticle-based biocompatible and long-life marker for lysosome labeling and tracking," *Analytical chemistry*, vol. 82, no. 6, pp. 2213–2220, 2010.

[125] T. Ha, T. Enderle, D. Ogletree, D. Chemla, P. Selvin, and S. Weiss, "Probing the interaction between two single molecules: fluorescence resonance energy transfer between a single donor and a single acceptor," *Proceedings of the National Academy of Sciences*, vol. 93, no. 13, pp. 6264–6268, 1996.

[126] T. Akagi, F. Shima, and M. Akashi, "Intracellular degradation and distribution of protein-encapsulated amphiphilic poly (amino acid) nanoparticles," *Biomaterials*, vol. 32, no. 21, pp. 4959–4967, 2011.

[127] K. Remaut, B. Lucas, K. Braeckmans, J. Demeester, and S. De Smedt, "Pegylation of liposomes favours the endosomal degradation of the delivered phosphodiester oligonucleotides," *Journal of controlled release*, vol. 117, no. 2, pp. 256–266, 2007.

[128] K. Langer, M. Anhorn, I. Steinhauser, S. Dreis, D. Celebi, N. Schrickel, S. Faust, and V. Vogel, "Human serum albumin (hsa) nanoparticles: reproducibility of preparation process and kinetics of enzymatic degradation," *International journal of pharmaceutics*, vol. 347, no. 1, pp. 109–117, 2008.

[129] P. I. Bastiaens and A. Squire, "Fluorescence lifetime imaging microscopy: spatial resolution of biochemical processes in the cell," *Trends in cell biology*, vol. 9, no. 2, pp. 48–52, 1999.

[130] A. Cser, K. Nagy, and L. Biczók, "Fluorescence lifetime of nile red as a probe for the hydrogen bonding strength with its microenvironment," *Chemical physics letters*, vol. 360, no. 5, pp. 473–478, 2002.

[131] S. Mukherjee, H. Raghuraman, and A. Chattopadhyay, "Membrane localization and dynamics of nile red: effect of cholesterol," *Biochimica et Biophysica Acta (BBA)-Biomembranes*, vol. 1768, no. 1, pp. 59–66, 2007.

[132] D. Reijngoud and J. Tager, "Measurement of intralysosomal pH," *Biochimica et Biophysica Acta (BBA)-General Subjects*, vol. 297, no. 1, pp. 174–178, 1973.

[133] G. Bjørkøy, T. Lamark, A. Brech, H. Outzen, M. Perander, A. Øvervatn, H. Stenmark, and T. Johansen, "p62/sqstm1 forms protein aggregates degraded by autophagy and has a protective effect on huntingtin-induced cell death," *The Journal of cell biology*, vol. 171, no. 4, pp. 603–614, 2005.

[134] C. de Duve and R. Wattiaux, "Functions of lysosomes," *Annual review of physiology*, vol. 28, no. 1, pp. 435–492, 1966.

[135] J. Panyam and V. Labhasetwar, "Biodegradable nanoparticles for drug and gene delivery to cells and tissue," *Advanced drug delivery reviews*, vol. 55, no. 3, pp. 329–347, 2003.

[136] D. J. Murphy and J. Vance, "Mechanisms of lipid-body formation," *Trends in biochemical sciences*, vol. 24, no. 3, pp. 109–115, 1999.

[137] E. Fattal, C. Vauthier, I. Aynie, Y. Nakada, G. Lambert, C. Malvy, and P. Couvreur, "Biodegradable polyalkylcyanoacrylate nanoparticles for the delivery of oligonucleotides," *Journal of Controlled Release*, vol. 53, no. 1, pp. 137–143, 1998.

[138] K. S. Soppimath, T. M. Aminabhavi, A. R. Kulkarni, and W. E. Rudzinski, "Biodegradable polymeric nanoparticles as drug delivery devices," *Journal of controlled release*, vol. 70, no. 1, pp. 1–20, 2001.

[139] V. Mohanraj and Y. Chen, "Nanoparticles-a review," *Tropical Journal of Pharmaceutical Research*, vol. 5, no. 1, pp. 561–573, 2007.

[140] A. Kumari, S. K. Yadav, and S. C. Yadav, "Biodegradable polymeric nanoparticles based drug delivery systems," *Colloids and Surfaces B: Biointerfaces*, vol. 75, no. 1, pp. 1–18, 2010.

[141] Y. Zhang, S. Zhu, L. Yin, F. Qian, C. Tang, and C. Yin, "Preparation, characterization and biocompatibility of poly (ethylene glycol)-poly(butyl cyanoacrylate) nanocapsules with oil core via miniemulsion polymerization," *European Polymer Journal*, vol. 44, no. 6, pp. 1654–1661, 2008.

[142] G. Yordanov, "Poly (alkyl cyanoacrylate) nanoparticles as drug carriers: 33 years later," *Bulg. J. Chem*, vol. 1, pp. 61–73, 2012.

[143] S. Eggen, S.-M. Fagerland, Ý. Mørch, R. Hansen, K. Søvik, S. Berg, H. Furu, A. D. Bøhn, M. B. Lilledahl, A. Angelsen, *et al.*, "Ultrasound-enhanced drug delivery in prostate cancer xenografts by nanoparticles stabilizing microbubbles," *Journal of Controlled Release*, vol. 187, pp. 39–49, 2014.

[144] P. Calvo, B. Gouritin, H. Chacun, D. Desmaële, J. D'Angelo, J.-P. Noel, D. Georgin, E. Fattal, J. P. Andreux, and P. Couvreur, "Long-circulating pegylated polycyanoacrylate nanoparticles as new drug carrier for brain delivery," *Pharmaceutical research*, vol. 18, no. 8, pp. 1157–1166, 2001.

Appendices

Appendix A

Fluorescence intensity

The fluorescence intensity from POCA NP (Targ 76) and PACA NP (Targ 67) was measured using a plate reader (figure A.1). The work was done by Eva von Haartman and Andreas Åslund prior to this master thesis.

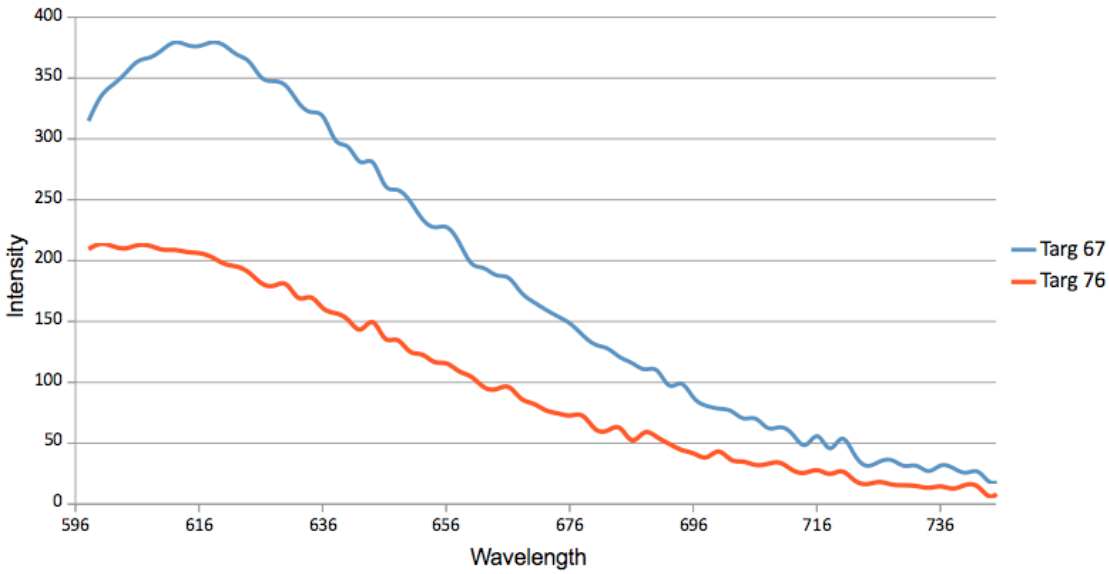

Figure A.1: Emission intensity of Targ 67 and Targ 76 from 596nm to 748nm. Excitation wavelength 561nm. Unpublished results from Eva von Haartman.

The normalized fluorescence intensity at wavelength 620 nm is presented in

table A.1, in order to compare the uptake of PBCA and POCA NP, the fluorescence intensity of POCA should therefore be multiplied by $\frac{1}{0.52} = 1.923$

Table A.1: Normalized fluorescence intensity at 620nm

Particle	Normalized intensity
PBCA (Targ 67)	1
POCA (Targ 76)	0.52

Appendix B

Endocytosis inhibition

Inhibition of endocytosis was done twice, and the bar plots in figure 4.10 comes from adding those two. These two experiments were performed at different cell density resulting from different time of cultivation before inhibitors and cells were added. The uptake of PBCA is seen in figure B.1 with the experiment of low density in A and high density in B. The same for POCA is seen in figure B.2.

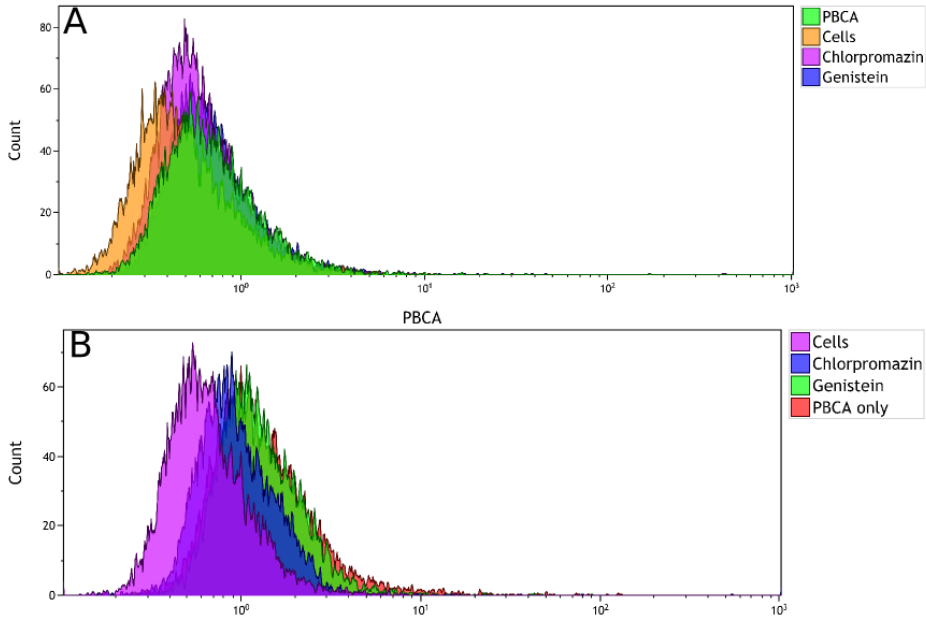

Figure B.1: Histograms from FC showing the uptake of PBCA suppressed by inhibitors in the experiment of low density (A), and high density of B.

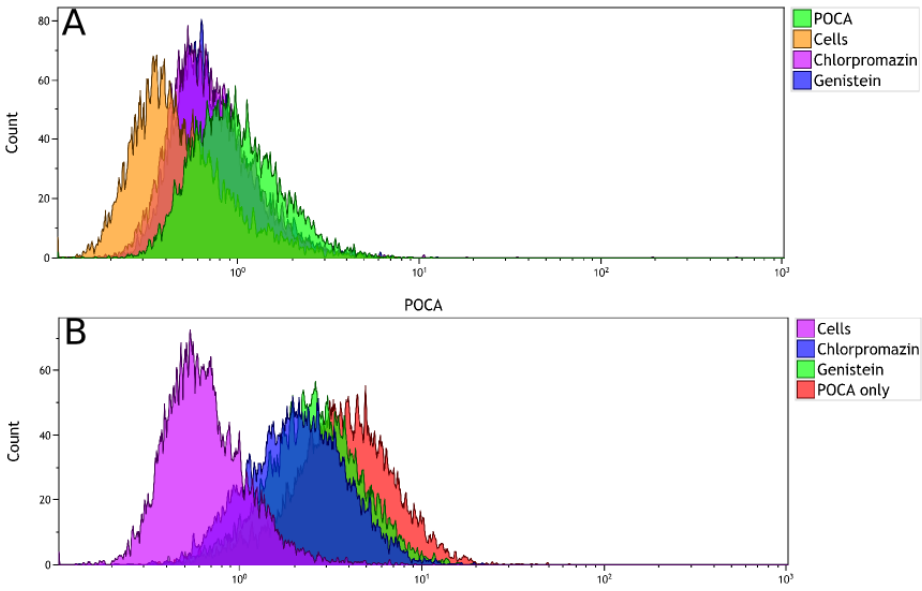

Figure B.2: Histograms from FC showing the uptake of POCA suppressed by inhibitors in the experiment of low density (A), and high density of B.

Appendix C

Fluorescence lifetimes

Table C.1 shows the exact lifetimes measured on the various time points after incubation.

Table C.1: Lifetimes of NR668 inside POCA and PBCA particles inside PC3 cells. Average and standard deviation based on 6 images.

PBCA		
Time	τ_1(ns)	τ_2(ns)
0h	0.72 (± 0.03)	3.15 (± 0.12)
5h	0.82 (± 0.08)	3.13 (± 0.11)
24-48h	1.05 (± 0.17)	3.44 (± 0.12)
6-7 days	1.22 (± 0.10)	3.58 (± 0.12)
POCA		
Time	τ_1(ns)	τ_2(ns)
0h	1.03 (± 0.36)	3.69 (± 0.20)
5h	1.05 (± 0.09)	3.64 (± 0.13)
24-48h	1.03 (± 0.09)	3.52 (± 0.13)
6-7 days	1.19 (± 0.29)	3.62 (± 0.19)
NR668		
Time	τ_1(ns)	τ_2(ns)
0h	-*	-*
5h	0.93 (± 0.21)	3.45(± 0.10)
24-48h	0.91 (± 0.11)	3.31 (± 0.12)
6-7 days	0.79 (± 0.17)	3.10 (± 0.14)

*Free NR668 could not be imaged at 0h because it is essentially quenched in water and does not attach to the sample chamber.